DESIGN OF INJECTABLE HYDROGELS FOR CELL- AND DRUG-DELIVERY IN TISSUE ENGINEERING APPLICATIONS

by

Bryan Russell Dollinger

Dissertation

Submitted to the Faculty of the

Graduate School of Vanderbilt University

in partial fulfillment of the requirements

for the degree of

DOCTOR OF PHILOSOPHY

in

Biomedical Engineering

December 18, 2021

Nashville, Tennessee

Approved:

Craig L. Duvall, Ph.D.

Jeffrey M. Davidson, Ph.D.

Todd D. Giorgio, Ph.D.

Scott A. Guelcher, Ph. D.

John T. Wilson, Ph.D.

To my mother, the warrior.

To my father, the rock.

To my sister, the solace.

To my friends, the beacon in the storm.

ACKNOWLEDGEMENTS

First and foremost, I'd like to thank my advisor, Dr. Craig Duvall. His support and guidance throughout my time as a graduate student enabled me to work to my potential. Dr. Duvall gracefully challenges his mentees and builds them into enthusiastic, impactful, and informed citizens of the science and engineering community. His ability to select lab members has assembled a highly cooperative and supportive group that promotes becoming your best.

With that said, I want to also thank all my lab mates who have been not just coworkers, but friends for life. Research professors Dr. Mukesh Gupta and Dr. Richard D'Arcy have been essential in helping me meet my goals as a scientist and professional. They've always been enthusiastic to help and more than willing to talk anything over at any time of day; I always left their office feeling much better about my research struggles. Dr. Fang Yu has played an essential role to my progress and supports the lab tremendously with her remarkable skills and patience as a surgeon. Last but certainly not least, I'd like to thank some of my closest friends in the lab: Isom Kelly, Dr. Prarthana Patil, Ella Hoogenboezem, Brock Fletcher, Shrusti Patel, Carli DeJulius, Juan Culazo, Jordan Hill, Will Tierney, Mariah Bezold and Josh McCune for always being a shoulder to lean on.

TABLE OF CONTENTS

LIST OF TABLES AND FIGURES

CHAPTER 3

CHAPTER 4

CHAPTER 5

CHAPTER 1

INTRODUCTION

1.1 Background

CELL-BASED THERAPIES ARE BECOMING AN INCREASINGLY POPULAR strategy for treating a multitude of pathologies, especially those characterized by loss of or atypical cellular function. However, acute and chronic immune rejection along with poor retention/engraftment remain the primary barriers in achieving potent and sustained therapeutic efficacy. To combat immune rejection, patients receiving donor cells will undergo systemic immune suppression, which often pairs with side-effects and toxicity [1,2]. Currently, the strategy for managing immune tolerance and graft acceptance is carefully fine-tuning systemic immunosuppressant drug treatments, but this approach has proven to be incredibly difficult in clinical translation [3]. To address the deleterious effects of systemic immunosuppression, researchers have begun to investigate the use of biomaterials that provide cell-protective effects locally at the graft site. The general principle behind these materials is to engineer a microenvironment suitable for graft survival and retention, immune evasion, and maintenance of therapeutic cellular function.

The most prolific target of cell-based therapies to produce systemic factors are aimed toward treating Type 1 Diabetes (T1D). T1D is an autoimmune disorder characterized by the loss of insulin-producing cells within the islets of Langerhans. The

peptide hormone insulin regulates metabolism by promoting absorption of glucose from the blood into fat, liver, and muscle cells while simultaneously inhibiting excretion of glucose from the liver into the blood. Thus, patients with T1D suffer from metabolic dysregulation and accumulation of supranormal levels of blood glucose. Currently, patients diagnosed with T1D must monitor their blood-glucose level and peripherally supplement their insulin levels with routine injections of exogenous insulin; a state referred to as insulin-dependence. However, the kinetics and dosages of exogenous insulin post-injection can often be misjudged. In some severe incidences, even vigilant monitoring of blood glucose in combination with strict adherence to prescribed insulin regimens, patients are susceptible to episodes of hypo/hyperglycemia that can require hospitalization [4,5]. One potentially curative route for achieving insulin-independence in T1D, is by replacing the insulin-producing cells that they have lost with those from external sources. Because cells are intrinsically capable of sensing and responding to cues in their environment, the successful institution of a cellular graft will lead to spontaneous and on-demand maintenance of target regulatory hormones and proteins – a fully autonomous system to cure T1D [6,7].

The objective of this introduction is to familiarize the reader with the immune response elicited by biomaterials and transplanted cells and highlight impactful strategies on the materials frontier to circumvent these responses. It provides a summary of the current outlook of challenges facing successful implementation of localized cellular transplantation and discusses the material frontier that aims to meet these challenges by localized of immune control and/or evasion along with other sustainable engraftment strategies.

1.2 The Immune Response to Transplanted Cells

Upon transplantation, the immune response to transplanted cells is initially associated with innate effector functions. This phase utilizes blood-mediated factors and recruitment of inflammatory cells to reduce a foreign body. Reports on syngeneic transplantation models have found that this initial phase of the immune response may account for the destruction of approximately 60% of transplanted islets [8].

Subsequently, adaptive effector functions will continue to reduce the foreign body content, via lymphocytes that recognize specific antigens.

1.2.1 The Initial Insult

Directly following the implantation of any material, the destruction of tissues resulting from the implantation procedure leads to a mediation in the immune response. This initial phase is characterized by paracrine factors distribute through the bloodstream and induce changes in immune cells that respond to the injury and lead to downstream inflammation. Mast cells, located throughout all connective tissues, play a critical role in tempering the immune response during this key-stage. Connective tissue injury leads to mast cell degranulation, where secretory vesicles fuse with the cell membrane and release histamine. In addition to acting as a chemokine and stimulating inflammatory cytokine production, histamine acts as a vasodilator, increasing localized blood flow that enables recruitment and increased migration of pro-inflammatory immune cells (i.e., neutrophils and monocytes). Previous work characterizing the immune response to implantation of polyethylene terephthalate disks in mast cell deficient mice demonstrated that loss of histamine releasing mast cells led to a significant reduction in immune-cell recruitment by histological analysis. This finding was further corroborated by the fact that histamine antagonists administered along with the implanted material in mast cell proficient mice yielded similar results. These results suggest that histamine release from activated mast cells plays a critical role in mediating the inflammatory response to an implanted material [9].

1.2.2 Blood-Mediated Biomaterial and Cellular Interactions

The collection of innate immune reactions that are coordinated during the interaction of a transplanted biomaterial with peripheral blood are known as the Instant Blood Mediated Inflammatory Reaction (IBMIR, also known as thromboinflammation). The IBMIR leads to activation of both the *coagulation* and *complement cascades*, which directly dictate the fate and therapeutic outcome of cellular transplants. The IBMIR, which occurs within the first 5 minutes of blood exposure, rapidly activates platelets and leads to infiltration by inflammatory leukocytes, [10].

1.2.2.1 Coagulation Activation and its Role in Transplant Rejection

Coagulation activation occurs via a cascade of events where inactive factors circulating in the blood undergo proteolytic cleavage and become activated. This process characteristically begins via the *extrinsic pathway*: destruction of local tissues and the resulting vascular damage leads to the exposure of the cell surface glycoprotein tissue factor (TF, also known as Factor III, thromboplastin, or platelet tissue factor) which is found outside of blood vessels and is normally not exposed to circulation. TF serves as the surface receptor for Factor VII, and, once bound to Factor VII, Factor VII is cleaved by different proteases (including thrombin and the TF-Factor VIIa complex itself) leading to its activated form. This TF-Factor VII complex then catalyzes the activation of Factor X into an active protease. Activated Factor X (Factor Xa) enzymatically cleaves the zymogen prothrombin, converting it into thrombin. In turn, thrombin acts as a serine protease that polymerizes fibrinogen into fibrin, which together with activated platelets forms a clot. In addition to converting fibrinogen into fibrin, thrombin also begins the *intrinsic pathway:* thrombin activates the serine protease Factor XI, which activates both the protease Factor IX and the transglutaminase Factor VIII (i.e., fibrin stabilizing factor that crosslinks fibrin). Activated Factor IX then hydrolyses and activates Factor X, which cleaves prothrombin into thrombin. In addition to polymerizing fibrin, thrombin activates platelet bound Factor V, which, in concert with activated Factor X, converts prothrombin to thrombin. This positive feedback loop is eventually inactivated by the serpin (serine protease inhibitor) antithrombin, which is produced in the liver and inactivates several enzymes of the coagulation system including thrombin and activated Factors X, IX, XI, and XII.

The concern with coagulation activation during cellular or organ transplantation is the possibility that this coagulation may lead to exclusion of the graft from blood vessels. Furthermore, thrombosis, or coagulation within a blood vessel, may occlude circulation to the transplant. These outcomes effectively prevent the transplant from being exposed to adequate blood flow and deprives the transplant of necessary nutrients and oxygenation required to maintain function and/or viability [13].

1.2.2.2 Complement Activation and its Role in Transplant Rejection

The complement system is responsible for innate recognition of “self” versus ‘‘non-self’’ antigens. It consists of nearly 30 plasma glycoproteins primarily produced in the liver that function as either enzymes to chemically dissociate foreign materials or binding proteins. It has three major functions: (1) opsonize “non-self” antigens to improve phagocytosis (2) form a membrane attack complex (MAC) on foreign pathogens to induce lysis, and (3) enhance inflammatory pathways by upregulating inflammatory cytokines. Complement proteins circulate in the blood as inactive prerequisites to prevent “self” activation. However, when they come in contact with guest antigens, they become active, and begin a cascade configured to reduce or destroy foreign pathogens. Central to this system is C3, which can become activated through three primary pathways: (1) the *classical pathway* (2) the *alternative pathway* and (3) the *lectin pathway*.

The *classical pathway* begins when circulating antibodies bind to antigens on the surface of the pathogen. The C1 complex will tether itself to the Fc region of these antibodies and cause cleavage of C4 into C4a and C4b subtypes. The *lectin pathway* works very similarly, however mannose binding lectin (MBL) will bind mannose or Ficolin will bind oligosaccharides causing the same cleavage of C4. Next, C4b will conjugate itself to the surface of the pathogen by adhering to a thioester binding site. C2 will then bind to this active C4b, causing cleavage into C2a and C2b subcomponents. It is at this stage that C4b2a is prepared. C4b2a is also referred to as C3 convertase because it is the enzyme that cleaves C3, the axis of this system. Once C3 is cleaved into its subtypes of C3a and C3b, complement activation of immunocyte recognition will begin. C3b will bind to the preexisting C4b2a complexes to form C4b2a3b, also known as C5 convertase. C5 convertase cleaves C5 into subcomponents C5a and C5b. C3b will also bind to the surface of the pathogen causing opsonization, acting as a site for phagocyte recognition. Phagocytic cells recognize C3b on the surface of a pathogen via CR1 receptors on the cell surface allowing them to bind to the pathogen. Phagocytosis of the pathogen then occurs when C5a binds to the C5a receptor of the phagocyte. Simultaneously, C3a is a humoral signal initially responsible for stimulating chemotaxis of inflammatory cell types – it causes degranulation of mast cells to produce histamine,

and influences leukocytes, monocytes and neutrophils to the site of this chemical message. Lastly, C5b, along with further downstream complement proteins, will cause the formation of the MAC on the surface of the pathogen, which essentially bores a hole in the plasma membrane of a cell or bacteria, causing lysis via osmotic pressure differences in ion concentration [14].

In contrast, the *alternative pathway* can be activated without the presence of antibody or immune complexes. It can be initiated by any "non-self" surface such as polysaccharides (PS), lipopolysaccharides (LPSs), and even biomaterial interfaces. Once C3b is bound to a surface after being formed during the *classical pathway*, a few other humoral proteins will initiate complement activation. Factor B, a single chain polypeptide will bind C3b and become cleaved by either Factor D or Factor P to prepare C3bBb, another form of C3 convertase. This will initiate positive feedback to complement by creating a larger quantity of C3 subtypes. However, it has also been noted that C3 can be hydrolyzed, preparing C3-H_2O, and leading to deposition of C3b onto the foreign object. Therefore, the *alternative pathway* can also become activated in the absence of the *classical pathway* [14].

Antibody-mediated rejection via *classical pathway* activation has long been identified as a challenge to transplantation. Donor-specific antibodies have led to the development of desensitization protocols prior to transplantation such as plasma exchange [15-17], but still lead to complications and early graft loss in as many as 40% of renal transplant recipients. When regimented with the complement inhibiting drug, eculizumab, an anti-C5 antibody this incidence decreased to nearly 7%, potentially confirming the notion that complement plays a major role in allograft rejection [18]. This is also identified as a source of rejection in xenotransplantation conditions. Human serum characteristically contains natural antibodies against α-linked galactose (α-Gal), which are commonly found in non-primate tissue. These antibodies are responsible for xenograft tagging, complement activation, and consequential graft rejection [19]. It has been shown in pigs deficient in α-Gal, that xenograft function can be prolonged, but rejection is still inevitable as they express other highly immunogenic epitopes [20, 21].

1.2.2.3 Mounting Evidence for Cell Destruction via IBMIR

It has been shown that this blood-mediated response to islets in particular is triggered by the expression of both TF and monocyte chemoattractant protein 1 (MCP-1) [22, 23]. As mentioned above, TF will lead to the activation of the *extrinsic pathway* and eventually lead to formation of the fibrin clot. It has also been shown that donor islets will often be accompanied by hitchhiking macrophages that contribute to the IBMIR by producing cytokines that are relevant to its initiation [24].

Even in autologous islet transplantation following total pancreatectomy, IBMIR has been observed as a source for cell loss. Immediately following islet transplantation into the hepatic portal vein of the liver, patients who received greater than 1000 islet equivalents (IEQ) per kg immediately showed an approximately 5-fold increase in thrombin-antithrombin III complex (TAT, an indicator of thrombosis and coagulation activation) in comparison to patients that received less than 1000 IEQ per kg [25]. C-peptide levels also showed a similar trend between these groups. C-peptide is produced in a 1:1 ratio with insulin, and a spike in its blood concentration has been shown to be the result of leaking insulin from the damaged islet graft. However, complement proteins measured were no different between groups, likely because the autologous grafts did not create direct immune activation via this mechanism – antibodies were not created for “self” tissue [25].

1.3 Inflammation

Acute inflammation, which lasts minutes to days, is typically characterized by the chemotaxis of polymorphonuclear cells that infiltrate the site of injury in a process referred to diapedesis. The cells involved in this phase are primarily neutrophils, but additionally include small levels of basophils and eosinophils. Neutrophils provide two major functions during inflammation: destroy foreign pathogens by acting as professional phagocytes and mediators of oxidative destruction, and signal circulating and distant leukocytes to migrate toward the site of inflammation. Additionally, resident cells within the tissue, particularly macrophages and dendritic cells will partake in this phase of the immune response.

Pathogens express topographical surface characteristics that enable recognition by both phagocytic cells and circulating proteins such as complement factors. These features are referred to as pathogen associated molecular patterns (PAMPs). The presence of PAMPs on a surface enable both the adsorption of complement proteins and recognition by toll-like receptors (TLRs) on a cell surface, which simultaneously contribute to phagocyte recognition. Once a phagocyte recognizes a pathogen by these features. It will then engulf the pathogen into the phagosome, and the phagosome will merge with a lysosome, which carries acidic enzymes to destroy and break apart the pathogen into its constituent components. To increase inflammation, tissue macrophages and dendritic cells will continually produce cytokines that begin to circulate through the blood stream. For example, interleukin-6 (IL6), tissue necrosis factor-α (TNF-α) and CXCL8 will collectively increase inflammation by upregulating the production of complement proteins and attracting more leukocytes to the site of injury [14].

If a pathogen is too large to be engulfed by a single macrophage, the macrophages will aggregate around the pathogen and begin to fuse together into a “foreign-body giant cell.” This is especially true regarding biomaterials and large transplants that are significantly larger than single cells. These cell conglomerates will begin to secrete cytokines that signal fibroblasts to initiate coagulation and fibrotic encapsulation, isolating the foreign body from the rest of the tissue [26].

Macrophages are also known to express two particularly distinct classes: a pro-inflammatory, classically activated type, or an anti-inflammatory, pro-angiogenic type known as alternatively activated. The classically activated macrophages will increase inflammation at the site of injury while the alternatively activated macrophages will decrease inflammation and initiate progression into a phase of wound healing [26]. Upregulation of inflammation is responsible for a significant loss in transplanted islets by host and donor (inflammatory cells that are transplanted along with islets) leukocytes [27]. Mediation in the production of cytokines along with reactive oxygen species has been a long-known source of islet cell destruction [28]. Therefore, gravely significant

loss of transplanted cells within this period of IBMIR inflammation is a likely cause for graft failure.

1.4 The Adaptive Immune Response

1.4.1 The Major Histocompatibility Complex

Central to cellular or tissue graft acceptance by the adaptive immune system is the major histocompatibility complex (MHC) antigen. In humans specifically, it is referred to as the Human Leukocyte Antigen (HLA). Class I MHC antigens are expressed on nearly all human cell types and are composed of more than 200 genes in humans, making it highly variable from person to person. The immense variability in this antigen is what allows the adaptive immune system to distinguish “self” from “non-self,” and mediate cell killing when there is an MHC-mismatch. Due to the scarcity in obtaining human islets and the high variability in MHC complex from person to person, obtaining donor cells with similarity in MHC complex as the host is virtually infeasible as a generalized clinical practice. Therefore, strategies to prevent direct and indirect recognition of the cellular graft, while challenging nonetheless, seems to be the most promising route to successful transplantation of islets. Because of the lack of antigen, fully synthetic materials are traditionally thought to be rejected through non-adaptive mechanisms, making exploration of them as encapsulation materials of particular interest.

Class II MHC antigen is phenotypically characteristic of antigen-presenting cells. Antigen is displayed on this complex after phagocytic lysis and used to communicate infection to the adaptive effector cells. Considered an “enabler” of adaptive immunity, dendritic cells are responsible for communication of pathogen presence to adaptive immunocytes via the MHC mechanism. When dendritic cells encounter a “non-self” pathogen, they will undergo a process referred to as licensing. Like macrophages, dendritic cells will engulf and lyse foreign objects. The remaining peptides from the lysed pathogen will become expressed on the MHC molecule in a process referred to as antigen presentation. Fully licensed dendritic cells express CCR7 which responds to lymph node produced CCL21, enabling dendritic cells to travel through the afferent

lymphatic vessels to the lymph node. Once in the lymph node, T cells and B cells, which individually express highly specific receptors, will approach the licensed dendritic cell. If these lymphocytes have high affinity for the presented antigen on the dendritic cell, the MHC molecule will become activated. This is a process referred to as “indirect” recognition. Indirect recognition of cellular grafts can occur due to both phagocytosed cellular material and protein metabolites created during normal cellular activity, making dendritic cells particularly important to transplant rejection by adaptive immunity [14].

1.4.2 T-Cells: Production of Cell-Mediated Immunity

Naive T cells reside in the lymph node and express a wide variety of receptors that make them highly antigen specific. They are typically broken into two major subtypes based upon the MHC class molecule that they interact with. A T cell becomes activated when its specific T cell receptor has a high binding affinity to an antigen peptide presented on an MHC complex and is engaged by costimulatory molecules on an antigen presenting cell surface. CD4+ T cells interact with antigen presented on dendritic cells via the MHC II molecule along with along with costimulators CD4 and CD28. When CD4+ T cells encounter a matching antigen to their receptor, they will become activated and differentiate into a subset of T helper cells, specifically T helper 1 (Th1), T helper 2 (Th2), T helper 17 (Th17) or regulatory T cells (Treg). The subset of differentiation is determined by cytokines released by the dendritic cells themselves. CD8+ T cells will interact with dendritic cells via the MHC I molecule along with costimulators CD8 and CD28. Activation of CD8+ T cells will lead to differentiation into T killer cells (also referred to as effector T cells), or T memory cells. Once activated, all these cells with the exception of memory T cells will migrate to the efferent lymph vessel and continue to the site of inflammation.

When dendritic cells release a combination of Interleukin 12 (IL-12) and IFN-gamma, Th1 cells will be produced. Th1 cells play important roles in activating macrophages by delivering IFN-gamma to the site of inflammation, increasing leukocyte presence via secretion of TNF-α and CXCL2, and assisting in the activation of B cells with matching antigen recognition. In the presence of IL-4, T cells will differentiate into Th2 cells. Th2 cells can also assist in B cell activation, but additionally activate

granulocytes to degranulate and produce relevant pro-inflammatory cytokines to recruit immune cells. A combination of Interferon Growth Factor β (IGF- β) and Interleukin 6 (IL-6) will lead to maturation into Th17 cells. Th17 cells produce Interleukin 17 (IL-17) which will cause endothelial cells to produce cytokines that induce migration of leukocytes to the inflamed area. However, in the absence of IL-6, but presence of IGF-β, Tregs will be produced. Tregs, as suggested by the name, will have an effect that is intended to decrease inflammation and cell killing. Tregs inhibit dendritic cells from becoming fully licensed and migrating to the lymph node. T killer cells will target specific cells and initiate cell killing [14].

1.4.3 B Cells: Production of Humoral Immunity

B cells are responsible for the production of antibody and can also act as highly efficient APCs. Like T cells, naïve B cells reside in the lymph node and express a wide variety of B cell receptors that initiate activation. Pathogens that move interstitially through the blood stream to different tissues can reach the lymph node and interaction with naïve B cells can cause B cell activation. The B cell will engulf this pathogen, presenting relevant antigen peptides on the MHC II surface antigen and then move into the germinal center of the lymph node and await activation by T cell subtypes. Activation will lead to differentiation into either a plasma cell or a memory B cell. Memory B cells will remain in the lymph node while plasma cells will migrate to either the site of inflammation or into the bone marrow. Within the site of inflammation, plasma cells will secrete antibody, but are rather short-lived. Plasma cells within the bone marrow secrete antibody into the blood stream indefinitely. The antibodies produced will enhance humoral immunity by neutralizing the pathogen and preventing them from adhering to cell types. This will also cause aggregation of the antibody target allowing the pathogen to be excreted. Antibodies also contribute to opsonization where phagocyte recognition and complement activation can occur [14].

1.5. Modeling T1D Immune Rejection of Islet Grafts

The non-obese diabetic mouse model (NOD), characterized by the spontaneous development of diabetes through insulin-producing cell destruction, is currently

considered the gold standard small animal model for T1D [29]. It is often referred to as "the 'workhorse' of the T1D preclinical 'stable' [30]." Through this model, T cell-mediated cell killing has been clearly identified as the primary effector population responsible for β-cell destruction and onset of NOD model diabetes [29, 31]. Further studies in B cell deficient NOD mice have shown that they will not spontaneously develop their diabetic state, suggesting the possibility that B cells are the primary APCs involved in diabetic onset [32-34]. It is through these similar mechanisms that transplantation of donor islets into host NOD mice will be destroyed [13]. However, the true underlying mechanisms for islet rejection in humans remains elusive, creating an obstruction in the development of models that can most accurately reflect the human pathology.

A less stringent model but still important to discuss for its widespread use is the practice of streptozotocin (STZ) injection to chemically induce insulitis, β-cell destruction, and eventually diabetes. The advantage of STZ models are that they increase the throughput of modeling hyperglycemia – there is no need to wait for diabetes to develop such as in the NOD model, and it is also cross-compatible between species – several species have been shown to achieve hyperglycemia when injected with STZ [35, 36]. However, this model might not be able to recapitulate the immune effects of the human T1D pathology most accurately and therefore reports that use it should be evaluated as such. Considering that autoimmune rejection of insulin producing cells is induced in a much more sophisticated way than chemically induced destruction, it's possible that this model can only reveal graft rejection in a more generalized sense rather than effector functions more likely responsible for the mechanisms behind T1D [29].

1.6 Biomaterial Strategies for Cell Delivery

In effort to prevent failure of cellular transplants, recent innovations in designing an exogenous interface that inhibits immune activation and cell-killing have been of major interest. Most of the reported work is subdivided into three major subcategories: bulk material systems that encapsulate the cells within a matrix to form a network of implanted cells, microencapsulation systems that coat cells either individually or in small cell numbers, and direct surface modification of cell surfaces via conjugation of

components that direct or limit immune reactions. All these approaches have a similar goal – they are intended to create a satisfactory interface between host immunocytes and guest therapeutic cells that will improve the likelihood of graft acceptance.

1.6.1 Microencapsulation Systems

Microencapsulation of cells, generally achieved via microfluidic fabrication or emulsification, is an auspicious tactic for preparing therapeutic cells for deployment that has been under investigation for nearly four decades. Encapsulation into spheroid structures have been shown to be beneficial to donor cell function through improved diffusion of available nutrients due to increased surface area in contact with host vasculature, in comparison to bulk encapsulation methods [37].

Alginate has been studied extensively for islet encapsulation to immunoisolate donor islet cells for transplantation. The first account of alginate used in the context of diabetes was in 1980 by Lim and Sun. They microencapsulated islets within alginate beads and showed maintenance in morphology and functionality of islets cultured *in vitro* for 15 weeks. *In vivo* implantation rescued diabetes in a streptozotocin (STZ)-induced rat model for approximately 3 weeks. In contrast, rats given unencapsulated islets returned to hyperglycemia after about 4 days [38]. For a fully comprehensive understanding of the history and development of alginates for cell encapsulation to treat diabetes, the reader is referred to a prior written review [39]. This section will focus specifically on immune compatibility of alginate capsules and developments thereof.

Alginate is a polysaccharide isolate from seaweed, composed of linear block co-polymers of β-D-mannuronic (M) and α-L-guluronic (G) acids, that form a gel in cationic solution. This composition (including molecular weight, G:M ratio, and cationic component) is particularly important to the material function as an encapsulant [39]. Regarding immunogenicity, there seem to be conflicting reports. It has been shown that high content of M in alginates are immunostimulating; originally it was reported that alginates composed primarily of M produced inflammatory cytokines approximately 10 times more effectively than high G counterparts [40]. More recently, this pathway was better elucidated – poly-M was shown to activate monocytes similarly to CD14 ligand,

lipopolysaccharide (LPS), and is recognized by toll-like receptors TLR2 and TLR4, causing monocyte upregulation of tumor necrosis factor (TNF) *in vitro* [41]. However, some reports state that high M content had the opposite effect. An incredibly thorough investigation into selecting the most suitable composition of alginate for cell-based therapeutics found that high M alginates were actually superior: lymphocyte and macrophage recruitment was statistically identical to high G alginates, there was no recognizable fibrosis (high G alginates showed clear evidence of fibrotic overgrowth), and they showed greater angiogenesis [42]. It's possible that such contradicting evidence in these reports might come from high variation in the alginate substrate itself. Because alginate is derived from a fully natural source, remaining impurities could be a likely cause for the described immune effects [43].

In efforts to prepare alginate derivates that better manage the foreign body response, and remove this possibility of inconsistency, Vegas *et al*. created a combinatorial library of modified alginates and tested their ability to mitigate fibrotic overgrowth based upon previously published high-throughput *in vivo* methods in mice [44]. Vegas's report shows the synthesis of nearly 800 different alginate materials via conjugation of various functional groups and compared them to a commercially available alginate SLG20. Based upon the results, three triazole functionalized alginates became the highest priority candidate materials in mouse models due to minimal fibrotic overgrowth as assessed histologically and via α-smooth muscle actin and collagen deposition by qPCR. They also showed an approximately 6-fold decrease in macrophage presence and 2-fold decrease in neutrophil presence as indicated by flow cytometry in comparison to SLG20 control. Similar fibrotic responses to these materials were also shown in non-human primate models [45]. Clearly these alginate derivatives have shown promise in these models, however their function as a carrier for islet encapsulation is still something to be explored. As discussed previously, while the material itself may mitigate fibrotic overgrowth, components of islets themselves such as production of TF may further contribute to initiation of coagulation.

Next-generation alginate systems are exploring the addition of biomolecules and pharmaceuticals to locally modulate the immune reaction to their implantation and/or

preserve islet function. In one study, a library small molecule anti-inflammatory drugs were screened for reduction in inflammation post-transplantation. They used PLGA microparticles as an initial test for inflammatory response and found curcumin and dexamethasone to be leading candidates for reduction in ROS and cathepsin as shown by fluorescent and bioluminescent imaging, respectively. Using these two candidate molecules they tested them individually with respect to in islet transplant function when fabricated into alginate microcapsules. Alginate solutions were mixed with curcumin or 1.0 mg/mL dexamethasone. The alginate solutions were then used to microencapsulate male Sprague-Dawley rat islets and were injected into the intraperitoneal space of C57B6/J mice with STZ-induced diabetes. They found that the inclusion of curcumin was more effective at decreasing fibrosis and maintaining blood glucose levels. Blood glucose was monitored in the animals over two months post-transplantation, and between day 29 to day 60, the blood glucose level of mice with curcumin capsules were statistically lower than that of the control mice. Dexamethasone-loaded alginate groups were not significant in comparison to controls. Additionally, the levels of several immune cells were assessed by qPCR and saw that there were significant reductions by curcumin loaded capsules in macrophages, cytotoxic T cells, dendritic cells, and B cells. Inflammatory cytokines TNF-α and TGF-β, and fibrosis markers collagen 1A1 and a smooth muscle actin, were also decreased by curcumin-loaded capsules in comparison to the dexamethasone-loaded and control capsules. Lastly, histological assessment of explanted samples saw decreased Hoechst staining in curcumin-loaded groups in comparison to dexamethasone-loaded and control capsules, which suggest that there was less cellular overgrowth and hence, fibrosis [46]. The results of this study certainly add to the body of literature suggesting that anti-inflammatory mechanisms could play a role in graft acceptance. It's possible as well that the kinetics of drug release might have been important to this study as the assessment of them saw dexamethasone released much more rapidly than the curcumin. The authors additionally suggest that it might be possible to conjugate dexamethasone onto the alginate itself, which may increase its persistence in maintaining graft acceptance and reducing immune rejection based upon their benchmarks.

C-X-C motif chemokine 12 ligand (CXCL12) has been shown previously to improve graft acceptance by binding C-X-C chemokine receptor type 4 (CXCR4), which is commonly expressed on lymphatic cell types. Increased local activity of the CXCL12/CXCR4 axis will repel effector T cells, responsible for transplant rejection, and encourage migration of regulatory T cells sedating local immune activity [47, 48]. Chen *et al*. incorporated CXCL12 by simply mixing it into the alginate solution at a concentration of 1 μg/mL prior to crosslinking [49]. First, they showed that caspase-3 (an apoptotic signaling protein) expression in encapsulated islets was decreased approximately 4-fold in alginates that contained 1 μg/mL CXCL12 ligand in comparison to no ligand controls. Unencapsulated islets of the same cohort of islets showed a 3-fold increase in caspase-3 in comparison to CXCL12 ligands. These results were in agreeance with prior evidence that there is a pro-survival mechanism that can be directly affiliated with CXCL12 inclusion [50]. Next, alloislets from C57BL/6 mice were encapsulated within these alginate microcapsules with the addition of CXCL12 and transplanted into the kidney capsule of STZ-induced diabetic NOD/LtJ mice (lineage mixing indicative of MHC-mismatch). Islets within capsules containing and void of CXCL12 remained functional for a mean of 136 days and 62 days, respectively. Next, they sensitized recipient mice using skin grafts to promote an immune memory response, and still saw maintenance of normoglycemia for 125 days in about 90% of mice receiving islets encapsulated in CXCL12-alginate capsules. Only about 20% of mice that received islets without CXCL12 remained euglycemic for this time period. Lastly, they explored xenotransplantation of porcine islets into the same C57BL/6 mouse model. Porcine islets encapsulated in CXCL12-alginate capsules restored normoglycemia in 60% of mice for 300 days. Hyperglycemia relapsed in all mice receiving islets without CXCL12 by about day 50 [49]. The results of these studies are indeed very striking and insinuate that localized chemotaxis of regulatory T cells might play a major role in graft survival by repelling effector cells responsible for chronic immune rejection.

Another naturally derived material used commonly for islet microencapsulation is agarose. Agarose, like alginate, is derived from seaweed, and was likely selected due to its longer history of purification for biomedical applications [51]. It is composed of a β-D-

galactopyranose polymer chain alternating with 3,6-anhydro-α-D-glactopyranose. Compared to alginates, agarose preparation into microbeads is minimally easier, but still incorporates the same principles – the major difference being that agarose will gel in aqueous solution in the absence of ionic components [52]. Luan *et al.* prepared islets encapsulated within agarose microcapsules that carried conjugated sCR1, a known complement inhibitor and saw extension in xenograft survival. Islets isolated from ACI/NSIc rats were encapsulated in agarose with or without sCR1 were injected into the peritoneal cavity of C57BL/6 mice. Mice that received 1000 IEQ within sCR1 conjugated agarose capsules remained normoglycemic for 34.1 ± 3.2 days, mice receiving the same number of islets in capsules without sCR1 exhibited normoglycemia for only 11.6 ± 3.8 days. They suggest that the sCR1 becomes denatured by proteases during inflammation, leading to limitation in long-term maintenance. However, histological evaluation of the immunocytes after explantation was not assessed making it somewhat difficult to draw conclusions on the mode of failure.

1.6.2 Bulk Materials for Cellular Transplantation

1.6.2.1 Chamber Devices

Some systems for islet transplantation make use of bulk chambers that physically isolate the therapeutic cellular components in a compatible device, while permitting the exchange of nutrients (oxygen, serum, etc.) and therapeutic outputs (insulin, glucagon, somatostatin, etc.). Because T cells can be directly activated by contact with MHCs expressed on the transplanted cell surface, seclusion of the therapeutic cells from immunocyte contact remains a promising strategy for successful graft acceptance.

The company Beta-O2 has developed the βAir device, which isolates the islet graft from direct contact with immune cell-types and pro-immune macromolecules (i.e. antibodies, complement proteins, etc.) through controlled porosity of the encapsulant and selection of an anti-fibrotic interfacial material, polytetrafluoroethylene (PTFE). The rigid, “puck-shaped” device consists of two sectors: an alginate disc to house the encapsulated islets, and a void space to permit gas exchange [53-55]. Unique to this device are accessible ports composed of polyurethane tubing for the exogenous

infusion of oxygen as a maintenance for cell loss due to hypoxia. In a preclinical model experiment with the βAir device, pig islets were isolated and casted into the device. Devices were implanted into the subcutaneous space of the lateral abdomen on both sides of two non-diabetic minipigs to create an allogeneic transplant model and supplemented daily with oxygen via port access. This 13-day study showed maintenance in the functional activity of islets, where glucose stimulation prior to implantation and after explantation were statistically identical. The explanted device showed no fibrotic development, and histologically sampled islets remained intact and maintained similar morphology [54]. Next, the device was used in a xenogeneic model. Rat islets were isolated and casted into the device, transplanted into a STZ-induced diabetic minipig, similarly to the previous study. Normoglycemia was maintained for the duration of the 30-day experiment, and rat c-peptide was present in the serum while the device was implanted. Regression to hyperglycemia and absence of rat c-peptide in minipig serum occurred immediately upon explantation of the device indicating success of the islet graft. Further, the alginate/islet samples were assessed for porcine DNA and no contamination was found. Anti-pancreatic rat antibodies were absent in the serum of the minipigs [53]. These results suggest that immune-cell infiltration during the implantation period was truncated, and elicitation of blood-mediated immune response to the cellular materials was hindered by entrapment of immune-stimulating, xenogeneic proteins.

Most recently, the device was transplanted with allogeneic islets from a deceased human donor into a single patient clinical trial. Current reports state that over the course of the 10-month study, islets retained function, but provided only modest reduction in exogenous insulin administration. However, there was no change in the islet autoantibody and donor alloantibody status compared to pre-transplantation levels, indicating that the humoral immune response was not upregulated in response to the islet graft. Lastly, they showed that isolated memory T cells remained unresponsive to glutamic acid decarboxylase 65 and to proinsulin at 5 days and at 9 months posttransplant, showing evidence of exclusion of islet proteins from immunocyte recognition [55].

While this device showed promise in preclinical trials, the underwhelming achievement of low insulin production responsiveness post-transplant was likely an effect of the bulkiness of the device and limited diffusion of therapeutic nutrients. The hampered immune response to the biomaterial permitted maintenance in viability of the encapsulated islets, but the desired outcome of insulin-independence was not achieved. It's possible that with this device, an increase in the number of encapsulated islets would permit stronger responsiveness to glucose-insulin exchanges, improving the result of the therapy. However due to the scarcity of human islets, this strategy may be unachievable. They have shown previously that the device maintains immune isolation of encapsulated cells in a xenotransplant model, perhaps exploration of this device in a clinical application of xenotransplantation will be explored in the future.

Similarly, the TheraCyte Encaptra system utilizes a PTFE membrane encapsulant with a controlled pore size for immunocyte exclusion, but free exchange of nutrients [56]. In a rigorous test of the immune isolating capacity of this device, encapsulated cells remained exclusive from immune detection, and did not stimulate any significant T cell mediated immunogenicity in comparison to a naïve control. The proposed device will encapsulate human embryonic stem cell (hESC)-derived insulin producing progenitor cells, this technology is discussed in later sections. When pancreatic progenitor cells were encapsulated within the intact device, T-cells of both indirect-specific and direct-specific alloimmune reactive populations did not proliferate. Further, when splenocytes were encapsulated within the device, increasing the number of MHC antigens encapsulated and likelihood of CD8+ T cell stimulation due to MHC mismatch, similar results were reported [57]. Together these results indicate that the device will block afferent and some efferent mechanisms of the immune system.

While macroencapsulation devices of this nature hold promise in clinical application for their clear ability to protect islets from immunocyte contact, and adaptive response priming, one significant drawback is that the sheer volume of them may lead to a restriction in implantation sites. Failure of islet grafts in the absence of well-established vasculature, and hence, poor nutrient diffusion, is a well-documented concern [3, 4, 58]. By limiting feasible implantation sites, this type of variable might limit

their success. Further, devices of this category, while able to physically isolate the encapsulated cell types from, they are admittedly incapable of protecting cells from various soluble factors that may induce apoptotic signaling and substantial graft failure. Immune effector cytokines such as IFN-γ, IL-1β or the myriad of reactive oxygen species produced during transplantation are certainly within the molecular weight range of size-inclusion to freely diffuse through the barrier.

1.6.2.2 Hydrogels

Growing attention has been given to hydrogels in the past few decades as vehicles for cell delivery. Hydrogels have very high water content by nature, and this hydrophilic character minimizes protein adsorption [59]. Hydrogels are also structurally like native tissues and extracellular matrix, making them palpable for design as a cell encapsulation and delivery material [60].

Like microencapsulation, alginates have been used as macroencapsulating hydrogels as well. Dufrane et. al developed a monolayer cellular device that supports islets on a monolayer of collagen which is then layered by high-M 3 wt.% alginate to create a “sheet” device that can be transplanted subcutaneously [61]. In a study of this device using porcine islets transplanted into the subcutaneous space of STZ-induced diabetic primates, euglycemia was restored for 6 months without immunosuppression. Nonencapsulated islets or microencapsulated islets within the same alginate composition of the hydrogel, either infused into the kidney capsules were rejected within 1 week and 2 weeks, respectively. Histological staining of CD3 (pan-T cell marker) and complement deposition, specifically C3d and C9 were present in rejected grafts, indicative of rejection by traditionally mediated immunity. Blood from the transplanted recipients was analyzed by flow cytometry and enzyme-linked immunosorbent assay during the experiments to assess the humoral immune response against xenografts. All the primates were positive for cytotoxic α-Gal, anti-porcine antibodies, prior to transplantation, and similar increases in antibody concentration profiles were observed across all groups in response to the transplant. The indication of blood-glucose maintenance over an extended period of 6 months suggests that the microencapsulation device was able to overcome what were at least the innate immune

effector functions such as antibody-mediated rejection. After the six-month time point, failure of the grafts within the hydrogel failed. These primates were reintroduced with new islet loaded hydrogels to the same subcutaneous pouch, and failure relapse occurred within 15-20 weeks. This indicates that while the hydrogel was able to protect against innate immunity, the onset of a sensitized immune system and memory response was an insurmountable challenge for this material alone [62]. In more sophisticated models of T1D, which are not chemically induced to be diabetic and are already pre-sensitized to islets [63], it's possible that a system of this nature may require more complex immune regulation.

Haque *et al*. reported the delivery of liposomal clodronate, a macrophage depletion reagent along with rat islets in a Matrigel® hydrogel into the subcutaneous space of mice. This xenogeneic transplant model saw approximately 60-day survival in approximately 80% of hosts with encapsulated islets with clodronate. Islets within Matrigel® without clodronate were all destroyed prior to day 10. Additionally, with the addition of clodronate, IL-1β and TNF-α were decreased to approximately 0.5% and 9%, respectively, in comparison to non-clodronate controls [64]. These results perhaps suggest that reduction in macrophage activation and cytokines relevant to acute inflammation can lead to increase in graft survival during the pro-inflammatory transplantation phase. This is also in agreeance with a prior report that showed similarly that depletion of macrophages improved survival porcine islets within alginate microcapsules when implanted into rats [65].

Particular attention has also been drawn toward zwitterionic surfaces to mitigate the foreign body response due to their ultra-low-fouling surface energy – they absorb astonishingly low protein content from plasma, preventing cellular adhesion. In one paper, poly(carboxybetaine methacrylate) (PCBMA) zwitterionic hydrogels composed of carboxybetaine monomer and carboxybetaine cross-linker were found to mitigate fibrin overgrowth and cellular adhesion when implanted subcutaneously in C57BL/6 mice. In comparison to a known anti-fouling material, poly(2-hydroxyethyl methacrylate) (PHEMA), that has been shown to minimize fibrotic overgrowth, PCBMA hydrogels showed a 50% reduction in collagen density on the surface of the material. They also

showed a decrease in pro-inflammatory cytokine production by macrophages and increase in anti-inflammatory macrophage markers as indicated by immunohistochemical examination [66]. Zwitterionic coatings, which are touted for their superior hydrophilicity, have also been shown in a more recent report to have similar effects on foreign body reaction [67].

1.6.2.3 Rigid Scaffolds

In contrast to hydrogels, another approach to microencapsulated islet delivery is the utilization of functional, rigid scaffolds. While these may not share similar mechanical properties to hydrogels, which are much similar to native tissue, the functional ability of either to undoubtedly be a superior therapeutic tool is still far from understood. However, similar to hydrogels, scaffolds can provide support for islets as a delivery vehicle and can be tuned to release and/or retain factors to improve graft survival and function.

Poly(lactide-co-glycolide) (PLG) has been explored in several accounts as a material for scaffold composition [68-72]. Because PLG is an approved material for medical applications, it has developed quite tremendous popularity for a diverse number of biomedical research applications [73, 74]. Hlavaty *et al*. reported PLG as a microporous scaffold capable of retaining and controllably releasing the proteins exendin-4 (Ex4) or insulin-like growth factor-1 (IGF-1) in addition to providing a vehicle for delivery of human islets. Ex4 has been shown to inhibit apoptosis of islets in several models of transplantation, and upregulate their cell cycle, encouraging them to proliferate [75-77]. IGF-1 has shown similar activity [78-80]. Scaffolds of either of these proteins were prepared by encapsulating the protein in PLG microspheres and using the microspheres to fill the center of two porous PLG outer layers. The scaffolds were then laden with human islets from donors aged 49.4 ± 12.1 years using a specially machined, customized micropipette. Scaffolds were then transplanted into the epididymal fat pad of male NOD-scid IL2Rgamma^{null} (NSG) mice rendered diabetic by STZ injection. Mice that received scaffolds containing IGF-1 were unable to restore euglycemia without external intervention, were still significantly lower than unloaded scaffold controls over 30 days. With scaffolds containing Ex4, 60% of mice achieved

euglycemia by day 30, compared to only 20% of control mice. Post-explantation analysis by histology of host tissue revealed no signs of fibrosis in either Ex4 scaffold recipients or control mice. Ki-67 staining (indicative of proliferation) revealed an approximately 4-fold increase in Ki-67 to nuclei ratio in Ex4 scaffold recipients compared to control mice, suggesting that the protein influenced islet proliferation [68].

Similar processing was also applied to the same scaffold to release transforming growth factor-beta1 (TGF-β1). TGF-β1 is a known mediator of innate immune function by suppressing diapedesis, recruitment and activation of leukocytes [81]. It has also been shown to restrain maturation and licensing of dendritic cells [82] and promote differentiation of CD4+ T cells into Tregs [83]. Islets from Balb/C mice were seeded onto scaffolds containing or not containing TGF-β1 and transplanted into diabetic C57BL/6 mice. Grafts containing TGF-β1 survived for 19 days in comparison to controls which lasted for 12 days. Several populations of cells were analyzed by flow cytometry to determine immunocyte cell number at the site of the transplant: macrophages, neutrophils, dendritic cells, monocytes, CD4+ T cells, CD8+ T cells, B cells, and natural killer cells. Numbers of macrophages, dendritic cells, and natural killer cells were reduced by 70%, 45%, and 45%, respectively, in the scaffolds delivering TGF-β1 relative to control. All other cell types assessed were statistically similar between TGF-β1 group and control [72].

1.6.3 Cell Surface Modifications

One strategy that has gained tremendous traction in manipulating the immune system for graft acceptance is coating therapeutic cell surfaces. These modifications provide an interface between guest and host, which can then be tuned to decrease immunogenicity of the foreign body. They can be made into a very thin layer on the outside of the transplant, decreasing graft volume and giving access to more transplantation sites [58].

Perhaps one of the most publicized of these methods is the use of poly(ethylene glycol) (PEG) as a cell-surface conjugate for the inhibition of immunocyte recognition, antibody binding, and blood-mediated inflammation. This surface modification is

generally achieved by preparing PEG chain with functional end-termination and chemically bonding it to free amines in the collagen matrix of isolated islets to form stable amide linkages. It was originally shown that conjugation of PEG to, or "PEGylation" of, the surface of red blood cells led to a marked reduction in antigenicity [84]. This method has been applied to islet grafts as an attempt to "camouflage" the cells from immune recognition and been shown to have nominal effects on islet function or viability *in vitro* [63]. However, only modest long-term immunoprotection of islets *in vivo* has been achieved using simple one-step PEGylation alone, leading to a variety of attempts to create more sophisticated surface modifications.

Lee *et al*. devised a strategy to create a three-step PEGylation procedure. They stated that single coatings offered only limited protection and incomplete coverage, and that cytokines induced by islets themselves mediate islet damage. They used a cationic polymer intermediate between PEGylation steps to amplify PEG content on the cellular surface and saw no adverse effects on *in vitro* viability or *in vivo* glucose responsiveness between the triply PEGylated islets versus the singly PEGylated islets. Next, they transplanted the triply PEGylated islets into the kidney capsule of STZ-induced diabetic rats in an allogeneic graft format. They reported that the rats that received singly PEGylated islets or uncoated islets returned to hyperglycemia with a median time of day 12 and 5 respectively. While some rats (42.9%, 3 of 7) that received triply PEGylated islets achieved glucose control for over 100 days without systemic immunosuppression, this was not exemplary of their entire dataset. The median time for regression to hyperglycemia in their rats that received triply PEGylated islets was 19 days with a standard deviation of 45.6 days, making it difficult to draw conclusions on the effect of the coating. However, immunohistochemical staining of recovered graft sections revealed infiltration of the singly PEGylated or unmodified islets by immunocytes, while triply PEGylated islets in all animals that remained euglycemic for 100 days remained intact [85].

Lee's study highlighted one of the potential drawbacks of surface modifications via conjugation of molecules to a cell membrane – the possibility that inadequate or insufficient coating might result in graft failure and direct immunocyte priming. However,

based upon the immense variability in their triply PEGylated islets with respect to maintenance of normoglycemia in rats, it's difficult to say whether this effect can repeatedly improve and prolong graft survival. The triply PEGylated islets that did fail to achieve long-term glucose maintenance failed within the first 19 days of transplantation, suggesting the possibility that acute immune effects might play a role in graft failure that is uncontrolled with PEGylation alone [85]. This result is consistent with previous *in vitro* findings that exposed islets, unmodified and PEGylated, to a co-culture of lymphocytes or macrophages [86]. Unmodified islets cultured with lymphocytes caused an approximately 3-fold increase in production of TNF-α and 2-fold increase in IL-2 cytokines in comparison to PEGylated islets after 1 day. At day 7 in culture, approximately twice the concentration of TNF-α and 3 times the amount of IL-2 were detected in unmodified islet cultures in comparison to PEGylated islets. However, when both types of islets were cultured with activated macrophages, both unmodified and PEGylated islet groups were destroyed within 2 days [85]. These results suggest that the PEG envelope inhibited direct MHC priming and lymphocyte but did not inhibit afferent immune destruction caused by macrophages characteristic of innate immunity.

Because of its ease of processing, some works have explored PEGylation to shorten the course and/or type of systemic immunosuppression drugs [87-89]. While this has shown promise in maintaining islet graft survival there are other methods that have employed other means of localized immune control. The conjugation of a material or cell surface with a biologically active component capable of inhibiting complement activation is one of these potential approaches.

The Iwata group of Kyoto University has shown multiple studies exemplifying promise in utilizing biomolecules such as heparin, sCR1 [90] and urokinase [91] to inhibit localized blood-mediated responses when used in conjunction with PEGylation of the islet surface. In one study where they combined heparin and sCR1 surface conjugation via layer-by-layer assembly onto the islet surface – PEG-maleimide was conjugated to the surface of C57BL6/C islets and thiolated sCR1 and heparin were added to the islet surface in alternating solutions. Next the islets were administered into the hepatic portal vein of the liver in STZ-treated C57BL6/C mice. Only 2 of 9 of the

mice that received uncoated islets demonstrated normoglycemia over the 50-day period, while all the mice that received coated islets demonstrated normoglycemia.

They also looked at insulin leakage in the post-transplant period. Destruction of islets, especially due to IBMIR-related action, will lead to a spike in blood-insulin content. Non-diabetic mice had a blood-insulin concentration of about 0.99 ng/mL, mice that received uncoated and coated islets had blood insulin concentrations of about 7.03 ng/mL and 3.6 ng/mL, respectively. They also reported severe fibrin deposition of most non-treated islets, indicating strong activation of coagulation once they encountered blood. On the contrary, little, if any, fibrin was deposited on the surface of the coated islets indicating that the heparin acted as a localized anti-coagulant [90].

Factor H, a highly abundant plasma protein, is a known regulator and inhibitor of complement activation by acting as a competitive substrate for activated C3 (C3b) binding therefore causing deactivation. By deactivating C3b, an essential molecule in complement activation, the amplification of the complement cascade can be effectively down-regulated, improving engraftment of the biomaterial and maintenance in viability of therapeutic cells [92, 93]. Therefore, it's possible that by binding Factor H to the surface of cells or biomaterials, the complement cascade can be mitigated. Wu *et al.* have developed a peptide that, in theory could be easily conjugated to the surface of these biomaterials or extracellular matrix of cells. They suggest that inclusion of this peptide on a surface could mitigate the effects of complement by promoting localized Factor H binding [94]. While this has not been tested with islets, biomaterials and cells alike could benefit from this type of surface modification.

1.7 Cell-based Immune-Modulation

One potential route to grant islet cells "immune privilege" upon implantation is to co-encapsulate them with cells that modulate immunocytes leading to reduction in inflammation and lymphocyte-mediated cell killing. Perhaps the most promising cell type that has been studied in this context are Sertoli cells of the testis. Sertoli cells have been shown in several accounts to create an "immune-privileged" environment via the secretion of immune modulating paracrine factors and the formation of a barrier against

lymphocyte infiltration [63, 95, 96]. Multiple reports have shown improvement in islet graft survival when they are co-transplanted with Sertoli cells [97, 98]. In a recent publication, islet-Sertoli cell co-aggregates were prepared. First, 3,000 Sertoli cells and single islets from BALB/c mice were cultured for 4 days using suspension under a hanging drop. The co-aggregates or unmodified islets were then transplanted into the hepatic portal vein of the liver in STZ-diabetic C57BL/6 mice. Mice receiving unmodified islets failed to achieve normoglycemia after 10 days post-transplantation, while mice receiving co-aggregates maintained normoglycemia for about 120 days. Therefore, protection of the islets by Sertoli cell inclusion was observed using this coaggregation method [99]. While the mechanism behind Sertoli cells contributing to islet graft acceptance remain unclear, it is speculated that one of the primary mechanisms is the high expression of Fas ligand. The Fas-Fas Ligand axis is responsible for induction of apoptosis of T lymphocytes, which may therefore contribute to long-term graft survival [100]. It should be noted that it has also been shown that conjugation of Fas-ligand to the islet surface showed remarkable improvement in graft survival in mouse models [101], signifying a potentially promising route to localized graft acceptance. While most of their work is unpublished, the Cell Pouch^{TM} system by Sernova Corp. utilizes Sertoli cells for immune modulation and encapsulation of allogeneic islets. The device is currently undergoing Phase II clinical trials [102].

1.8 Conclusions and Future Outlook

Modulation of the immune system, whether by localized material control other means is of utmost concern for the successful transplantation of islets to treat T1D. However, it should be noted that this cannot be considered the one and only focus hindering the success of making cellular transplantation feasible for all patients with T1D. Other considerations must be taken to ensure that function of the graft is not decreased or jeopardized due to immune isolation such as restriction of nutrients or on-demand hormone transaction, and material design parameters should consider these with similar importance.

One potential circumstance that would be enormously impactful to reaching a curative route for cellular transplantation is the use of cell sources other than human

donor islets. There is a clear shortage of human donor pancreata, and islets isolated from these donor populations are typically highly variable, leading to complications with consistency in the clinic [103]. It has been suggested that genetic manipulation of xenogeneic sources such as genetically engineered pigs might be a potential route toward achieving what is a much larger source for donor islets. However, as mentioned previously and throughout several reviews, the immunogenicity of xenografts is far from being adequately controlled for acceptance [104]. Another alternative cell source that is being explored is the use of pluripotent stem cells that can be differentiated to produce insulin [105-110]. It's certainly conceivable that the possibility of employing autologous stem cells to prepare insulin producing cells might mitigate several of the obstacles of cellular transplantation related to adaptive immunity.

1.9 References

1. McCall, M and Shapiro, A. *Update on Islet Transplantation*. Cold Spring Harb Perspect Med, vol. 2, no. 7, p. a007823, Jul. 2012
2. Belle, T and von Herrath, M. *Immunosuppression in islet transplantation* J Clin Invest, vol. 118, no. 5, pp. 1625–1628, May 2008, doi: 10.1172/JCI35639.
3. Desai, T. and L.D. Shea, *Advances in islet encapsulation technologies.* Nat Rev Drug Discov, 2016.
4. Gibly, R.F., et al., *Advancing islet transplantation: from engraftment to the immune response.* Diabetologia, 2011. 54(10): p. 2494-2505.
5. Shapiro, A. M. J. et al*. Islet Transplantation in Seven Patients with Type 1 Diabetes Mellitus Using a Glucocorticoid-Free Immunosuppressive Regimen.* New England Journal of Medicine 343, 230–238. 2000.
6. Robertson, R. P. *Islet Transplantation a Decade Later and Strategies for Filling a Half-Full Glass.* Diabetes 59, 1285–1291. 2010.
7. Barton, F.B., et al., *Improvement in outcomes of clinical islet transplantation: 1999-2010.* Diabetes Care, 2012. 35(7): p. 1436-45.
8. Fotino, N., C. Fotino, and A. Pileggi, *Re-engineering islet cell transplantation.* Pharmacol Res, 2015. 98: p. 76-85.
9. Orive, G., et al., *Cell encapsulation: technical and clinical advances.* Trends Pharmacol Sci, 2015. 36(8): p. 537-46.
10. Linn, T., et al., *Ischaemia is linked to inflammation and induction of angiogenesis in pancreatic islets.* Clinical & Experimental Immunology, 2006. 144(2): p. 179-187.
11. Tang, L., Jennings, T. A. & Eaton, J. W*. Mast cells mediate acute inflammatory responses to implanted biomaterials.* Proc Natl Acad Sci U S A 95, 8841–8846. 1998*.*

12. Bennet, W. et al*. Incompatibility between human blood and isolated islets of Langerhans: a finding with implications for clinical intraportal islet transplantation?* Diabetes 48, 1907–1914. 1999.
13. Huang, X., et al., *Resolving the conundrum of islet transplantation by linking metabolic dysregulation, inflammation, and immune regulation.* Endocr Rev, 2008. 29(5): p. 603-30.
14. Murphy, K., *Janeway's Immunobiology*. Vol. 8. 2012, New York, NY: Garland Science.
15. Montgomery, R.A. and A.A. Zachary, *Transplanting patients with a positive donor-specific crossmatch: a single center's perspective.* Pediatr Transplant, 2004. 8(6): p. 535-42.
16. Burns, J.M., et al., *Alloantibody levels and acute humoral rejection early after positive crossmatch kidney transplantation.* Am J Transplant, 2008. 8(12): p. 2684-94.
17. Vo, A. A. *et al. Rituximab and intravenous immune globulin for desensitization during renal transplantation.* N Engl J Med 359, 242–251. 2008.
18. Stegall, M.D., et al., *Terminal complement inhibition decreases antibody-mediated rejection in sensitized renal transplant recipients.* Am J Transplant, 2011. 11(11): p. 2405-13.
19. Pierson, R.N., 3rd, *Antibody-mediated xenograft injury: mechanisms and protective strategies.* Transpl Immunol, 2009. 21(2): p. 65-9.
20. Sacks, S.H. and W. Zhou, *The role of complement in the early immune response to transplantation.* Nat Rev Immunol, 2012. 12(6): p. 431-42.
21. Hawthorne, W.J., et al., *Control of IBMIR in neonatal porcine islet xenotransplantation in baboons.* Am J Transplant, 2014. 14(6): p. 1300-9.
22. Piemonti, L., et al., *Human Pancreatic Islets Produce and Secrete MCP-1/CCL2: Relevance in Human Islet Transplantation.* Diabetes, 2002. 51(1): p. 55-65.
23. Moberg, L., et al., *Production of tissue factor by pancreatic islet cells as a trigger of detrimental thrombotic reactions in clinical islet transplantation.* The Lancet. 360(9350): p. 2039-2045.
24. Barshes, N.R., et al., *Achievement of insulin independence via pancreatic islet transplantation using a remote isolation center: a first-year review.* Transplantation Proceedings, 2004. 36(4): p. 1127-1129.
25. Naziruddin, B., et al., *Evidence for instant blood-mediated inflammatory reaction in clinical autologous islet transplantation.* Am J Transplant, 2014. 14(2): p. 428-37.
26. Anderson, J.M., A. Rodriguez, and D.T. Chang, *Foreign body reaction to biomaterials.* Semin Immunol, 2008. 20(2): p. 86-100.
27. Yang, Z., et al., *Inflammatory Blockade Improves Human Pancreatic Islet Function and Viability.* American Journal of Transplantation, 2005. 5(3): p. 475-483.
28. Rabinovitch, A. and W.L. Suarez-Pinzon, *Cytokines and Their Roles in Pancreatic Islet β-Cell Destruction and Insulin-Dependent Diabetes Mellitus.* Biochemical Pharmacology, 1998. 55(8): p. 1139-1149.
29. Atkinson, M.A. and E.H. Leiter, *The NOD mouse model of type 1 diabetes: As good as it gets?* Nat Med, 1999. 5(6): p. 601-604.

30. von Herrath, M. & Nepom, G. T. *Animal models of human type 1 diabetes. Nat Immunol* 10, 129–132. 2009.
31. Bach, J.F. and D. Mathis, *The NOD mouse.* Res Immunol, 1997. 148(5): p. 285-6.
32. Greeley, S.A.W., et al., *Impaired Activation of Islet-Reactive CD4 T Cells in Pancreatic Lymph Nodes of B Cell-Deficient Nonobese Diabetic Mice.* The Journal of Immunology, 2001. 167(8): p. 4351-4357.
33. Wong, F. S. et al*. Investigation of the Role of B-Cells in Type 1 Diabetes in the NOD Mouse*. Diabetes 53, 2581–2587. 2004.
34. Noorchashm, H., et al., *B-cells are required for the initiation of insulitis and sialitis in nonobese diabetic mice.* Diabetes, 1997. 46(6): p. 941-6.
35. Thomas, J. M. et al*. Successful reversal of streptozotocin-induced diabetes with stable allogeneic islet function in a preclinical model of type 1 diabetes.* Diabetes 50, 1227–1236. 2001.
36. Furman, B. L. *Streptozotocin-Induced Diabetic Models in Mice and Rats*. Curr Protoc Pharmacol 70, 5.47.1-5.47.20. 2015.
37. Espona-Noguera, A. et al. *Review of Advanced Hydrogel-Based Cell Encapsulation Systems for Insulin Delivery in Type 1 Diabetes Mellitus*. Pharmaceutics 11, 597. 2019.
38. Lim, F. and A.M. Sun, *Microencapsulated Islets as Bioartificial Endocrine Pancreas.* Science, 1980. 210(4472): p. 908-910.
39. de Vos, P., et al., *Alginate-based microcapsules for immunoisolation of pancreatic islets.* Biomaterials, 2006. 27(32): p. 5603-17.
40. Otterlei, M., et al., *Induction of Cytokine Production from Human Monocytes Stimulated with Alginate.* Journal of Immunotherapy, 1991(4).
41. Flo, T.H., et al., *Involvement of toll-like receptor (TLR) 2 and TLR4 in cell activation by mannuronic acid polymers.* J Biol Chem, 2002. 277(38): p. 35489-95.
42. Sophie Ve´riter, et al., *In Vivo Selection of Biocompatible Alginates for Islet Encapsulation and Subcutaneous Transplantation.*
43. Lee, K.Y. and D.J. Mooney, *Alginate: properties and biomedical applications.* Prog Polym Sci, 2012. 37(1): p. 106-126.
44. Bratlie, K.M., et al., *Rapid biocompatibility analysis of materials via in vivo fluorescence imaging of mouse models.* PLoS One, 2010. 5(4): p. e10032.
45. Vegas, A.J., et al., *Combinatorial hydrogel library enables identification of materials that mitigate the foreign body response in primates.* Nat Biotechnol, 2016. 34(3): p. 345-52.
46. Dang, T.T., et al., *Enhanced function of immuno-isolated islets in diabetes therapy by co-encapsulation with an anti-inflammatory drug.* Biomaterials, 2013. 34(23): p. 5792-801.
47. Righi, E., et al., *CXCL12/CXCR4 Blockade Induces Multimodal Antitumor Effects That Prolong Survival in an Immunocompetent Mouse Model of Ovarian Cancer.* Cancer Research, 2011. 71(16): p. 5522-5534.
48. McCandless, E.E., et al., *CXCL12 Limits Inflammation by Localizing Mononuclear Infiltrates to the Perivascular Space during Experimental*

Autoimmune Encephalomyelitis. The Journal of Immunology, 2006. 177(11): p. 8053-8064.
49. Chen, T., et al., *Alginate encapsulant incorporating CXCL12 supports long-term allo- and xenoislet transplantation without systemic immune suppression.* Am J Transplant, 2015. 15(3): p. 618-27.
50. Liu, Z. and J.F. Habener, *Stromal cell-derived factor-1 promotes survival of pancreatic beta cells by the stabilisation of beta-catenin and activation of transcription factor 7-like 2 (TCF7L2).* Diabetologia, 2009. 52(8): p. 1589-1598.
51. Iwata, H. et al. *Agarose for a bioartificial pancreas*. Journal of Biomedical Materials Research 26, 967–977. 1992.
52. Gin, H., et al., *Agarose encapsulation of islets of Langerhans: reduced toxicity in vitro.* J Microencapsul, 1987. 4(3): p. 239-42.
53. Neufeld, T., et al., *The efficacy of an immunoisolating membrane system for islet xenotransplantation in minipigs.* PLoS One, 2013. 8(8): p. e70150.
54. Ludwig, B., et al., *A novel device for islet transplantation providing immune protection and oxygen supply.* Horm Metab Res, 2010. 42(13): p. 918-22.
55. Ludwig, B., et al., *Transplantation of human islets without immunosuppression.* Proc Natl Acad Sci U S A, 2013. 110(47): p. 19054-8.
56. E. Rafael, A.W., P. Arner, A. Tibell,, *In vivo Studies on Insulin Permeability of an Immunoisolation Device Intended for Islet Transplantation Using the Microdialysis Technique.* 1999.
57. Faleo, G., et al., *Assessment of Immune Isolation of Allogeneic Mouse Pancreatic Progenitor Cells by a Macroencapsulation Device.* Transplantation, 2016. 100(6): p. 1211-8.
58. Wilson, J.T. and E.L. Chaikof, *Challenges and emerging technologies in the immunoisolation of cells and tissues.* Adv Drug Deliv Rev, 2008. 60(2): p. 124-45.
59. Song, S. and S. Roy, *Progress and challenges in macroencapsulation approaches for type 1 diabetes (T1D) treatment: Cells, biomaterials, and devices.* Biotechnol Bioeng, 2016. 113(7): p. 1381-402.
60. Schmidt, J.J., J. Rowley, and H.J. Kong, *Hydrogels used for cell-based drug delivery.* J Biomed Mater Res A, 2008. 87(4): p. 1113-22.
61. Dufrane, D., Gianello, P. & Melvik, J*. Alginate coated, collagen matrix cellular device, preparative methods, and uses thereof.* 2008*.*
62. Dufrane, D., R.M. Goebbels, and P. Gianello, *Alginate macroencapsulation of pig islets allows correction of streptozotocin-induced diabetes in primates up to 6 months without immunosuppression.* Transplantation, 2010. 90(10): p. 1054-62.
63. Vergani, A. et al. *A Novel Clinically Relevant Strategy to Abrogate Autoimmunity and Regulate Alloimmunity in NOD Mice*. Diabetes 59, 2253–2264. 2010.
64. Haque, M.R., et al., *Local co-delivery of pancreatic islets and liposomal clodronate using injectable hydrogel to prevent acute immune reactions in a type 1 diabetes.* Pharm Res, 2014. 31(9): p. 2453-62.
65. Omer, A. et al. *Macrophage depletion improves survival of porcine neonatal pancreatic cell clusters contained in alginate macrocapsules transplanted into rats*. Xenotransplantation 10, 240–251. 2003.
66. Zhang, L., et al., *Zwitterionic hydrogels implanted in mice resist the foreign-body reaction.* Nat Biotechnol, 2013. 31(6): p. 553-6.

67. Yesilyurt, V., et al., *A Facile and Versatile Method to Endow Biomaterial Devices with Zwitterionic Surface Coatings.* Adv Healthc Mater, 2017. 6(4).
68. Hlavaty, K.A., et al., *Enhancing human islet transplantation by localized release of trophic factors from PLG scaffolds.* Am J Transplant, 2014. 14(7): p. 1523-32.
69. Gibly, R.F., et al., *Extrahepatic islet transplantation with microporous polymer scaffolds in syngeneic mouse and allogeneic porcine models.* Biomaterials, 2011. 32(36): p. 9677-84.
70. Kheradmand, T., et al., *Permanent protection of PLG scaffold transplanted allogeneic islet grafts in diabetic mice treated with ECDI-fixed donor splenocyte infusions.* Biomaterials, 2011. 32(20): p. 4517-24.
71. Graham, J.G., et al., *PLG scaffold delivered antigen-specific regulatory T cells induce systemic tolerance in autoimmune diabetes.* Tissue Eng Part A, 2013. 19(11-12): p. 1465-75.
72. Liu, J.M., et al., *Transforming growth factor-beta 1 delivery from microporous scaffolds decreases inflammation post-implant and enhances function of transplanted islets.* Biomaterials, 2016. 80: p. 11-9.
73. Lü, J.-M., et al., *Current advances in research and clinical applications of PLGA-based nanotechnology.* Expert Review of Molecular Diagnostics, 2009. 9(4): p. 325-341.
74. Danhier, F., et al., *PLGA-based nanoparticles: An overview of biomedical applications.* Journal of Controlled Release, 2012. 161(2): p. 505-522.
75. Goke, R., et al., *Exendin-4 is a high potency agonist and truncated exendin-(9-39)-amide an antagonist at the glucagon-like peptide 1-(7-36)-amide receptor of insulin-secreting beta-cells.* J Biol Chem, 1993. 268(26): p. 19650-5.
76. Sharma, A., et al., *Exendin-4 treatment improves metabolic control after rat islet transplantation to athymic mice with streptozotocin-induced diabetes.* Diabetologia, 2006. 49(6): p. 1247-53.
77. Cechin, S.R., et al., *Anti-inflammatory properties of exenatide in human pancreatic islets.* Cell Transplant, 2012. 21(4): p. 633-48.
78. Giannoukakis, N., et al., *Prevention of beta cell dysfunction and apoptosis activation in human islets by adenoviral gene transfer of the insulin-like growth factor I.* Gene Ther, 2000. 7(23): p. 2015-22.
79. Mabley, J.G., et al., *Insulin-like growth factor I reverses interleukin-1beta inhibition of insulin secretion, induction of nitric oxide synthase and cytokine-mediated apoptosis in rat islets of Langerhans.* FEBS Lett, 1997. 417(2): p. 235-8.
80. Agudo, J., et al., *IGF-I mediates regeneration of endocrine pancreas by increasing beta cell replication through cell cycle protein modulation in mice.* Diabetologia, 2008. 51(10): p. 1862-72.
81. Yang, L., Y. Pang, and H.L. Moses, *TGF-beta and immune cells: an important regulatory axis in the tumor microenvironment and progression.* Trends Immunol, 2010. 31(6): p. 220-7.
82. Bonham, C.A., et al., *TGF-β1 pretreatment impairs the allostimulatory function of human bone marrow-derived antigen-presenting cells for both naive and primed T cells.* Transplant Immunology, 1996. 4(3): p. 186-191.

83. Fu, S., et al., *TGF-β Induces Foxp3 + T-Regulatory Cells from CD4 + CD25 − Precursors.* American Journal of Transplantation, 2004. 4(10): p. 1614-1627.
84. Scott, M. D., et. al. *Chemical camouflage of antigenic determinants: Stealth erythrocytes*. PNAS 94, 7566–7571. 1997.
85. Lee, D.Y., et al., *Highly poly(ethylene) glycolylated islets improve long-term islet allograft survival without immunosuppressive medication.* Tissue Eng, 2007. 13(8): p. 2133-41.
86. Jang, J.Y., et al., *Immune reactions of lymphocytes and macrophages against PEG-grafted pancreatic islets.* Biomaterials, 2004. 25(17): p. 3663-9.
87. Lee, D.Y., et al., *Minimization of immunosuppressive therapy after islet transplantation: combined action of heme oxygenase-1 and PEGylation to islet.* Am J Transplant, 2006. 6(8): p. 1820-8.
88. Lee, D.Y., et al., *A combination therapy of PEGylation and immunosuppressive agent for successful islet transplantation.* J Control Release, 2006. 110(2): p. 290-5.
89. Giraldo, J.A., et al., *The impact of cell surface PEGylation and short-course immunotherapy on islet graft survival in an allogeneic murine model.* Acta Biomater, 2017. 49: p. 272-283.
90. Luan, N.M. and H. Iwata, *Inhibition of instant blood-mediated inflammatory responses by co-immobilization of sCR1 and heparin on islets.* Biomaterials, 2013. 34(21): p. 5019-24.
91. Teramura, Y. and H. Iwata, *Improvement of Graft Survival by Surface Modification With Poly(ethylene glycol)-Lipid and Urokinase in Intraportal Islet Transplantation.* Transplantation, 2011. 91(3): p. 271-278.
92. Nilsson, P.H., et al., *Autoregulation of thromboinflammation on biomaterial surfaces by a multicomponent therapeutic coating.* Biomaterials, 2013. 34(4): p. 985-94.
93. Tu, Z., et al., *Mesenchymal stem cells inhibit complement activation by secreting factor H.* Stem Cells Dev, 2010. 19(11): p. 1803-9.
94. Wu, Y.Q., et al., *Protection of nonself surfaces from complement attack by factor H-binding peptides: implications for therapeutic medicine.* J Immunol, 2011. 186(7): p. 4269-77.
95. Naito, M. et. al. *Patterns of infiltration of lymphocytes into the testis under normal and pathological conditions in mice*. Am J Reprod Immunol 59, 55–61. 2008.
96. Griffith, T. S., et. al. *Fas Ligand-Induced Apoptosis as a Mechanism of Immune Privilege.* Science 270, 1189–1192. 1995.
97. Suarez-Pinzon, W. et al. *Testicular sertoli cells protect islet beta-cells from autoimmune destruction in NOD mice by a transforming growth factor-beta1-dependent mechanism*. Diabetes 49, 1810–1818. 2000.
98. Selawry, H. P. et. al. *Sertoli cell-enriched fractions in successful islet cell transplantation. Cell Transplant.* 2, 123–129. 1993.
99. Takemoto, N., et al., *Transplantation of co-aggregates of Sertoli cells and islet cells into liver without immunosuppression.* Transplantation, 2014. 97(3): p. 287-93.
100. Dhein, J., et al., *Autocrine T-cell suicide mediated by APO-1/(Fas/CD95).* Nature, 1995. 373(6513): p. 438-441.

101. Yolcu, E.S., et al., *Pancreatic islets engineered with SA-FasL protein establish robust localized tolerance by inducing regulatory T cells in mice.* J Immunol, 2011. 187(11): p. 5901-9.
102. Sernova. *Corporate Investor Deck Q3*. [Powerpoint Slides]. 2021.
103. Chhabra, P., D.E.R. Sutherland, and K.L. Brayman, *Overcoming barriers in clinical islet transplantation: Current limitations and future prospects.* Current Problems in Surgery. 51(2): p. 49-86.
104. Zhu, H., et al., *Pig-Islet Xenotransplantation: Recent Progress and Current Perspectives.* Frontiers in Surgery, 2014. 1(7).
105. Kroon, E., et al., *Pancreatic endoderm derived from human embryonic stem cells generates glucose-responsive insulin-secreting cells in vivo.* Nat Biotechnol, 2008. 26(4): p. 443-52.
106. Baetge, E.E., *Production of beta-cells from human embryonic stem cells.* Diabetes Obes Metab, 2008. 10 Suppl 4: p. 186-94.
107. Kelly, O.G., et al., *Cell-surface markers for the isolation of pancreatic cell types derived from human embryonic stem cells.* Nat Biotechnol, 2011. 29(8): p. 750-6.
108. McCall, M.D., et al., *Are stem cells a cure for diabetes?* Clin Sci (Lond), 2009. 118(2): p. 87-97.
109. Schulz, T.C., et al., *A scalable system for production of functional pancreatic progenitors from human embryonic stem cells.* PLoS One, 2012. 7(5): p. e37004.
110. Pagliuca, F.W., et al., *Generation of functional human pancreatic beta cells in vitro.* Cell, 2014. 159(2): p. 428-39.

CHAPTER 2

SPECIFIC AIMS

2.1 Background

Hydrogels are a distinct class of hydrophilic polymeric materials defined by the formation of a physical/covalent, three-dimensional mesh and high retention of aqueous solutions. They're of particular interest for biomedical applications because their intrinsic properties mimic those of native, soft tissues. This unique architecture along with their tunable degradation has inspired their use as a persistent repository for drug- and/or cell-based therapeutics. The central purpose of this work was to develop hydrogel systems for cell- and drug-delivery. The first aim looked to establish a previously prepared hydrogel system as a cell-encapsulating material with antioxidant capabilities. The subsequent aims looked to generate a novel, shear-thinning hydrogel and test its performance *in vitro* and *in vivo*.

2.2 Aim 1: Develop a ROS-protective hydrogel for cell delivery

A ROS-scavenging ABC triblock polymer, poly[(propylene sulfide)-block-(N,N-dimethyl acrylamide)-block-(N-isopropylacrylamide)] (PPS_{135}-b-$PDMA_{152}$-b-$PNIPAAM_{225}$, PDN) that self-assembles into a hydrogel by thermal gelation was previously prepared in our lab and shown to protect 3t3 fibroblasts from cytotoxic levels of H_2O_2 in 2D culture. However, translation of this platform to a clinically relevant material for cell delivery requires maintenance of this feature in 3D culture. Therefore, in this aim, we looked to demonstrate maintenance in viability following cell-encapsulation.

2.2.1 *Aim 1A: Characterize incorporation of a structural protein into PDN hydrogel*

We recognized that PDN hydrogels lack intrinsic cellular adhesion motifs which can contribute to loss in delivered cell viability *in situ*. Therefore, as a design consideration, we considered compositing our material with naturally derived type-1 collagen (T1C), to present adhesion sites and influence cell-survival/morphology. Characterization of this composite involved determination of homogeneity, influence on material mechanics, and assessment of changes to encapsulated-cell behavior.

Completion of this aim prepared a mechanically stable composite material consisting of a homogenously incorporated collagen structure that enables native morphology of encapsulated, adherent cells.

2.2.2 Aim 1B: Demonstrate maintenance in viability of adherent and nonadherent cell types within PDN hydrogel against ROS insult

To establish this platform as feasible for cell-delivery, we chose to optimize *in vitro* assays that demonstrated protection from ROS-challenge in multiple different cell types cultured within the hydrogel. We utilized common therapeutic cells such as human MSCs, and for proof of concept, mouse insulinoma pancreatic β-cells (MIN6) which can be easily formed into aggregates as a facile model for primary islets. An analogous, ROS-inert hydrogel was also synthesized as a control. The results of this aim showed significant improvement in the maintenance of viability of cells encapsulated with the antioxidant hydrogel in comparison to these controls.

2.3 Aim 2: Develop and characterize fully synthetic shear-thinning hydrogel for cell and drug delivery

Shear-thinning hydrogels have gained tremendous traction as a class of injectable biomaterials for tissue engineering applications. Their distinguishing property is that they undergo a pseudo-solid to liquid transition under shear force and recover as a hydrogel following alleviation of force. This supramolecular structure gains integrity through non-covalent physical bonds that are broken by mechanical disruption. In this aim, we looked to prepare a novel shear-thinning hydrogel with tunable properties via controlled, RAFT polymerization techniques.

2.3.1 Aim 2A: Prepare and characterize a shear-thinning polymer matrix

Synthesis of a shear-thinning hydrogel library began with RAFT polymerization of a hydrophilic polymer backbone composed of N,N-dimethylacrylamide (DMA) as a matrix building block copolymerized with variable percentages of primary amine post-modifiable 2-vinyl-4,4-dimethyl azlactone (VDMA). This library of polymers was post-modified with guest/host-complexing side-groups, aminated cyclodextrin (Cd) or

adamantane (Ad) on complementary macromers (DMA-co-Cd or DMA-co-Ad) and mixed to spontaneously assemble hydrogels. These hydrogels were characterized by rheometry to assess (1) strength, stiffness, and viscoelasticity, (2) stress-relaxation behavior, (3) yield strain and (4) shear-thinning/recovery. Lastly, we used cryogenic electron microscopy to preserve and visualize the nanostructure of the hydrogels, assessing homogeneity and pore size/structure. A lead candidate hydrogel was selected by a combination of optimized mechanics: greater modulus and yield strain, longest stress-relaxation time, and self-healing/shear-thinning behavior.

2.3.2 Aim 2B: Prepare and nanoparticles compatible with shear-thinning matrix

Modifying this hydrogel system to enable drug-loading capabilities was achieved by synthesis of a poly(ε-caprolactone) (PCL) block followed by analogous DMA-co-Ad copolymerization chemistry utilized in bulk matrix synthesis. Monomer feed of DMA-co-Ad was adjusted to include variable content of guest-molecule Ad and prepare a library of polymers for nanoparticle formation. Polymers were then dissolved in aqueous solution and characterized by dynamic light scattering (DLS) for detection of dispersity and size. Nanoparticles in library were then mixed into lead hydrogel matrix from prior aim and reassessed by rheometry, varying nanoparticle species (distinguished by adamantane density) and concentration. Completion of this aim showed improvement or maintenance in mechanics due to incorporation of nanoparticles surface-modified with Ad, and preparation of a nanoparticle-laden, shear-thinning hydrogel.

2.3.3 Aim 2C: Characterize function of cells encapsulated in hydrogel

Mouse MSCs derived from C57BL/6J bone marrow (mMSCs) were first transduced to express secreted embryonic alkaline phosphatase (SEAP) engineered protein. Next, mMSCs were encapsulated within hydrogels and assessed for viability after 10 days in culture and media supernatant was assayed for SEAP to demonstrate extravasation of a cell-produced protein from the hydrogel. Cell-inclusive hydrogels were then reassessed by rheometry for mechanical stability and maintenance in shear-thinning properties. Successful completion of this aim identified this hydrogel platform as a viable cell-encapsulating material *in vitro*.

2.4 Aim 3: Test in vivo performance of shear-thinning hydrogel

Logical progression to explore the feasibility of this cell-/drug-delivery platform was to test it in a pre-clinical, *in vivo* model. We chose to explore this aim in mice for their ease of handling, low cost, and established infrastructure for mouse-work within our lab.

2.4.1 Aim 3A: Evaluate host response, resorption kinetics and drug release from hydrogel substrate

Hydrogel materials containing nanoparticles with (NP(+)Ad) or without (NP(-)Ad) surface-presence of Ad and loaded with Nile Red fluorophore were injected subcutaneously into the ventral region of albino C57BL/6J mice. Fluorophore was tracked intravitally using an IVIS imaging system to show release kinetics of a model drug from the hydrogel overtime and demonstrate prolonged retention of Ad-modified nanoparticles into comparison to unmodified control. Histological examination of the hydrogels after 28 days was used to evaluate host response/-cell infiltration along with resorption of the hydrogel substrate. By concluding this sub-aim, we identified an inert material resistant to host-cell infiltration capable of persistent, localized drug-release by inclusion of NP(+)Ad.

2.4.2 Aim 3B: Characterize function of delivered cells in subcutaneous mouse model

To assess this platform for *in vivo* cell-delivery, we implanted our cell-laden materials subcutaneously in BALB/C mice, preparing an allogeneic model of cell-transplantation for delivery of systemic paracrine/trophic factors. SEAP protein was intravitally monitored in the plasma compartment for the duration of the study to assess function of the allograft as a source of protein production overtime. Successful completion of this sub-aim demonstrated a prototype for a hydrogel for use as a cell-delivery vehicle that prolongs production of a cell-secreted protein in comparison to clinically-relevant PBS-excipient control.

CHAPTER 3

REDUCING ROS AS A DESIGN CONSIDERATION FOR IMPROVING CELL-ENGRAFTMENT

Adapted From:

Dollinger, B. R., Gupta, M. K., Martin, J. R. & Duvall, C. L. *Reactive Oxygen Species Shielding Hydrogel for the Delivery of Adherent and Nonadherent Therapeutic Cell Types*. Tissue Engineering Part A 23, 1120–1131 (2017)

3.1 Abstract

Cell therapies suffer from poor survival post-transplant due to placement into hostile implant sites characterized by host immune response and innate production of high levels of reactive oxygen species (ROS). We hypothesized that cellular encapsulation within an injectable, antioxidant hydrogel would improve viability of cells exposed to high oxidative stress. To test this hypothesis, we applied a dual thermo- and ROS-responsive hydrogel comprising the ABC triblock polymer poly[(propylene sulfide)-block-(N,N-dimethyl acrylamide)-block-(N-isopropylacrylamide)] (PPS_{135}-b-$PDMA_{152}$-b-$PNIPAAM_{225}$, PDN). The PPS chemistry reacts irreversibly with ROS such as hydrogen peroxide (H_2O_2), imparting inherent antioxidant properties to the system. Here, PDN hydrogels were successfully integrated with type 1 collagen to form ROS-protective, composite hydrogels amenable to spreading and growth of adherent cell types such as mesenchymal stem cells (MSCs). It was also shown that, using a control hydrogel substituting nonreactive poly-caprolactone in place of PPS, the ROS-reactive PPS chemistry is directly responsible for PDN hydrogel cytoprotection of both MSCs and insulin-producing β-cell pseudo-islets against H_2O_2 toxicity. In sum, these results establish the potential of cytoprotective, thermogelling PDN biomaterials for injectable delivery of cell therapies.

3.2 Introduction

Cell therapies are promising for many biomedical applications such as tissue regeneration, immunomodulation, and replacement of lost cell function. [1–5] Stem cells

have the potential to comprise impactful therapies that promote myocardial, cutaneous, or orthopedic tissue repair.[6–10] In particular, it has been demonstrated that undifferentiated mesenchymal stem cells (MSCs) have immunomodulatory functions through the secretion of paracrine factors [11] that can positively direct tissue regeneration. Other diseases, such as type 1 diabetes (T1D), are characterized by loss of a specific functional cell type (β-cells that produce insulin); T1D could potentially be cured by the transplantation and long-term survival of donated pancreatic islets [12] or delivery of stem cell-derived, insulin-producing cells [13] into diabetic patients.

While cell therapies have a broad range of potential applications, survival of the delivered cells is hampered by the host's innate and acquired immune response [14,15] and minimal cellular engraftment and retention at the implantation site. [16,17] These translational difficulties and the subsequent limited success of cell delivery in the clinic has motivated the development of next generation biomaterials to improve cell-based therapies.

Polymeric hydrogels are particularly advantageous for cell encapsulation and delivery due to their hydrated state and ability to be engineered with multiple functions such as cell adhesiveness and degradability. Furthermore, injectable hydrogels that undergo in situ gelation through temperature change, [18] ultraviolet (UV) irradiation, [19] shear forces, [20] or guest-host interactions [21] offer a strategy for mixing cells with gel precursors before minimally invasive injection and gelation.

Poly(N-isopropylacrylamide) (PNIPAAM) has been studied extensively as an injectable, thermogelling material due to its distinguishing lower critical solution temperature (LCST) behavior at around 34°C, [18] allowing for thermogelation between ambient and physiological temperatures. However, hydrogels synthesized from PNIPAAM homopolymers are limited as cell delivery vehicles because they can undergo syneresis (hydrophobic expulsion of liquid as they thermoform), [18] are minimally biodegradable, and do not provide recognizable extracellular matrix cues for cellular attachment. [22]

To leverage the LCST behavior of PNIPAAM in a more cytocompatible format, we recently developed an ABC triblock polymer, poly[(propylene sulfide)-block-(N,N-

dimethyl acrylamide)-block-(N-isopropylacrylamide)] (PPS_{135}-b-$PDMA_{152}$-b-$PNIPAAM_{225}$, PDN), which forms an injectable, cell-protective hydrogel.[18] Mechanistically, the hydrophobic PPS ‘‘A’’ block triggers micelle formation in aqueous solution, the hydrophilic PDMA ‘‘B’’ block stabilizes the hydrophilic corona and prevents syneresis of the assembled gels, and the PNIPAAM ‘‘C’’ block endows thermal gelation properties at temperatures consistent with PNIPAAM homopolymer. The core-forming PPS component enables loading of hydrophobic drugs and is also sensitive to reactive oxygen species (ROS); oxidation of sulfides to sulfones and sulfoxides causes PPS to become more hydrophilic, [23] driving micellar disassembly, hydrogel degradation, and controlled release of encapsulated drugs. [24]

High, localized concentrations of ROS, or oxidative stress, are produced at sites of biomaterial implantation [25,26] and can lead to detrimental, cytotoxic effects such as irreparable DNA/protein modification and the triggering of bystander cell apoptosis [27]. As such, oxidative stress can cause failure of cellular therapies. [28] PPS-containing PDN hydrogels have been shown to minimize the toxicity of hydrogen peroxide (H_2O_2) when overlaid onto NIH 3T3 mouse fibroblasts grown in two-dimensional (2D) tissue culture plates. [18] This result motivates the current exploration of PDN hydrogels for encapsulation and delivery of more therapeutically relevant cell types such as human mesenchymal stem cells (hMSCs) and pancreatic islets in a three-dimensional (3D) format that is more relevant to in vivo cell delivery.

One of the challenges of application of PDN hydrogels for cell delivery is that they do not feature intrinsic cellular adhesion motifs that can support long-term viability of adherent cell types. Previous reports have demonstrated that natural extracellular matrix components (i.e., collagen, hyaluronic acid, fibronectin, etc.) can be homogenously incorporated into PNIPAAM-based materials to promote cell adhesion with minimal impact on overall hydrogel LCST behavior. [22] This significantly improves the cell adhesive properties of the hydrogel matrix, and produces comparable results to growth in the natural material alone.[22] In particular, type 1 collagen (T1C) is one of the most abundant structural proteins found in almost all tissue and promotes robust cellular adhesion. [29] Similar to PNIPAAM-based polymers, T1C solutions also undergo

thermoresponsive gel formation, [30] therefore making incorporation of T1C into PDN hydrogels an attractive strategy for increasing the cellular adhesion capacity of these materials. Herein, we have extended the utility and retained the injectability of PDN hydrogels by incorporating collagen into these materials to improve the adhesion, growth, and proliferation of both adherent and nonadherent cells in 3D culture. Furthermore, we explored the potential of PDN hydrogels to protect both the suspension culture of therapeutically relevant insulin-producing MIN6 pseudo-islets (PIs) and adherent hMSCs from cytotoxic levels of ROS. To our knowledge, this work represents the first successful demonstration of long-term 3D encapsulation and ROS protection of therapeutic cells within antioxidant, injectable hydrogels.

3.3 Materials

Normal cell medium (NCM) was prepared from Gibco (Grand Island, NY) 1 · Dulbecco's modified Eagle's medium (DMEM) with 4.5 g/L d-Glucose, l-Glutamine, 25 mM HEPES, and supplemented with 10% fetal bovine serum (FBS) and 1% penicillin/streptomycin (P/S). Normal MSC medium (NMM) was prepared from Gibco 1 · MEM Alpha with l-Glutamine, Ribonucleosides, and Deoxyribonucleosides (Ref. No. 12571-063), and supplemented with 15% FBS and 1% P/S. Imaging cell medium (ICM) was prepared from Gibco Fluorobrite DMEM with high d-Glucose and 3.7 g/L sodium bicarbonate, and supplemented with 10% FBS. Rat-Col, rat tail type I collagen (T1C), was purchased from Advanced Biomatrix (Carlsbad, CA). Mouse insulinoma pancreatic β-cells (MIN6) were a generous gift from the David Jacobson Laboratory at Vanderbilt University. Human bone marrow-derived hMSCs were purchased from Lonza (Walkersville, MD). Unless otherwise mentioned, all other materials were purchased from Sigma-Aldrich Corp. (St. Louis, MO).

3.4 Methods

3.4.1 Synthesis of PPS_{135}-b-$PDMA_{152}$-b-$PNIPAAM_{225}$ (PDN) triblock copolymer

The PDN triblock polymer was synthesized as previously described. [18] Briefly, hydroxyl functional poly(propylene sulfide) (PPS135-OH) was prepared via anionic ring-

opening polymerization of propylene sulfide (135 mmol, 9.99 g, 10.56 mL) using 1,8-diazabicyclo[5.4.0]undec-7-ene (DBU; 3 mmol, 0.46 g, 0.45 mL) as a base and 1-butane thiol (1 mmol, 0.122 g, 0.138 mL) as an initiator in tetrahydrofuran (THF, 10 mL) solvent at ambient temperature followed by quenching of the polymerization after 2 h with 2-iodo ethanol. The polymerization mixture was purified by three precipitations into cold methanol. The resultant PPS_{135}-OH (0.6 mmol, 6.0 g) polymer was then conjugated to the reversible addition-fragmentation chain transfer (RAFT) chain transfer agent (CTA) 4-cyano-4-(ethylsulfanyltiocarbonyl) sulfanylpentanoic acid (ECT, 2.4 mmol, 0.628 g) using Steglich esterification coupling with dicyclohexylcarbodiimide (DCC, 2.4 mmol, 0.495 g) and 4-dimethylaminopyridine (DMAP, 0.18 mmol, 0.021 g) for 24 h at room temperature to yield PPS_{135}-ECT as a RAFT macro-CTA. The obtained PPS_{135}-ECT in dichloromethane (DCM) was purified through three precipitations into cold methanol. To prepare the diblock copolymer PPS_{135}-b-$PDMA_{152}$, N,N-dimethylacrylamide (DMA, 0.445 mL, 4.5 mmol) was RAFT polymerized from the PPS macro-CTA (0.3 g, 0.03 mmol) in 1,4-dioxane at 35°C for 16 h using the radical initiator 2,2-azobis(4-methoxy-2,4-dimethylvaleronitrile) (V-70) (0.92 mg, 0.003 mmol) at a CTA:initiator molar ratio of 10:1. The polymer was purified by precipitation into a 10-fold excess of cold diethyl ether.

Finally, the diblock copolymer, PPS_{135}-b-$PDMA_{152}$ (0.015 mmol, 0.37 g), was used for RAFT polymerization of N-isopropyl acrylamide (NIPAAM, 2.7 mmol, 0.30 g) in 1,4-dioxane using V-70 (0.0015 mmol, 0.46 mg) as an initiator at 35°C for 15 h at 5:1 ratio of CTA to V-70 to yield PPS_{135}-b-$PDMA_{152}$-b-$PNIPAAM_{225}$ (PDN) triblock copolymer. The crude mixture was purified by precipitation into cold diethyl ether. The precipitated polymer was dissolved into methanol and dialyzed against water for 48 h before lyophilization to yield the final product. The PDN triblock copolymer and precursor polymers at each step of synthesis were analyzed by ^{1}H nuclear magnetic resonance (NMR, 400 MHz, CDCl3), and product molecular weight was determined using gel permeation chromatography (GPC; Agilent Technologies, Santa Clara, CA) run with a mobile phase of N,N-dimethylformamide (DMF) with 100 mM LiBr and in-line light scattering (Wyatt Technology Corporation, Santa Barbara, CA) and refractive index detectors.

3.4.2 Synthesis of PCL_{85}-b-$PDMA_{150}$-b-$PNIPAAM_{150}$ (CDN)

The synthesis of PCL_{85}-b-$PDMA_{150}$-b-$PNIPAAM_{150}$ was performed using a modified protocol from the synthesis of the PDN polymer. In the first step, hydroxyl functional PCL_{85}-OH was synthesized by the ring opening polymerization of ε-caprolactone (64 mmol, 7.23 g) using benzyl alcohol (0.8 mmol, 0.086 g) as an initiator and Sn(Oct)2 (0.04 mmol, 0.014 g, 0.014 mL) as the catalyst for 2 h at 140°C. The crude polymer was dissolved in DCM and purified through precipitation into cold diethyl ether. The resulting PCL_{85}-OH (0.6 mmol, 6 g) was conjugated with ECT (2.4 mmol, 0.63 g) at room temperature, using DCC (0.49 g, 2.4 mmol)/DMAP (0.021 g, 0.18 mmol) esterification for 24 h to obtain PCL_{85}- ECT as a RAFT macro-CTA. The crude polymer in DCM was purified by three precipitations into cold methanol. The PCL_{85}-ECT (5 g, 0.5 mmol) macro CTA was used to RAFT polymerize DMA (75 mmol, 7.425 g) using V-70 (0.025 mmol, 0.0077 g) as an initiator (5:1 ratio of macro CTA to V-70) in a 1,4-dioxane/DCM solvent mixture at 35°C for 16 h to prepare PCL_{85}-b-DMA_{150}. The resultant crude diblock copolymer solution was purified by precipitation into cold diethyl ether.

In the final step, the PCL_{85}-b-DMA_{150} (0.2 mmol, 5 g) macro-CTA was used to polymerize NIPAAM (45 mmol, 5.08 g) using V-70 (0.02 mmol, 0.0061 g) as an initiator (5:1 ratio CTA to V-70) in 1,4-dioxane solvent at 35°C for 15 h to yield PCL_{85}-b-$PDMA_{150}$-b-$PNIPAAM_{150}$ (CDN). The crude polymerization mixture was purified through precipitation into a 10-fold excess of cold diethyl ether. The vacuum-dried polymer was dissolved into methanol, dialyzed against water for 48 h, and then lyophilized. The structure and molecular weight of the lyophilized CDN triblock copolymer and precursors at each synthetic step were characterized by ^{1}H NMR and GPC, respectively.

3.4.3 Preparation and rheological characterization of polymer-collagen composites

To select the appropriate concentration of collagen to maximize growth and viability of adherent cell types within our hydrogels, we used fibroblasts as a model cell type (Fig. A.A.1). To determine the storage modulus (G′) of our materials, lyophilized PDN polymer was weighed and dissolved in either 0.9 mL of phosphate-buffered saline

(PBS) or a solution of 0.2 wt. % acid-solubilized rat tail, T1C to prepare two different polymer solutions at 3 or 5 wt. % PDN polymer. The polymers were allowed to dissolve for 48 h at 4°C, permitting polymer micellization.

For collagen-only control gels, 950 mL of 0.2 wt. % T1C was pipetted into a separate tube, and 50 mL of the included neutralization solution was added to the tube. Five hundred microliters of each solution were dispensed onto 25 mm aluminum rheological base plates and allowed to gel for 1 h in a humidified incubator at 37°C. Each plate was then transferred to a rheometer (AR 2000 · Rheometer; TA Instruments, New Castle, DE), with the solidified hydrogel being compressed between the parallel plates at a gap distance of 1000 mm. The G′ values were then measured over a frequency range of 0.1–100 rad/s at a constant strain of 1% and a constant temperature of 37°C. To demonstrate the injectability and thermogelation behavior of our PDN hydrogel+collagen composites, lyophilized PDN polymer was weighed and dissolved in 950 mL of 0.2 wt.% acid-solubilized T1C to prepare two aliquots of 3 wt. % PDN polymer solutions. The polymers were allowed to dissolve for 48 h at 4°C, permitting polymer micellization. The first polymer/collagen sample was then mixed with 50 mL of the included neutralization solution, and 500 mL of the solution was immediately dispensed onto a 25 mm aluminum rheological base plate attached to the rheometer. The solution was then compressed at 1000 mm gap distance. The dynamic viscosity was then measured over a strain rate range of 100–6000/ s (the upper machine limit) at a constant temperature of 20°C.

Next, the second polymer/collagen solution sample was similarly neutralized and dispensed onto the base plate using the same solution volume and plate gap distance. To demonstrate the injectability of the material, the sample's viscosity was measured at 20°C, 6000/s shear rate for 30 s. The shear rate was then stepped immediately down to 0.100/s, while temperature was held at 20°C for the next 30 s. Temperature was then stepped up to 37°C while shear rate was held at 0.100/s, and measurements were continued for the next 60 s.

3.4.4 Scanning electron microscopy of polymer-collagen composites

PDN or CDN polymer solutions, with and without collagen, or collagen-alone solutions were prepared as described above. One hundred microliters of each solution was dispensed into microcentrifuge tubes (Fisherbrand Polyethylene Sample Vials with Hinged Cap, Size 1A; Fisher Scientific, Hampton, NH) and placed in an incubator at 37°C for 30 min. Following gelation, the tubes were maintained at 37°C using a hot plate, and the gel samples were carefully covered with 500 mL of 37°C PBS before being incubated at 37°C overnight.

To prepare the collagen-only and PDN/CDN hydrogel+ collagen composites for scanning electron microscopy (SEM), the PBS solution covering the gels was aspirated and replaced with prewarmed 2.5% glutaraldehyde in PBS for fixation. The tubes were kept at 37°C for 3 h. The glutaraldehyde solution was removed, and the gels were successively incubated at 37°C with solutions of 50%, 60%, 70%, 80%, 90%, and 100% ethanol for 30 min each.

The materials were carefully cut out of the tubes and critical point dried against liquid CO2 for 5 h. The materials were then bisected and placed onto carbon tape on SEM posts to enable imaging of the gels' internal morphology. For the PDN-only and CDN-only hydrogels, the PBS solution covering the gel was aspirated, and the gel was flash frozen in liquid nitrogen to preserve the thermoresponsive architecture. The materials were quickly cut out of the tubes and placed onto carbon tape e on precooled SEM posts in a cooler filled with dry ice before being lyophilized. All SEM samples were gold sputter coated and imaged using a ZEISS MERLIN SEM (Carl Zeiss Microscopy, LLC, ZEISS Group, Thornwood, NY).

3.4.5 Human mesenchymal stem cell culture and protection from hydrogen peroxide-induced cell death

Bone marrow-derived hMSCs below passage 8 were seeded in a tissue culture flask at a density of ~1500 cells/cm^2 and cultured in NMM. Media were changed every 4 days until the cells reached ~90% confluence. Cells were then dissociated with 0.25% Trypsin-EDTA and used directly for hydrogel experimentation. Polymer solutions of 0.2

wt. % T1C, 3 wt. % CDN with 0.2 wt. % T1C, or 3 wt. % PDN with 0.2 wt. % T1C were prepared as described above.

Harvested hMSCs (500,000 cells/tube) were pelleted and then dispersed into 1 mL of each respective polymer solution. The cell-polymer solutions were then dispensed into six separate wells of a black-walled 96-well plate at a volume of 75 mL/ well (37,500 cells per gel sample). The plate was then incubated at 37°C, 5% CO2 for 30 min to allow gel formation. After the gels were solidified, the plate was placed on a hot plate at 37°C to ensure that the thermally responsive gels remained intact. Next, 150 mL of 37°C NMM, with or without 200 mM H_2O_2, was added on top of each gel (all treatments done in triplicate). The plate was incubated at 37°C, 5% CO_2 for 24 h.

After 24 h, each well was incubated with 200 mL of freshly prepared 0.5 mg/mL collagenase P (Roche Life Sciences, Pleasanton, CA), and the plates were placed on an orbital shaker (100 rpm) in an incubator at 37°C for 15 min. Each plate was then placed on ice for 15 min, permitting the thermoresponsive materials to de-gel. The solutions from each well were placed into 0.6 mL microcentrifuge tubes and centrifuged at 300 g for 5 min. The supernatant was then carefully aspirated from each tube, and 200 mL of CellTiter-Glo solution (CellTiter-Glo Luminescent Cell Viability Assay Kit; Promega, Madison, WI) was used to resuspend the cells. Solutions were pipetted back into the respective wells of the original plate and mixed. After 10 min, total luminescent flux of each well was read for 2 s using an IVIS imaging system (IVIS Lumina Series III, Caliper LifeSciences; Perkin Elmer, Waltham, MA).

To establish the ROS-protective capacity of the PDN hydrogel+collagen groups over longer time points, the previous experiment was repeated using MSC-laden PDN hydrogel+collagen composites seeded in three separate plates with and without 200 mM H_2O_2 in NMM. Media with and without H_2O_2 was replaced every 48 h, and viability screening was performed as described above on plates at 2-, 4-, and 6-day time points.

3.4.6 *Confocal microscopy of hydrogel-encapsulated human mesenchymal stem cells*

Cells were dissociated and suspended into the polymer solutions (0.2 wt. % T1C, 3 wt. % CDN with 0.2 wt. % T1C, or 3 wt. % PDN with 0.2 wt. % T1C) as described

above. Thirty mL of the polymer/cell solutions were then dispensed into the well of a 35 mm glass bottom plate with a 7 mm inset (35 mm dish, no. 0 coverslip, 7 mm glass diameter, uncoated; MatTek Corporation, Ashland, MA) and allowed to solidify for 30 min in an incubator at 37°C, 5% CO_2. The gelled material was overlaid with 2 mL of ICM with or without 200 mM H_2O_2. Cells were then incubated for 24, 48, or 144 h.

After incubation, cells were stained with 3 mM calcein-AM (green stain, indicating live cells) and 3 mM ethidium homodimer (red stain, indicating dead cells). Cells were imaged with a confocal scanning laser microscope (Nikon Eclipse Ti Microscope with D-Eclipse C1 laser; Nikon Instruments, Inc., Melville, NY) using a 488 nm (green) and 532 nm (red) laser line on a heated stage set to 37°C. Z-stacks of each sample were taken and averaged 4 times per frame to minimize light-scattering and background noise caused by the opacity of the materials. Maximum intensity projections were acquired, and the resulting images were processed by splitting the green and red channels from the maximum intensity projections. The red channels were thresholded, converted to binary, and then background subtracted before being overlaid above the green channel images.

3.4.7 MIN6 culture and PI generation

Mouse insulinoma pancreatic β-cells (MIN6) below passage 10 and stably transduced to express luciferase and mApple fluorescent protein were seeded into a tissue culture flask at a density of $1.5x10^4$ cells/cm^2 and cultured at 37°C, 5% CO2 for ~4 days or until confluent. Next, the cells were prepared into PI aggregates based upon previously reported methods. [31] The cells were dissociated with 0.25% trypsin for 5 min, suspended in NCM, and centrifuged at 300 g for 5 min to form a pellet. The media was aspirated, and the pelleted cells were resuspended in NCM to a density of $5x10^5$ cells/mL. Fifteen mL of the cell solution was pipetted into a T-75 flask, which was placed on an orbital shaker within an incubator at 70 rpm (to prevent adherence). After 48 h, the cells were viewed using an inverted optical microscope to confirm PI formation.

3.4.8 Protection of PIs from hydrogen peroxide-induced cell death

First, 50 mg of lyophilized PDN or CDN polymer was weighed and dissolved in 1 mL of sterile PBS (5 wt. % polymer solutions) and allowed to dissolve for 48 h at 4°C. Fully aggregated PIs (~$7.5x10^7$ MIN6 cells in about 3,000 aggregates) were pipetted into a 15 mL conical tube and centrifuged at 50 g for 1 min to form a cell pellet. The media was aspirated, and the PIs were carefully resuspended in 5 mL of NCM using a wide-orifice pipette tip, dispensed evenly into five, 2-mL microcentrifuge tubes, and centrifuged again at 50 g for 1 min. The media was aspirated and replaced with 1 mL of (1) 5 wt. % PDN, (2) 5 wt. % CDN, or (3) PBS. PIs were then carefully and homogenously resuspended into the overlaid solution using a wide-orifice pipette.

Next, each solution was dispensed into six wells per group of a black-walled 96-well plate at a volume of 75 mL/well to embed ~200 PIs per gel sample. The plate was then incubated at 37°C, 5% CO2 for 30 min to allow gel formation. After 30 min, the plate was placed on a 37°C hot plate, and each well was given 150 mL of 37°C NCM containing 0.45 mg/mL d-Luciferin monopotassium salt. After 10 min, the plate was placed on a heated stage set to 37°C in an IVIS imaging system, and total luminescent flux was read for 2 min. The plate was then transferred back to the hot plate, and the supernatant was replaced with 150 mL of prewarmed 37°C PBS. This washing step was repeated two times more to ensure removal of the d-Luciferin monopotassium salt.

Next, 150 µL was aspirated from each well and replaced with NCM with or without 100 mM H_2O_2 such that each group and treatment was performed in triplicate. The plate was then incubated at 37°C, 5% CO2 for 24 h. After 24 h of incubation, each well was washed as described above and replaced with NCM containing 0.45 mg/mL d-Luciferin monopotassium salt. Luminescence readings were taken again, the wells were rewashed, and new solutions of NCM with or without 100 mM H_2O_2 were replaced into each respective well. Solutions were replaced every 24 h, and measurements were taken three more times up until 120 h after the initiation of the experiment. Based on using vital bioluminescence as a readout, we were able to take longitudinal data on the same samples over time. To confirm the veracity of this approach, a cell number versus

bioluminescence curve was generated, validating that bioluminescence readings directly correlate to cell number for the MIN6 cells (Fig A.A.2).

3.4.9 Statistical Analysis

Data are expressed as mean ± SEM. All statistical analyses were performed by one-way analysis of variance (ANOVA), and post hoc Sidak's multiple comparisons were tested via GraphPad Prism 6 software. For all tests, $p < 0.05$ was considered statistically significant.

3.5 Results and Discussion

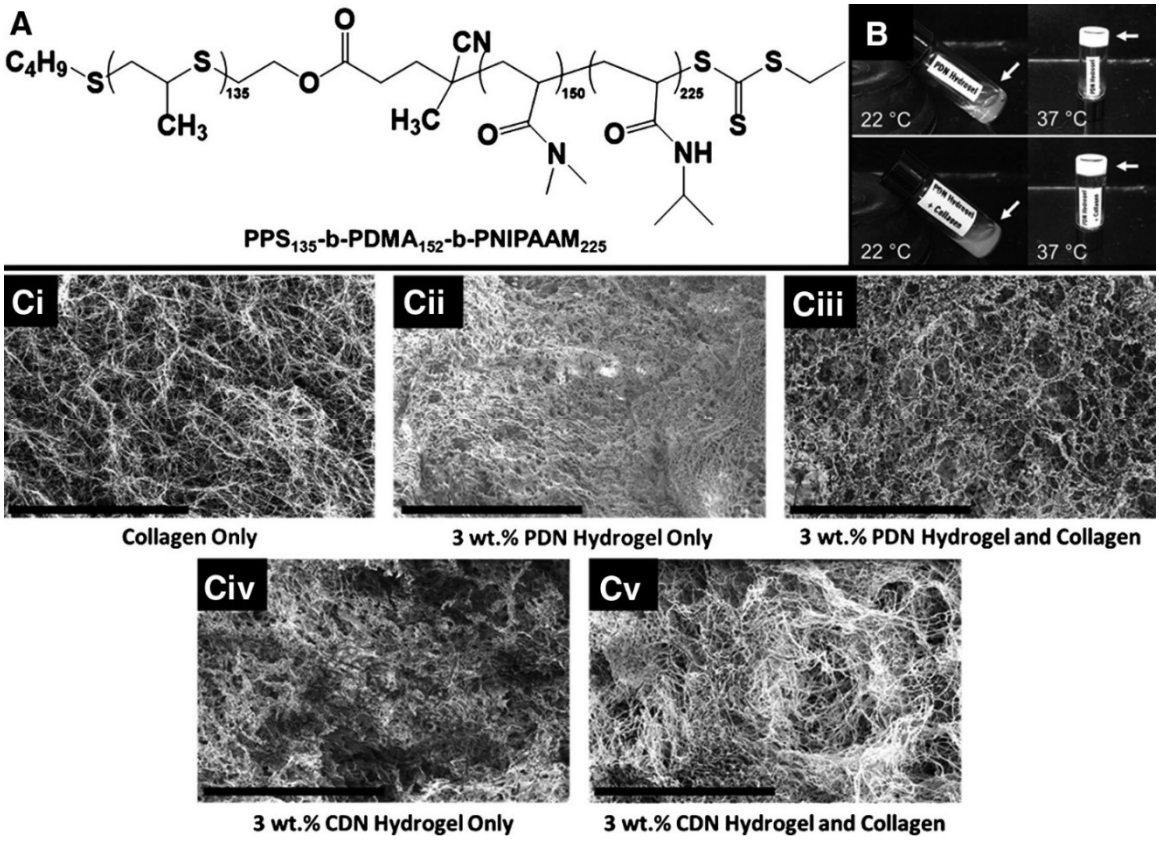

Figure 3.1 *(A) Chemical structure of PPS_{135}-b-$PDMA_{152}$-b-$PNIPAAM_{225}$, PDN hydrogel. (B) Vial inversion demonstrates thermal gelation of the hydrogel at 37°C. At 22°C, PDN hydrogel with (bottom images) or without (top images) collagen is a liquid. Both self-assemble into gels when heated. (C) The collagen network is homogeneously incorporated into the PDN and CDN polymer hydrogels, forming composite materials. Scale bar: 20 mm. (Ci) Collagen only. (Cii) 3 wt. % PDN hydrogel only. (Ciii) Collagen with 3 wt. % PDN hydrogel. (Civ) 3 wt. % CDN hydrogel. (Cv) 3 wt. % CDN hydrogel and collagen. PPS135-b-PDMA152-b-PNIPAAM225, PDN, poly[(propylene sulfide)-block-(N,N-dimethyl acrylamide)-block-(N-isopropylacrylamide)].*

3.5.1 PDN and CDN polymer synthesis and hydrogel formation

ABC triblock polymers, PPS_{135}-b-$PDMA_{152}$-b-$PNIPAAM_{225}$ (PDN, Fig. 3.1A) and PCL_{85}-b-$PDMA_{150}$-b-$PNIPAAM_{150}$ (CDN), were successfully synthesized and characterized by NMR and GPC (Figs A.A.3 and A.A.4). Polymeric solutions in water visibly gel when heated from ambient to physiologic temperature as demonstrated in Figure 3.1B. Furthermore, acid-disassociated T1C added to the PDN micelle solution can be neutralized and seamlessly incorporated into the thermogelling PDN hydrogels (Fig. 3.1B). SEM images of hydrogels made from T1C alone, PDN alone, CDN alone, or the polymers combined with T1C suggest that there is homogenous integration of the collagen network into the thermoresponsive polymers, forming uniform material composites (Fig. 3.1C).

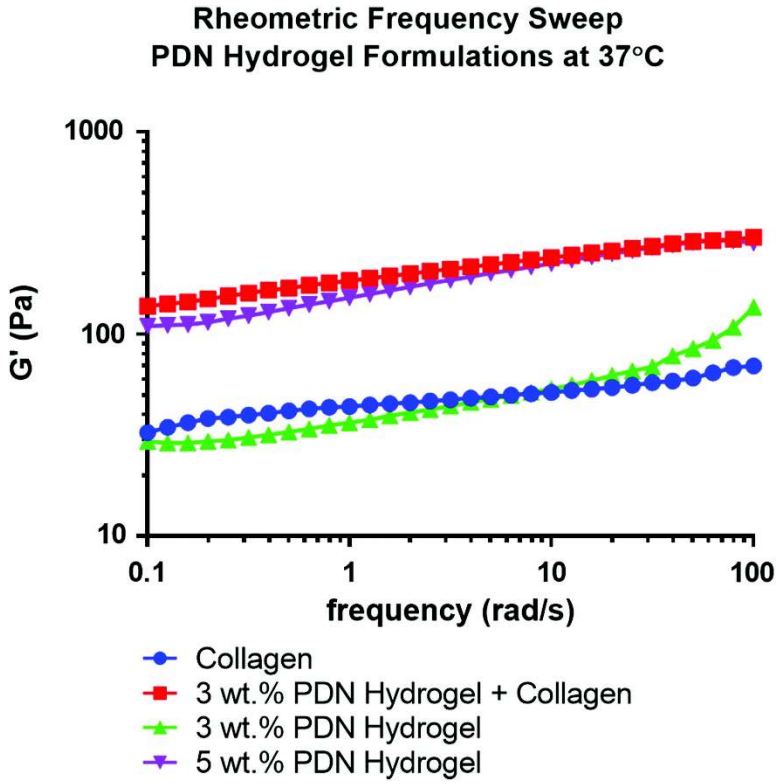

Figure 3.2 *Rheometric analysis of the PDN hydrogel at 37°C with or without collagen addition demonstrates that incorporation of the collagen into the 3 wt. % PDN hydrogel increases the storage modulus of the composite material to relative equivalence with hydrogels made solely with 5% PDN polymer.*

3.5.2 Rheometric characterization of hydrogels

To assess the mechanical properties of these materials, rheometric characterization of hydrogel storage moduli (G′) was performed across a range of frequencies at 37°C. As shown in Figure 3.2, 2 mg/mL collagen gels provided similar mechanical properties to a 3 wt.% PDN hydrogel (an average G′ value of ~50 Pa). As seen in previous work, increasing the wt.% of PDN from 2.5 to 5 increased the stiffness of the hydrogels to 100–200 Pa. Interestingly, the addition of collagen (2 mg/mL) to a 3 wt. % PDN solution significantly increased G′ values relative to collagen or PDN alone (Fig. 3.2), and the composite materials had similar mechanical characteristics to those shown in the 5 wt. % PDN-only hydrogels (G′ value of ~200 Pa).

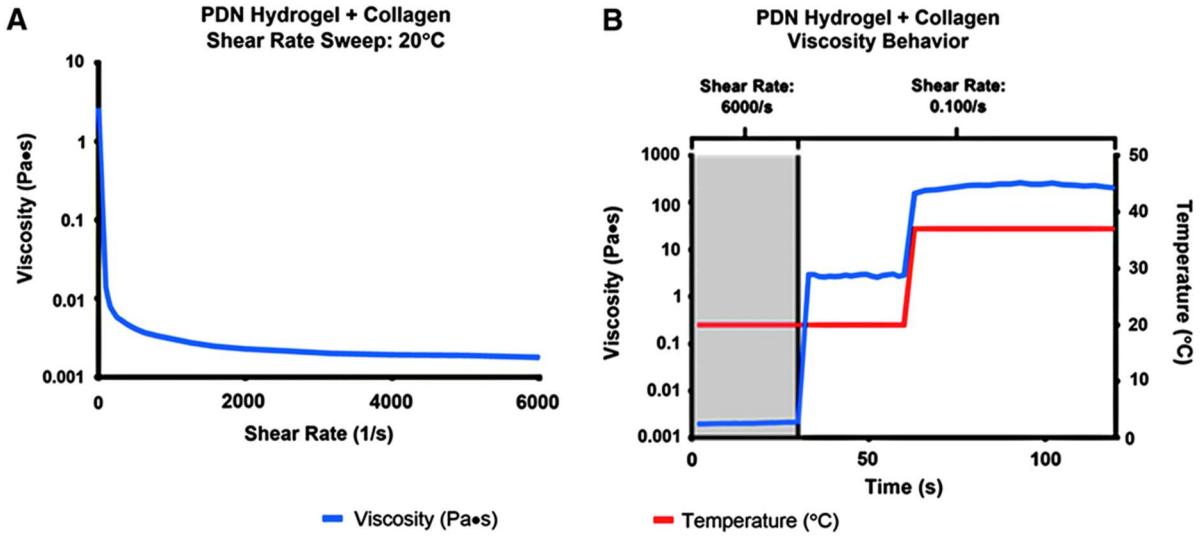

Figure 3.3 (A) The PDN hydrogel+collagen composites have shear-thinning behavior at 20°C as demonstrated by a substantial decrease in viscosity over a shear sweep from 0.100/ s to 6000/s. (B) The PDN hydrogel+collagen composite is injectable. At high shear rate (6000/s) and low temperature (20°C), the viscosity of the composite is very low, comparable to a liquid. At low shear rate (0.100/s) and low temperature, the viscosity recovers. At low shear rate and physiological temperature (37°C), the viscosity undergoes an *100-fold increase, indicative of gelation.

To assess the utility of the PDN hydrogel+collagen composite as an injectable substrate, rheometric flow tests were performed to measure dynamic viscosity as a function of shear rate and temperature. The viscosity of the PDN+collagen solution at 20°C (liquid state) is substantially decreased as the shear rate is increased from 100 to

6000/s (Fig. 3.3A). As demonstrated in Figure 3.3B, the viscosity is ~0.002 Pa x s at 20°C and a 6000/s shear rate, but at the same temperature and a lower shear rate of 0.100/s, the viscosity increases to ~2.0 Pa x s. While maintaining the shear rate at 0.100/s and increasing the temperature to 37°C the viscosity of the composite material increases to ~200 Pa x s indicating gelation.

A related study was done to confirm that the PDN materials could be utilized as an injectable vehicle for cell delivery. In this additional proof-of-concept experiment, fibroblasts were used as a model cell type (Fig A.A.5). Cells were suspended in the PDN+collagen precursor solution and injected through a 16G needle onto a plate warmed to physiologic temperature; the resultant cell-laden gels were then overlaid with media. The hydrogel encapsulated cells remained viable and exclusively associated with the hydrogel material after 24 h.

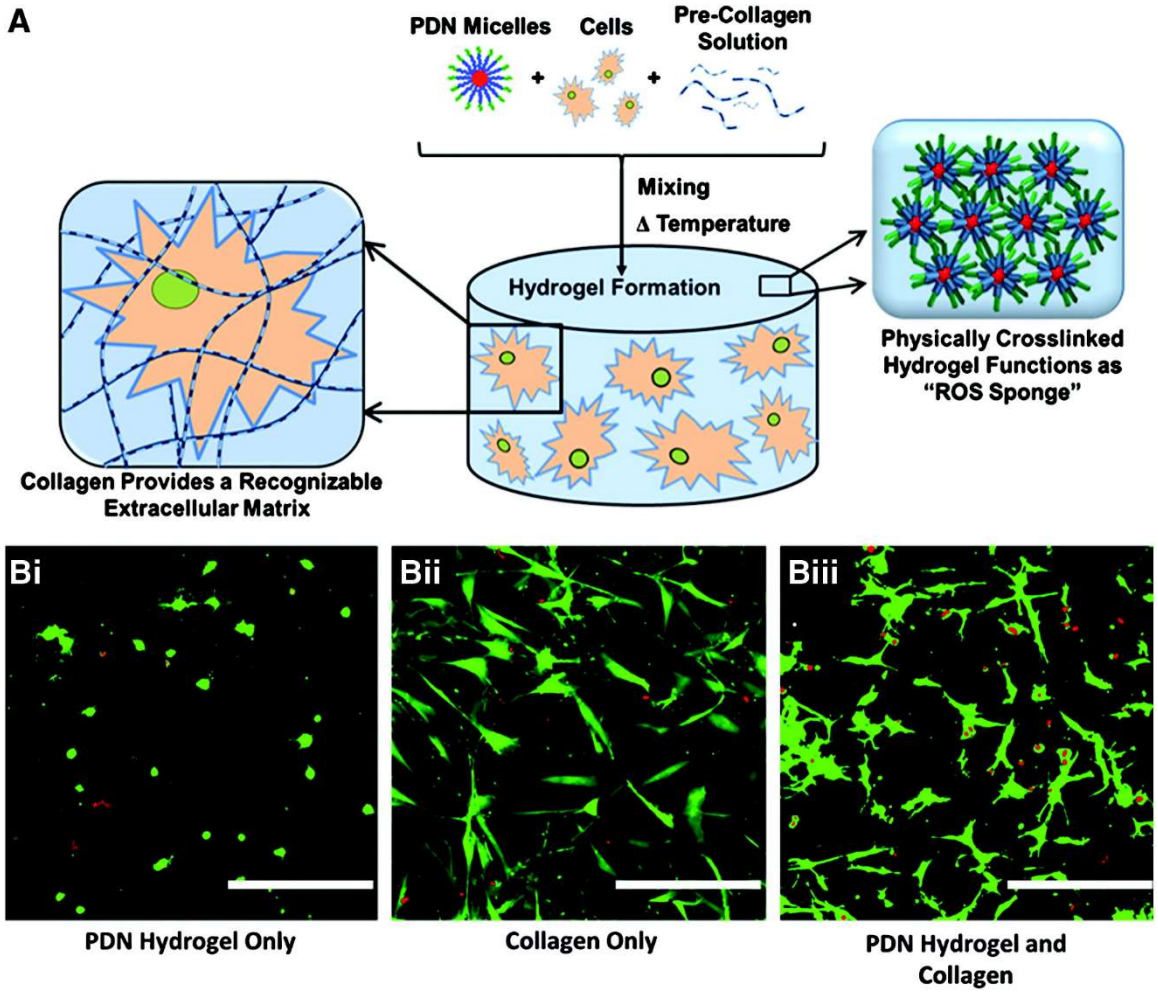

Figure 3.4 (A) Scheme depicting the formation of the cell-encapsulating hydrogel. PDN micelles, precollagen solution, and hMSCs are mixed and then incubated at 37°C to prepare an ROS-protective, cell-adherent construct. (B) After 24 h in culture, Calcein-AM (green, live stain)/Ethidium Homodimer (red, dead stain) staining reveals hMSC adherence to the composite PDN hydrogel when collagen is incorporated. Cells in the PDN hydrogel alone were unable to spread and adhere, indicating that the inclusion of collagen contributes to a more suitable environment for the encapsulation of adherent hMSCs. Images taken with 20x objective lens. hMSCs cultured in 3D in (Bi.) Three wt. % PDN hydrogel alone; (Bii) collagen alone, or (Biii) 3 wt. % PDN hydrogel with collagen (scale bar = 500 μm).

3.5.3 Protection of hMSCs from ROS-induced toxicity

Mixing hMSCS into PDN–collagen precursor solutions resulted in the formation of a cell-laden hydrogel (Fig. 3.4A). As shown in Figure 3.4B, hMSCs encapsulated in hydrogels solely comprised of PDN possessed a rounded morphology, indicating the cells' inability to either migrate through or adhere to the material substrate. However, cells seeded in T1C hydrogels featured robust attachment and spreading through the material. Consequently, cells in the PDN hydrogel+collagen composite were able to spread to a level comparable to that seen in the T1C-only hydrogels, demonstrating the cell adhesiveness imparted to these hybrid materials with the inclusion of collagen.

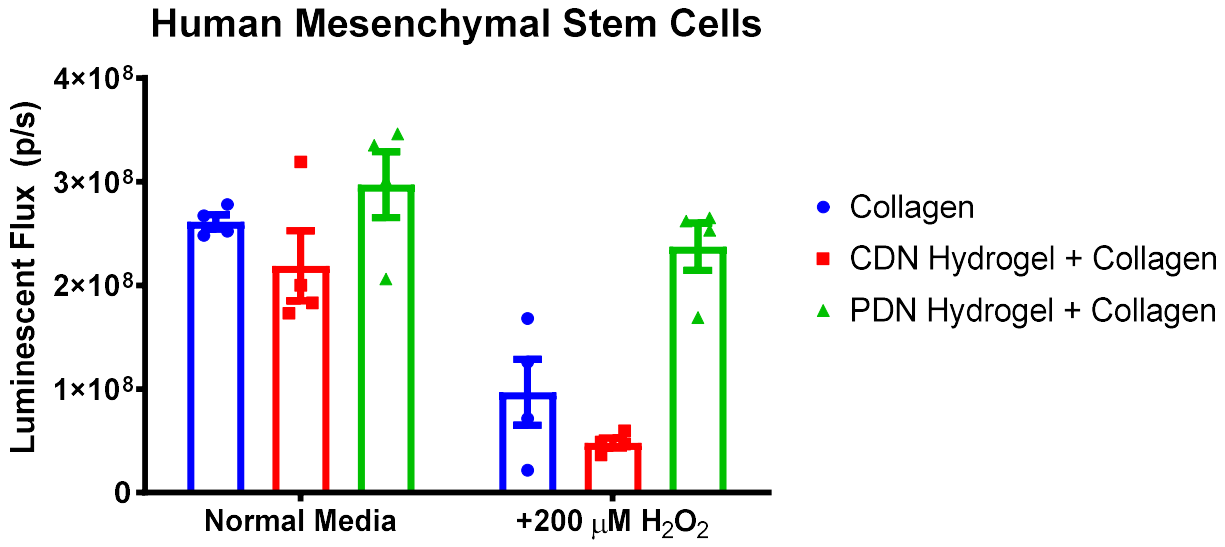

Figure 3.5 Adherent hMSCs encapsulated in collagen, CDN hydrogel+collagen composites, or PDN hydrogel+collagen composites for 24 h maintain similar levels of viability in normal media. However, media supplemented with 200 μM H_2O_2 causes significant cytotoxicity in collagen and CDN hydrogel+collagen composite materials, while the PDN hydrogel+collagen composite

protects adherent hMSCs from H_2O_2-induced cell death (Two-way ANOVA with Sidak's Multiple Comparison test, *$p < 0.05$, $n = 5$, data expressed as mean – standard error of the mean).

To demonstrate the ROS-detoxifying effect of PPS-based hydrogels, hMSCs were encapsulated in collagen gels, PDN hydrogels with 2 mg/mL T1C, and CDN hydrogels with 2 mg/mL T1C. The control CDN hydrogels were developed to provide thermogelling, cell-encapsulating material that does not contain the ROS-reactive, antioxidant PPS component. After 24 h of culture in normal MSC media (n = 5 gels for all groups), viability as determined by luminescence measurements of ATP content through a Cell Titer Glo assay showed that there were no significant differences between the number of viable encapsulated hMSCs in the three hydrogel formulations (Fig. 3.5). However, when 200 μM H_2O_2 was added to provide an oxidative stress-mimicking environment, the PDN hydrogel protected the cells from H_2O_2-induced cell death, while the other two groups displayed a statistically decreased number of viable cells. Importantly, there was no significant difference in viable cell number for normal MSC media versus the 200 μM H_2O_2 media for cells encapsulated within the PDN hydrogels (Fig. 3.5). Representative confocal microscopy maximum intensity z-stack images taken after the cells were cultured for 48 h confirm the results found in the quantitative measurements of cell number (Fig. 3.6).

As assessed by calcein-AM staining of live cells within the three formulations, embedded hMSCs possessed a similar density and spread morphology when treated with NMM. However, for cells in both the collagen-only and the CDN+collagen groups, media containing 200 μM H_2O_2 was cytotoxic as visualized by red ethidium homodimer staining. Conversely, cells encapsulated within PDN+collagen show a much higher ratio of live/dead cells following 200 μM H_2O_2 treatment in agreement with the quantitative findings in Figure 3.5, demonstrating the antioxidative behavior of PDN+collagen composite materials. Furthermore, the viability of hMSCs encapsulated in PDN hydrogel+collagen was maintained for at least 4 days in the presence of cytotoxic H_2O_2 concentrations (Fig. 3.7A). After 6 days and reapplication of H_2O_2 every 2 days, there was a statistically significant decrease in the viability of hydrogel-encapsulated hMSCs versus day 2 levels. However, ~80% of viable cells were still maintained at day 6, in

agreement with qualitative live/dead staining images of hydrogel encapsulated (Fig. 3.7B).

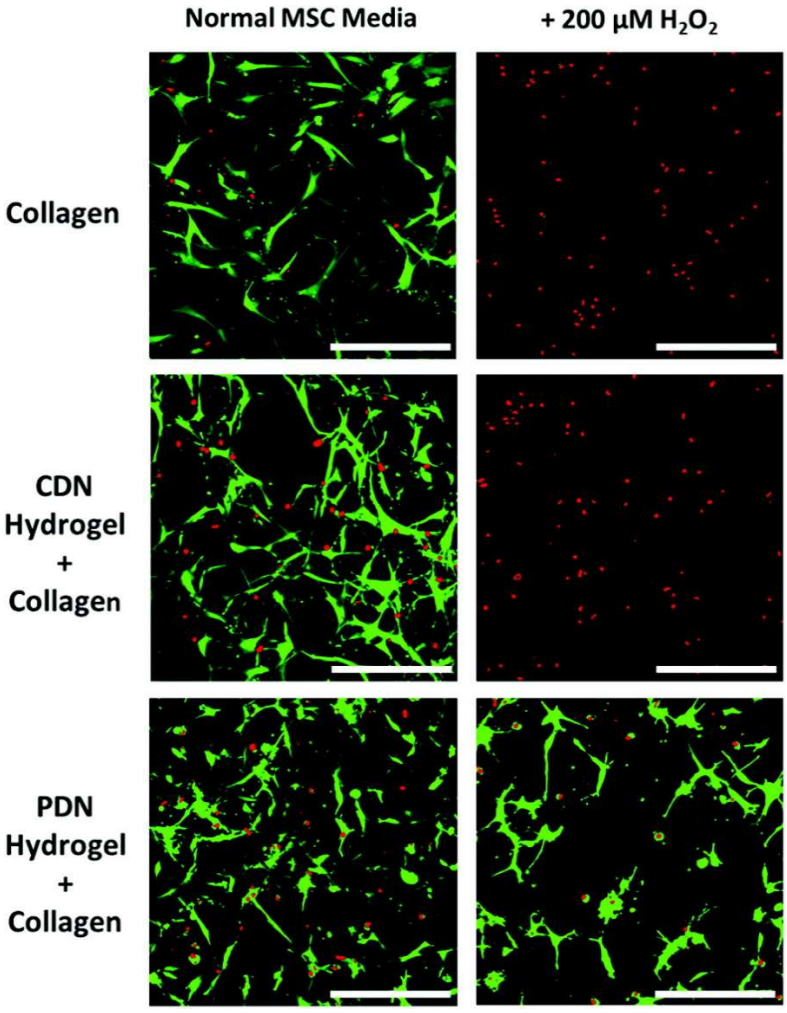

Figure 3.6 Confocal microscopy images of hydrogel-encapsulated hMSCs at 24 h confirm that all gels maintain similar levels of cell viability in normal media, while only PDN hydrogels protects adherent hMSCs from H_2O_2- induced cell death. Images taken with 20x objective lens. Cells were stained with Calcein-AM (green, live stain)/ Ethidium Homodimer (red, dead stain) (scale bar = 500 µm).

3.5.4 Protection of pseudo-islet, suspension culture from ROS

PIs created from MIN6 cell aggregates (Fig. 3.8A) were cultured within 5 wt.% PDN and CDN hydrogels or on 2D tissue culture polystyrene for 4 days. When the cells were overlaid with normal cell media, there were no significant differences between the groups, indicating that the PDN hydrogels are not cytotoxic to PIs in comparison to 2D culture (Fig. 3.8B). However, when 100 µM H_2O_2 was added to the cell media to mimic

in vivo oxidative stress, PIs encapsulated in PDN hydrogels had a statistically higher number of viable cells than PIs cultured in CDN gels or on tissue culture polystyrene (TCPS). The CDN material control gels also had higher viable cell signal than TCPS PIs, indicating that thermogels without inherent antioxidant capacity have some nonspecific protective effect (Fig. 3.8B). These data demonstrate that PDN hydrogels effectively protect PIs from cytotoxic levels of ROS and that cell aggregates (and potentially other nonadherent cell types) can be effectively delivered/ protected by PDN hydrogels without the addition of cell-adhesive T1C.

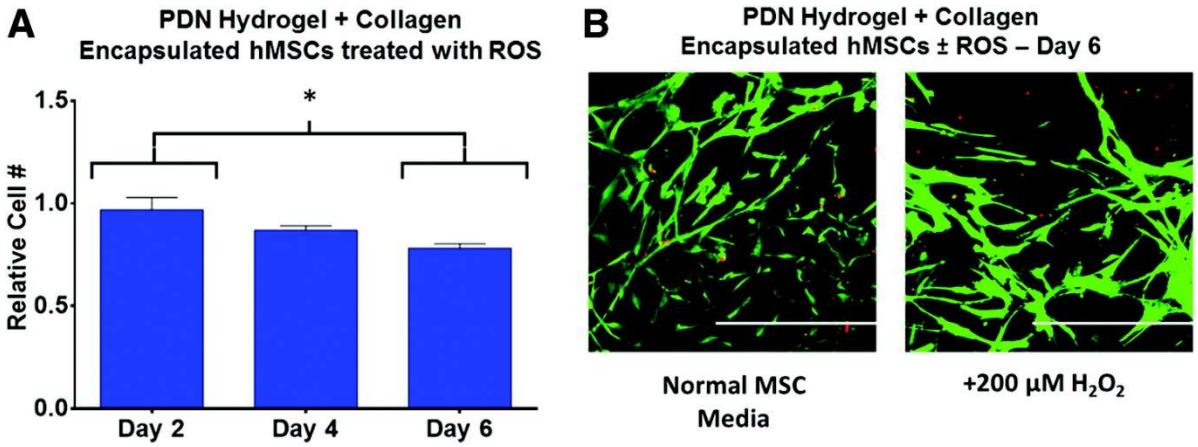

Figure 3.7 (A) hMSCs encapsulated within PDN hydrogel+collagen composites maintain *80% viability over 6 days of in vitro culture when treated with 200 mM H2O2 every 2 days in comparison to normal MSC media controls (*p < 0.05, n = 3, data expressed as mean – standard error of the mean, normalized to gel-encapsulated cells in normal MSC media). (B) Confocal z-stack images of gel-encapsulated hMSCs in media– three doses 200 µM H2O2 at day 6 taken with 20x objective lens. Cells were stained with Calcein-AM (green, live stain)/Ethidium Homodimer (red, dead stain). Scale bar = 500 µm.

3.5.5 Discussion

Hydrogels fabricated from PDN polymers feature effective thermogelation at 37°C, are noncytotoxic, possess an inherent cell-protective antioxidative capacity, and can serve as depots for local drug delivery in vivo. [18] It was hypothesized that these thermoresponsive materials would also be effective vehicles for 3D cell encapsulation and in vivo delivery applications due to their gelation characteristics and antioxidative qualities.

Though encapsulation of nonadherent cell aggregates is feasible with the initial PDN hydrogel design, this material lacks inherent cell adhesion motifs, motivating the exploration of a composite architecture that integrates a naturally derived substrate to promote attachment. Other NIPAAM-based thermogels have been fabricated to include natural components such as hyalauronic acid, [32] gelatin, [33] and T1C [22]; these composites demonstrate improved local adhesion of cells, enhanced integration of peripheral tissue with the material substrate, and boost revascularization of the transplant. In particular, T1C is a ubiquitous component of the extracellular matrix and features integrin binding domains that permit cell spreading within a 3D microenvironment. [34] To this end, PDN hydrogel+collagen composites were successfully fabricated and were subsequently evaluated for mechanical robustness, cell adhesion, and ROS-detoxification.

As an important and highly relevant benchmark control to better elucidate that the PPS chemistry was responsible for this ROS-detoxification effect, the CDN hydrogel was employed. By using the CDN hydrogel as our control, we were able to test the hypothesis that the primary ROS protective function of PDN hydrogels is achieved by the inclusion of the propylene sulfide monomer into the backbone of the PDN hydrogel rather than any chemical or structural components affiliated with other portions of the polymer.

Through a qualitative initial comparison of PDN hydrogel+ collagen composites with PDN-only gels, the gelation properties of PDN polymer-only hydrogels were preserved in the new hybrid materials. (Fig. 3.1B). As assessed by SEM, the PDN hydrogel+collagen composites uniformly incorporate the fibrillar network of polymerized T1C into the more globular structure of the polymeric PDN materials to form a homogenous, composite hydrogel featuring both synthetic and naturally derived components (Fig. 3.1C). Natural materials often lack robust mechanical properties, and composites consisting of natural and synthetic components can be utilized to enhance strength of biomaterials. [22,35] The inclusion of the collagen into the PDN hydrogel increased the storage modulus of the composite relative to PDN alone (Fig. 3.2), achieving G′ values (around 200 Pa), which favorably compares with the stiffness of

native soft tissues. [36,37] Through a more rigorous quantitative assessment, the PDN hydrogel+collagen composite was shown to be intrinsically shear-thinning at 20°C (Fig. 3.3A). At 20°C and a high shear rate (6000/s, the upper machine limit) the viscosity approaches a minimum of *0.002 Pa x s, comparable to and on the same order of magnitude as the viscosity of water (~0.001 Pa x s). [38] The maximum shear rate used is approximately one order of magnitude less than the experimentally measured maximum (26,800/s) of flow through a 28G syringe needle at 1000 mL/min, [39] though lower shear rates can be attained with both lower gauge (larger diameter) needles and decreased flow rates. Since a low viscosity was achieved at 6000/s, we expect our PDN hydrogel+collagen composite material to display low viscosity at shear rates relevant to syringe or catheter injection of cell-polymer solutions before in situ gelation.

For the PDN hydrogel+collagen composites at 20°C (liquid state), the shear-thinning behavior is exemplified by the rapid, three orders of magnitude-increase in viscosity as the shear rate is decreased from 6000/s to 0.100/s (Fig. 3.3B). By increasing the temperature to 37°C while maintaining the 0.100/s shear rate, the hydrogel viscosity increased another two orders of magnitude, indicative of the thermogelling behavior of the material (Fig. 3.3B). These experiments collectively exhibit the injectability of these materials due to their shear-thinning behavior at ambient temperature while also conclusively demonstrating their potential as in situ gelling materials due to the LCST-mediated increase in viscosity at body temperature.

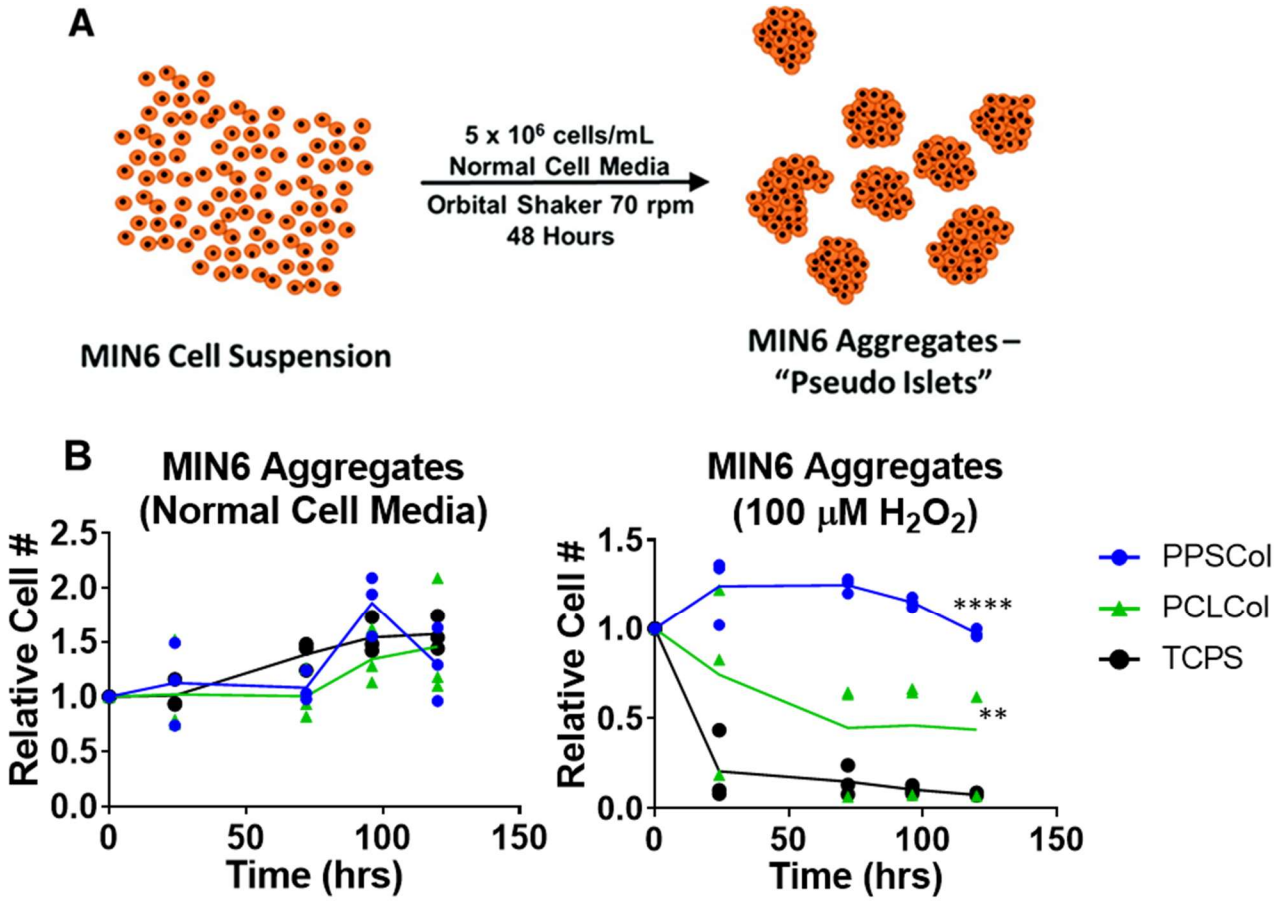

Figure 3.8 (A) Scheme for preparation of pseudo-islet cell aggregates from a high-density MIN6 cell suspension. (B) PDN hydrogels protect nonadherent MIN6 aggregates from H_2O_2-induced cell death. When cultured in normal cell media, differences between cellular viability in the different substrates were insignificant, indicating that the hydrogels are not cytotoxic to the pseudo-islets. When 100 μM H_2O_2 was added to the cell media, the PDN hydrogel significantly protected viability of cultured cells compared to CDN and TCPS, while the CDN provided an intermediate level of protection relative to PDN and TCPS. (Two-way ANOVA with Tukey's Multiple Comparison Test, ****$p < 0.0001$ PDN versus TCPS and CDN, **$p < 0.01$, CDN vs. TCPS, $n = 3$)

For most cell delivery applications, adherent cells grown in a 3D material can more readily spread and migrate through a matrix when they can proteolytically cleave the material substrate. [40] The inclusion of collagen within these hydrogels provides both motifs for cellular adhesion and the opportunity to remodel the substrate through cell-produced metalloproteinases. Consequently, adherent hMSCs seeded in hydrogels comprised solely of PDN polymer were incapable of spreading within these materials and showed a rounded morphology (Fig. 3.4Bi) while cells grown in collagen hydrogels

were able to spread through the matrix (Fig. 3.4Bii). When T1C was integrated into the PDN hydrogels, the hMSC morphology was similar to that of cells grown in collagenonly hydrogels (Fig. 3.4Biii), and the relative number of viable cells supported by composites (either PDN or CDN) was similar to that of collagen-only gels or control, 2D culture conditions. The need to include an adhesive component such as collagen to support adherent cell types is also analogous to the strategies employed with commonly utilized polyethylene glycol (PEG) hydrogels. For example, incorporation of arginylglycylaspartic acid (RGD) tripeptide (an integrin binding domain) into PEG hydrogels is necessary to promote robust cell-spreading and adhesion. [41] In sum, these data indicate that integration of collagen as an adhesion motif within PDN hydrogels renders these materials more suitable for the delivery of adherent cell types.

Long-term engraftment of patient-implanted cells is hindered by a number of difficulties [1,2] including oxidative stress produced by the host's innate immune response, with H2O2 serving as a key cytotoxic component implicated with reperfusion injury at transplantation sites. [42–44] In excess, H_2O_2 triggers cell apoptotic mechanisms via lipid peroxidation of the cellular membrane [45] and irreversible damage to proteins and DNA. [46] Wong et al. reported that an antioxidant biomaterial scaffold composed of the carbohydrate glucan pullalan improved MSC survival in the presence of H_2O_2 in vitro and in vivo. [47,48] However, their system is prefabricated into a specific geometry and therefore noninjectable, limiting its utility for some applications. In this work, we have shown that the cytotoxic effects of H_2O_2 can be mitigated by encapsulating adherent MSCs in injectable PDN hydrogel+collagen composites (Fig. 3.5). The composite PDN gels, featuring ROS-sensitive PPS in the polymer structure, [18,23,24] absorb H_2O_2 and prevent cell death of encapsulated MSCs in contrast to cells in collagen gels. Moreover, hydrogels made with the thermoresponsive CDN polymers comprised of ROS-insensitive PCL instead of PPS do not protect encapsulated cells from H_2O_2-mediated toxicity, indicating that the PPS component is the main driver of the retention in cellular viability. These results were qualitatively confirmed in confocal microscopy imaging of Live/Dead stained cells encapsulated in the hydrogel formulations with or without H_2O_2 treatment (Fig. 3.6).

The ROS-detoxifying behavior of PDN hydrogel+collagen composites was also sustained over an extended time frame as the viability of encapsulated hMSCs was maintained at 80% or higher for at least 6 days (Fig. 3.7), whereas the other nonantioxidant treatment groups saw minimal protection even after 24 or 48 h in culture (Figs. 3.5 and 3.6). In all, the PDN hydrogels+collagen composites feature a superior injectable cell delivery format and protect encapsulated cells from cytotoxic levels of H_2O_2.

We have also shown in proof-of-concept experiments that the PDN hydrogels provide protection to model PIs, suggesting future utilization of this system for delivery of insulin-producing cell therapies to cure T1D. Because these cells, like the cells that comprise native islets, are adhered to one another, they are less dependent on adhesion to an extracellular matrix. Thus, the requirement of adhesion proteins for cell spreading is not crucial, and the cells can survive for longer periods in the PDN-only gels.

For islets transplanted into patients in the clinic, many islets experience hypoxia-induced intracellular ROS generation that often causes a significant loss in islet mass. [49] Furthermore, most islets naturally produce lower amounts of antioxidant enzymes compared with other tissue types, making islets acutely susceptible to ROS-mediated toxicity. [50] Therefore, many groups have explored strategies for delivering islets while simultaneously detoxifying ROS. Weaver and Stabler encapsulated PIs in composite microparticles composed of an alginate bulk matrix and interstitial cerium oxide nanoparticles to preserve islets metabolic activity even in the presence of 10 mM superoxide. [51] Additionally, Dang et al. previously explored the use of encapsulating islets in microcapsules alongside antioxidant drugs, showing a significant improvement in islet graft survival and function upon implantation. [52]

In contrast to these and other previously developed systems, we have prepared a material that inherently functions as an antioxidant, and consequently, the complexity of material drug loading and tailoring release kinetics do not need to be considered. In this study, we showed that the hydrogel-encapsulated PIs maintained their viability (~100% or greater of the initial cell number) on par with PIs on 2D TCPS for 4 days of

culture (Fig. 3.8B). However, with the addition 100 μM H_2O_2 only the PDN hydrogel maintained full viability of the PIs (Fig. 3.8B). The toxicity of PIs in CDN hydrogels also provides further validation that the specific ROS-reactive PPS chemistry mediates protection from ROS, though the control CDN materials do act as a nonspecific barrier to limit ROS-mediated toxicity and preserve some encapsulated PI viability.

Though the PPS component of the injectable hydrogel system is primarily used to neutralize cytotoxic levels of ROS in the presented work, the degradability of the PDN hydrogels in the presence of ROS is also a key component in this system. [18] As demonstrated by other groups, [53,54] tissue remodeling and local vascularization of the islet-delivering biomaterial implant is critical for oxygenating the implanted cells, improving the glucose transaction efficiency, and producing/delivering therapeutic levels of insulin. We anticipate that the antioxidant PDN hydrogels will protect encapsulated PIs from initial immune-generated ROS levels before being gradually remodeled into a well-vascularized construct for improved islet engraftment and survival post-implantation.

As the current system does not provide longstanding, physical isolation from the immune system, we also intend to explore the use of islet surface coatings and/or immunomodulatory drugs that can be hydrophobically loaded in the micellar core of these materials to protect islets from longer term rejection by the acquired immune response.

3.6 Conclusion

In summary, we have validated the utility of our previously described antioxidant PDN hydrogel chemistry [18] for use in 3D culture of therapeutically relevant cell types. Furthermore, PDN hydrogels have been proven to enact cell-protective benefits against cytotoxic levels of oxidative stress induced by H_2O_2 in both adherent (hMSC) and suspension/aggregate (MIN6 PIs) cell models. It was found that spreading and growth of adherent cells within PDN gels benefits from integration of native matrix proteins such as T1C and that PDN hydrogel+collagen composites harness the beneficial cell adhesive properties of T1C while maintaining the thermogelling and ROS-protective

capacity of the PDN hydrogels. These results motivate preclinical exploration of PDN hydrogels for hMSC delivery in models of tissue regeneration and for delivery of primary pancreatic islets or other engineered insulin-producing cells in models of diabetes.

3.7 Acknowledgements

Experiments were performed in part using resources provided and maintained by VUMC Cell Imaging Shared Resource (CISR) (supported by NIH grants CA68485, DK20593, DK58404, HD1502, DK59637, and Ey008126) and the Vanderbilt Institute of Nanoscale Science and Engineering (VINSE). Funding was provided in part by the National Institute of Health Integrated Training in Engineering and Diabetes Training Grant (NIH 1T32DK101003-01A1) and the National Science Foundation CAREER Award (DMR) (BMAT 1349604)

3.8 References

1 Kean T.J., Lin P., Caplan A.I., and Dennis J.E. MSCs: delivery routes and engraftment, cell-targeting strategies, and immune modulation. Stem Cells Int 2013, 2013.
2 Orive G., Santos E., Pedraz J.L., and Hernández R.M. Application of cell encapsulation for controlled delivery of biological therapeutics. Adv Drug Deliv Rev 67–68, 3, 2014.
3 Malafaya P.B., Silva G.A., and Reis R.L. Natural-origin polymers as carriers and scaffolds for biomolecules and cell delivery in tissue engineering applications. Adv Drug Deliv Rev 59, 207, 2007.
4 Mooney D.J., and Vandenburgh H. Cell delivery mechanisms for tissue repair. Cell Stem Cell 2, 205, 2008.
5 Gill S., and June C.H. Going viral: chimeric antigen receptor T-cell therapy for hematological malignancies. Immunol Rev 263, 68, 2015.
6 Griffin M.D., Ritter T., and Mahon B.P. Immunological aspects of allogeneic mesenchymal stem cell therapies. Hum Gene Ther 21, 1641, 2010.
7 Pittenger M.F., and Martin B.J. Mesenchymal stem cells and their potential as cardiac therapeutics. Circ Res 95, 9, 2004.
8 Lam M.T., Nauta A., Meyer N.P., Wu J.C., and Longaker M.T. Effective delivery of stem cells using an extracellular matrix patch results in increased cell survival and proliferation and reduced scarring in skin wound healing. Tissue Eng Part A 19, 738, 2013.
9 Bianco P., and Robey P.G. Stem cells in tissue engineering. Nature 414, 118, 2001.
10 Fisher J.P., Jo S., Mikos A.G., and Reddi A.H. Thermoreversible hydrogel scaffolds for articular cartilage engineering. J Biomed Mater Res A 71, 268, 2004.

11 Parekkadan B., and Milwid J.J. Mesenchymal stem cells as therapeutics. Annu Rev Biomed Eng 12, 87, 2010.
12 Shapiro A.M.J., et al. Islet transplantation in seven patients with type 1 diabetes mellitus using a glucocorticoid-free immunosuppressive regimen. N Engl J Med 343, 230, 2000.
13 Assady S., et al. Insulin production by human embryonic stem cells. Diabetes 50, 1691, 2001.
14 Tilney N.L. Transplantation and its biology: from fantasy to routine. J Appl Physiol 89, 1681, 2000.
15 Wood K.J., and Goto R. Mechanisms of rejection: current perspectives. Transplantation 93, 1, 2012.
16 Hou D., et al. Radiolabeled cell distribution after intramyocardial, intracoronary, and interstitial retrograde coronary venous delivery: implications for current clinical trials. Circulation 112, 150, 2005.
17 Blocklet D., et al. Myocardial homing of nonmobilized peripheral-blood CD34+ cells after intracoronary injection. Stem Cells 24, 333, 2006.
18 Gupta M.K., et al. Cell protective, ABC triblock polymer-based thermoresponsive hydrogels with ROS-triggered degradation and drug release. J Am Chem Soc 136, 14896, 2014.
19 Burdick J.A., and Anseth K.S. Photoencapsulation of osteoblasts in injectable RGD-modified PEG hydrogels for bone tissue engineering. Biomaterials 23, 4315, 2002.
20 Park H., Kang S.W., Kim B.S., Mooney D.J., and Lee K.Y. Shear-reversibly crosslinked alginate hydrogels for tissue engineering. Macromol Biosci 9, 895, 2009.
21 Koopmans C., and Ritter H. Formation of physical hydrogels via host-guest interactions ofβ-cyclodextrin polymers and copolymers bearing adamantyl groups. Macromolecules 41, 7416, 2008.
22 Barnes A.L., Genever P.G., Rimmer S., and Coles M.C. Collagen–poly(N-isopropylacrylamide) hydrogels with tunable properties. Biomacromolecules 17, 723, 2016.
23 Napoli A., Valentini M., Tirelli N., Müller M., and Hubbell J. a. Oxidation-responsive polymeric vesicles. Nat Mater 3, 183, 2004.
24 Gupta M.K., Meyer T.A., Nelson C.E., and Duvall C.L. Poly(PS-b-DMA) micelles for reactive oxygen species triggered drug release. J Control Release 162, 591, 2012.
25 Anderson J.M., Rodriguez A., and Chang D.T. Foreign body reaction to biomaterials. Semin Immunol 20, 86, 2008.
26 Liu W.F., et al. Real-time in vivo detection of biomaterial-induced reactive oxygen species. Biomaterials 32, 1796, 2011.
27 Lopez-Neblina F., Toledo A.H., and Toledo-Pereyra L.H. Molecular biology of apoptosis in ischemia and reperfusion. J Invest Surg 18, 335, 2005.
28 Ingulli E. Mechanism of cellular rejection in transplantation. Pediatr Nephrol 25, 61, 2010.
29 Yeung T., et al. Effects of substrate stiffness on cell morphology, cytoskeletal structure, and adhesion. Cell Motil Cytoskeleton 60, 24, 2005.

30 Lapworth J.W., Hatton P.V., Goodchild R.L., and Rimmer S. Thermally reversible colloidal gels for three-dimensional chondrocyte culture. J R Soc Interface 9, 362, 2012.
31 Jia D., Dajusta D., and Foty R.A. Tissue surface tensions guide in vitro self-assembly of rodent pancreatic islet cells. Dev Dyn 236, 2039, 2007.
32 Ohya S., Nakayama Y., and Matsuda T. Thermoresponsive artificial extracellular matrix for tissue engineering: hyaluronic acid bioconjugated with poly(N-isopropylacrylamide) grafts. Biomacromolecules 2, 856, 2001.
33 Chen J.-P., Leu Y.-L., Fang C.-L., Chen C.H., and Fang J.-Y. Thermosensitive hydrogels composed of hyaluronic acid and gelatin as carriers for the intravesical administration of cisplatin. J Pharm Sci 100, 655, 2011.
34 Knight C.G., et al. The collagen-binding A-domains of integrins alpha(1)beta(1) and alpha(2)beta(1) recognize the same specific amino acid sequence, GFOGER, in native (triple-helical) collagens. J Biol Chem 275, 35, 2000.
35 Burdick J.A., Chung C., Jia X., Randolph M.A., and Langer R. Controlled degradation and mechanical behavior of photopolymerized hyaluronic acid networks. Biomacromolecules 6, 386, 2005.
36 Dikovsky D., Bianco-Peled H., and Seliktar D. Defining the role of matrix compliance and proteolysis in three-dimensional cell spreading and remodeling. Biophys J 94, 2914, 2008.
37 Engler A.J., Sen S., Sweeney H.L., and Discher D.E. Matrix elasticity directs stem cell lineage specification. Cell 126, 677, 2006.
38 Kestin J., Sokolov M., and Wakeham W.A. Viscosity of liquid water in the range −8C to 150C. J Phys Chem Ref Data 7, 941, 1978.
39 Aguado B.A., et al. Improving viability of stem cells during syringe needle flow through the design of hydrogel cell carriers. Tissue Eng Part A 18, 806, 2012.
40 Raeber G.P., Lutolf M.P., and Hubbell J.A. Molecularly engineered PEG hydrogels: a novel model system for proteolytically mediated cell migration. Biophys J 89, 1374, 2005.
41 Phelps E.A., et al. Maleimide cross-linked bioactive PEG hydrogel exhibits improved reaction kinetics and cross-linking for cell encapsulation and in situ delivery. Adv Mater 24, 64, 2012.
42 Zeng W., et al. Antioxidant treatment enhances human mesenchymal stem cell anti-stress ability and therapeutic efficacy in an acute liver failure model. Sci Rep 5, 11100, 2015.
43 Kunduzova O.R., Bianchi P., Parini A., and Cambon C. Hydrogen peroxide production by monoamine oxidase during ischemia/reperfusion. Eur J Pharmacol 448, 225, 2002.
44 Pendergrass K.D., et al. Acute preconditioning of cardiac progenitor cells with hydrogen peroxide enhances angiogenic pathways following ischemia-reperfusion injury. Stem Cells Dev 22, 2414, 2013.
45 Sevanian A., and Ursini F. Lipid peroxidation in membranes and low-density lipoproteins: similarities and differences. Free Radic Biol Med 29, 306, 2000.
46 Elliott R.M., Astley S.B., Southon S., and Archer D.B. Measurement of cellular repair activities for oxidative DNA damage. Free Radic Biol Med 28, 1438, 2000..

47 Wong V.W., et al. Pullulan hydrogels improve mesenchymal stem cell delivery into high-oxidative-stress wounds. Macromol Biosci 11, 1458, 2011.
48 Wong V.W., Rustad K.C., Galvez M.G., Neofytou E., Glotzbach J.P., Januszyk M., Major M.R., Sorkin M., Longaker M.T., Rajadas J., and Gurtner G.C. Engineered pullulan–collagen composite dermal hydrogels improve early cutaneous wound healing. Tissue Eng Part A 17, 631, 2011.
49 Monfared S.S.M.S., Larijani B., and Abdollahi M. Islet transplantation and antioxidant management: a comprehensive review. World J Gastroenterol 15, 1153, 2009.
50 Lenzen S., and Drinkgern J. Low antioxidant enzyme gene expression in pancreatic islets compared with various other mouse tissues. Free Radic Biol Med 20, 463, 1996.
51 Weaver J.D., and Stabler C.L. Antioxidant cerium oxide nanoparticle hydrogels for cellular encapsulation. Acta Biomater 16, 136, 2015.
52 Dang T.T., et al. Enhanced function of immuno-isolated islets in diabetes therapy by co-encapsulation with an anti-inflammatory drug. Biomaterials 34, 5792, 2013.
53 Dufour J.M., et al. Development of an ectopic site for islet transplantation, using biodegradable scaffolds. Tissue Eng 11, 1323, 2005.
54 Phelps E.A., Headen D.M., Taylor W.R., Thulé P.M., and García A.J. Vasculogenic bio-synthetic hydrogel for enhancement of pancreatic islet engraftment and function in type 1 diabetes. Biomaterials 34, 4602, 2013.

CHAPTER 4

DESIGNING A SYNTHETIC SHEAR-THINNING HYDROGEL FOR CELL- AND DRUG-DELIVERY

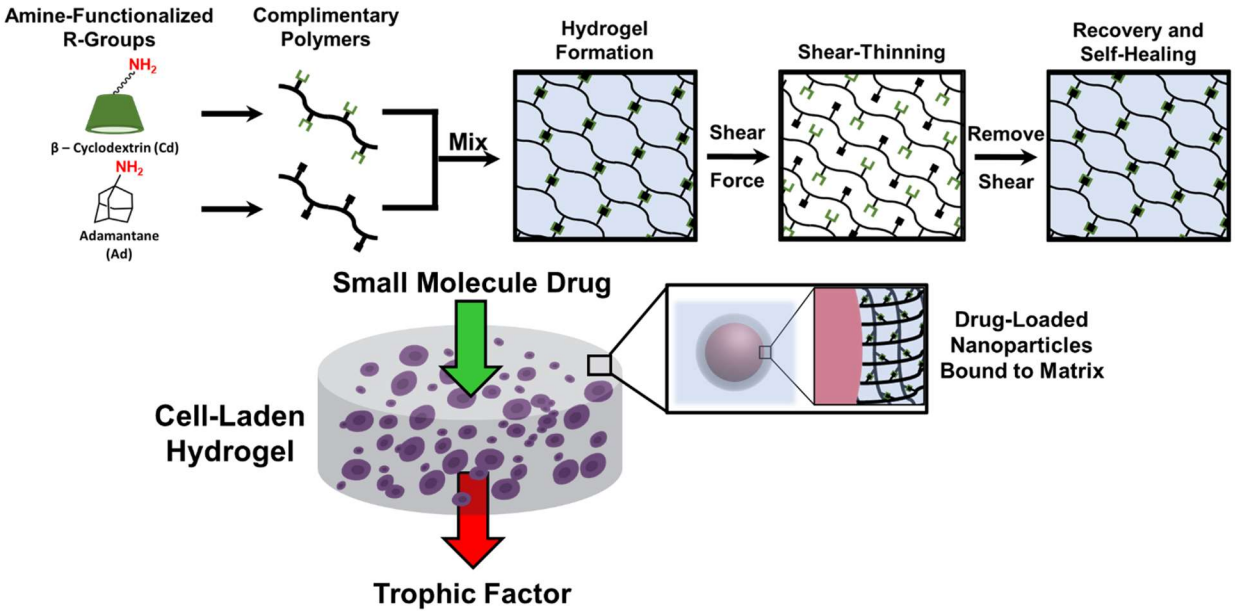

Figure 4.1 Graphical Abstract for Chapter 4

4.1 Abstract

Shear-thinning hydrogels, defined by the formation of a physically bound, three-dimensional network with high retention of aqueous solutions and transition to a fluid-like state during mechanical disruption, have gained immense attention in the biomedical community as an injectable substrate. This unique set of properties has inspired their application as a persistent repository for drug and/or cell-based therapeutics. In this work, we have explored the preparation and design considerations of a fully synthetic hydrogel that assembles through guest-host complexation of complementary polymers containing cyclodextrin or adamantane side pendants. We demonstrate control of intrinsic properties by tuning polymer architecture and reporting changes to mechanics to derive an ideal material for injection, self-healing, and *in vivo* retention. We further establish matrix-bound nanoparticles and their improved persistence of localized drug-retention *in vivo* when surface-modified to include adamantane, thus directly integrating into the hydrogel network. Lastly, we exhibit prolonged plasma detection of a protein produced by allografted cells encapsulated in our lead-candidate material in comparison to clinically relevant injection in aqueous excipient.

4.2 Introduction

Shear-thinning hydrogels have emerged as a popular class of injectable biomaterials that undergoes a pseudo-solid to liquid transition under application of mechanical shear force. Shear-thinning hydrogels comprise a supramolecular structure that gains mechanical integrity through non-covalent bonds. These bonds are formed through hydrophobic interactions or guest-host complexes between two or more underlying hydrogels components, creating reversible adhesions across polymer chains or between polymers and nanoparticles [1]. These physical interactions are susceptive to slip-dislocations under shear stress. A popular guest-host chemistry used to generate reversible, noncovalent bonds is the β-cyclodextrin (Cd, host) and adamantane (Ad, guest) complex. The Cd/Ad interaction has a high affinity with an association equilibrium constant (K_a) of 5.2×10^4 M^{-1}. The Cd/Ad complex has been proven useful in formation

of shear-thinning hydrogels, particularly for shear-thinning hydrogels based on modified hyaluronic acid (HA) [2].

The overall goal of this work was to prepare a fully-synthetic, shear-thinning hydrogel for cell and/or drug delivery that is based on well-defined linear polymers with precisely tuned molecular weight and Cd/Ad densities. The majority of currently utilized shear thinning hydrogel systems are based on naturally-derived materials like hyaluronic-acid or cellulose [3], [4]. However, fully-synthetic systems notably provide advantages such as (1) better control and higher reproducibility of physical, degradation, and chemical properties, (2) higher control of polymer molecular weight and density of pendant moieties one the polymer backbone, (3) more facile precursor sourcing and scalability, and (4) less probability of immunogenicity [5]. To demonstrate the tunability and elucidate the structure-function relationships of a fully synthetic polymer-based shear-thinning hydrogel system, herein we prepared a library of polymers with controlled variation of guest-host molecule backbone density and degree of polymerization using the controlled free radical polymerization technique RAFT combined with the amine reactive monomer 2-vinyl-4,4-dimethyl azlactone (VDMA) which enables highly-efficient post-polymerization modifications [6].

Shear thinning and other classes of hydrogel systems have great promise for therapeutic application for both cell and drug delivery [1], [7], [8]. We also sought, in this work, to demonstrate these features of the new fully synthetic, shear-thinning hydrogel platform. Local, sustained release from biomaterials can be used to reduce exposure to non-target sites and maximize drug efficacy. However, hydrated structures provide fairly low diffusional barrier to drugs encapsulated during hydrogel fabrication. To better explore this avenue, we integrated varied wt% of nanoparticles into our shear thinning hydrogel system and explored how surface functionalization with guest Ad molecules impacted hydrogel retention and controlled release in vivo.

Cell-based therapies, on the other hand, can be utilized to promote tissue repair or other therapeutic outcomes through both active cell participation in tissue formation or through paracrine mechanisms. However, paracrine mechanisms are hypothesized to potentially outweigh transplanted cell participation in tissue formation. For example,

mesenchymal stem cells (MSCs) can serve as progenitors for a myriad of cell types (i.e., adipocytes, chondrocytes, myocytes, and osteoblasts), but preclinical and clinical data suggest that transplanted cell differentiation and stable integration into tissue is a fairly rare event [9]–[11]. On the contrary, MSC benefits are thought to be more primarily derived from the function of their secreted factors, and there are also opportunities to genetically engineer MSCs or other cell types prior to implant to generate cell factories with upregulated expression of specific factors such as growth factors, insulin, or factor VIII [12]–[15].

One of the hurdles that limits production of effective, long-term cell-based paracrine therapies is poor cell retention and immune destruction of the transplanted cells, especially if they are derived from non-autologous, “off-the-shelf” sources. Encapsulation and delivery within a nonfouling, stable hydrogel that blocks immune cell infiltration can serve the dual functions of providing a persistent matrix and reducing interactions with immune cells. Herein, we’ve also sought to establish proof-of-concept of applying this new shear-thinning hydrogel platform as a cell delivery technology that prolongs the release of cell-secreted factors.

4.3 Materials and Methods

4.3.1 Poly(DMA-co-VDMA) synthesis

Random copolymers of N,N-dimethylacrylamide (DMA) and 2-vinyl-4,4-dimethyl azlactone (VDMA, Polysciences, Inc., Warrington, PA) were synthesized by RAFT polymerization. DMA was distilled at 65°C through a short-pass column under vacuum to purify away from the 4-methoxyphenol inhibitor and then stored at -20°C prior to use. DMA, VDMA, 4-cyano-4-(ethylsulfanylthiocarbonyl) sulfanylpentanoic acid (ECT, chain transfer agent (CTA)), 2,2′-azobis(isobutyronitrile) (AIBN, initiator), and trioxane (inert NMR standard) were dissolved in anhydrous dioxane at molar ratio 1:5, initiator to CTA, in a round bottom flask. An aliquot of the reaction mixture was sampled for ^{1}H-NMR, and the remainder of the solution was purged with nitrogen for 30 min and heated to 65 °C for 24 hours in a temperature-controlled oil bath under positive nitrogen pressure. The crude mixture was then cooled to room temperature and sampled for ^{1}H-NMR prior

to thrice drop-wise precipitation of the product in diethyl ether. Diethyl ether was carefully decanted, and the resulting precipitate, poly(DMA-*co*-VDMA), was dried under vacuum.

4.3.2 β-cyclodextrin-amine synthesis

β-cyclodextrin-amine (Cd-NH2) was synthesized based upon previously reported methods [16], [17]. Briefly, β-cyclodextrin was co-dissolved with p-toluenesulfonyl chloride in DI water on ice and then brought to room temperature for 2 hours. NaOH was dissolved in DI water and added dropwise, followed by stirring for an additional 30 minutes. The pH was adjusted to 8.5 by gradual addition of solid ammonium chloride, and then the solution was cooled on ice. The product was then filtered through a fritted disc. The solid residue was transferred into a vigorously stirring bath of acetone and allowed to stir for 2 hours. Next, the acetone suspension was filtered, and the residue was dried under vacuum overnight to prepare dried tosylated-Cd (Cd-TosO).

1,8-diamino-3,6-dioxaoctane (ethylene glycol diamine, ~50 mol eq) was dissolved in DMF, added to a round bottom flask, purged with nitrogen for 30 minutes, and heated to 80°C. Cd-TosO was dissolved in DMF and added dropwise to the reaction bath over the course of one hour under positive nitrogen pressure. This reaction was then allowed to proceed for approximately 24 hours. It was then cooled to room temperature and added dropwise to a stirring bath of acetone, creating a slurry suspension that was then stirred for 1 hour. After stopping the stirring, the slurry was allowed to settle. The acetone solution was siphoned from the bath and replaced with fresh acetone. Acetone was replaced 5 times total prior to filtering the precipitate, Cd-NH2, and drying under vacuum.

4.3.3 Poly(DMA-co-VDMA) Conjugation to Cd/Ad

Poly(DMA-*co*-VDMA) and either: Cd-NH2 (from prior synthesis, 2 mol eq compared to amine reactive groups) or Adamantylamine (purchased from Sigma, 2 mol eq compared to amine reactive groups) were codissolved in DMF, purged with nitrogen for 30 min, and heated to 50 °C for 3 hours in a temperature-controlled oil bath under positive nitrogen pressure. The resulting solution was transferred to a dialysis tube and

dialyzed against water for approximately 5 hours, replacing the dialysis bath every hour. An aliquot was dried prior to analysis by FTIR. Cyclodextrin macromer (Poly(DMA-*co*-Cd), Cd-Macromer) was then dialyzed against 50:50 DMSO:DI-H_2O for one week, replacing bulk solution every day. The product was subsequently dialyzed against 100% DI-H_2O for 10 days, replacing the dialysis bath daily. Adamantane macromer (DMA-co-Ad, Ad-Macromer) was then dialyzed against MeOH for one week, replacing MeOH every day, followed by dialysis against water for 10 days, replacing water every day. Both macromers were then lyophilized.

4.3.4 Nanoparticle Synthesis

Poly(ε-caprolactone)$_{90}$-ECT (PCL_{90}-ECT, CTA) was prepared through a ring-opening and conjugation scheme as described previously [18]. Briefly, the ring-opening polymerization of ε-caprolactone formed a hydroxyl-terminated, PCL_{90}-OH that was then conjugated to the carboxylated RAFT chain transfer agent ECT to prepare PCL_{90}-ECT macro-chain transfer agent. Next, DMA, 1-acryloyloxy-3-hydroxyadamantane (adamantane monomer, TCI Chemicals, Portland, OR, REF# A2859), PCL_{90}-ECT, AIBN, and trioxane were dissolved in anhydrous dioxane at molar ratio 1:5, initiator to CTA, in a round bottom flask for RAFT polymerization as described above.

4.3.5 Hydrogel formulation

Ad-macromer (with or without Ad-functionalized nanoparticles) and Cd-macromer were dissolved in PBS in separate vials at a concentration of 10 weight percent (wt%) and vortexed for approximately one hour. Dissolved Ad-macromer was then mixed into Cd-macromer using a positive displacement pipette, resulting in a rapid gelation. The resulting hydrogel was then vortexed for 30 minutes.

4.3.6 Nanoparticle-embedded hydrogels

Diblock copolymer PCL-*b*-(DMA-*co*-Ad) was dissolved in tetrahydrofuran at a concentration of 125 mg/mL. PBS was then carefully added dropwise to drive micellar nanoparticle self-assembly at a 2 wt% solution. The nanoparticle solution was left on the benchtop for about 1 hour, vigorously vortexed, and rotary evaporated to remove THF. Samples were then assessed by dynamic light scattering to ensure homogeneous

dispersity. In some samples, a fluorophore (Nile red) was co-dissolved in THF to yield fluorescent nanoparticles.

Nanoparticle solutions were then used to dissolve Ad-macromer to prepare solutions at 10 wt.% total material (*e.g.*, 1 mg/mL nanoparticles, 99 mg/mL Ad-macromer). Ad-macromer/nanoparticle solution was then mixed with a Cd-macromer solution as described above.

4.3.7 Rheological Characterization

Hydrogels were prepared and stored at 4°C overnight prior to rheometric characterization. Rheometry conditions were followed as described previously [19]. Briefly, a TA Instruments AR2000 EX rheometer was fitted with a cone (0° 59′ 42″, 20 mm) and plate geometry. Then, 100 µL of hydrogel were transferred onto the lower plate, and the upper cone was lowered to a gap size of 25 µm. For measurements of moduli, frequency was set to 10 Hz, and strain was set to 0.5%. For frequency sweeps, strain was set to 0.5%. For strain sweeps, frequency was set to 10 Hz. For time sweeps demonstrating self-healing behavior, low strain was set to 0.5%, high strain was set to 500%, and frequency was maintained at 10 Hz.

4.3.8 Cryo-SEM

100 µL of the hydrogel were prepared and stored at 4°C overnight. The following morning, a copper hole TEM aperture grid (3.0mm outer diameter) was dipped into the hydrogel material and quickly removed to produce a thin sample. The TEM grid was then snap frozen in a vitreous, liquid nitrogen slurry and fitted onto a cryo-SEM shuttle under liquid nitrogen to maintain the frozen sample. The sample was shuttled into a preparation chamber maintained at -180°C and sublimated at -90°C for 45 minutes. The temperature was reduced back to -180°C, and the sample was sputter-coated with platinum for 20 seconds and shuttled into the imaging chamber.

4.3.9 In Vivo Fluorophore Tracking

PCL-b-DMA-co-Ad nanoparticles and Nile red fluorophore (Sigma, CAS Number 7385-67-3) were co-dissolved in tetrahydrofuran at concentrations of 125 mg/mL

nanoparticles, 10 mg/mL fluorophore. This nanoparticle fluorophore solution was prepared as described above to create nanoparticles and nanoparticle-laden hydrogels.

10 to 15-week-old B6(Cg)-Tyr^{c-2J}/J (Albino B6, Jackson Laboratory) were shaved and injected with 50 µL of hydrogel in the lower ventral region to the right of midline using a positive displacement pipette. The mice were then imaged by an IVIS imaging system using 525/650 fluorescent excitation/emission filters to acquire an initial day 0 reading. Mice were imaged at intermittent time points throughout the course of the study, and signal was normalized to day 0 reading to derive percent release of Nile red, used as a model hydrophobic drug.

At days 14 and 28, mice from each group were anesthetized with isoflurane and then euthanized by cervical dislocation. Each hydrogel was excised along with surrounding skin and muscle and fixed for 48 hours in 4% paraformaldehyde. Samples were then processed, paraffin embedded, and sectioned for H&E staining.

4.3.10 Transduction of mMSCs and SEAP Detection

Two self-inactivating lentiviral expression plasmids were used to produce lentiviral vectors. Lentiviral vectors were generated by co-transfecting 2.0 µg of the respective transfer plasmid, 1.5 µg of the packaging plasmid pCMVdr8.91 (citation: doi: 10.1038/nbt0997-871), and 0.6 µg of envelope plasmid pMD2G (a gift from Didier Trono (Addgene plasmid # 12259; http://n2t.net/addgene:12259 ; RRID:Addgene_12259) into Lenti-X 293T cells (Takara) cultured at confluence in the well of a 6-well plate using Lipofectamine 3000. The next day, medium from 293T virus producer cells was changed, and conditioned medium containing lentivirus was collected approximately 36 and 60 hours after transfection. The lentiviral supernatant was filtered through 0.45 mm PVDF filters prior to cell transduction into primary bone-derived mMSCs from C57BL/6J mice (Cyagen Biosciences, Inc, Santa Clara, CA)

Transduced cells were seeded into a 96-well plate and treated with media ± variable doses of doxycycline. 24 hours later, media was collected and assayed for presence of SEAP protein by Great EscAPe™ SEAP chemiluminescence kit (Takara Bio, Cat# 631737, San Jose, CA).

4.3.11 In Vitro Cell Encapsulation

Hydrogel components were dissolved individually as described above. Cells were grown in culture until day of encapsulation, dissociated with trypsin, pelleted, and then mixed into Ad-Macromer prior to mixing with Cd-Macromer. Cell-laden hydrogels at a final concentration of 6000 cells/μL were then dispensed into a glass bottom dish and overlaid with media. 10 days later, the samples were assessed using the LIVE/DEAD™ Viability/Cytotoxicity Kit (ThermoFisher, Cat# L3224, Waltham, MA).

4.3.12 In Vivo Cell Delivery

Cells were encapsulated in hydrogels as described above at a concentration of 6000 cells/μL. BALB/c mice received cell-laden hydrogels subcutaneously as described above. The following day and every three days, mice were placed inside of a restraint housing and blood was sampled by tail vein collection into a heparinized micro-capillary tube. Blood was then dispensed into a micro-centrifuge tube and spun down at 10,000 rcf for 10 minutes. The plasma supernatant was transferred into a separate tube. Equal plasma amounts for each mouse were then used to measure SEAP content in blood using the Great EscAPe™ SEAP chemiluminescence kit.

4.4 Results and Discussion

4.4.1 Preparation and characterization of guest-host assembled hydrogel library

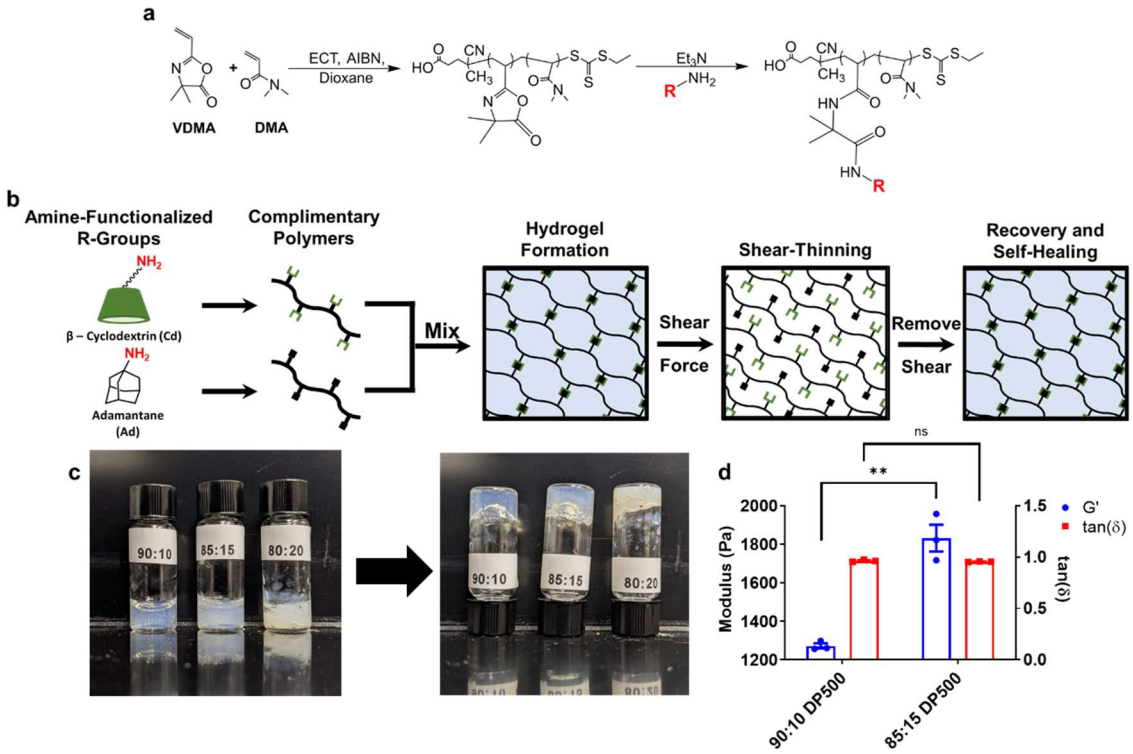

Figure 4.2 Hydrogel matrices are constructed from hydrophilic, random copolymer building blocks and physically crosslinked through guest-host complexation of their pendant side groups. (A) Monomers dimethylacrylamide (DMA) and vinyl azlactone (VDMA) are randomly polymerized through RAFT polymerization and post-modified by ring-opening conjugation of a primary amine-bearing molecule. (B) Cyclodextrin (host) and adamantane (guest) covalently conjugated to separate polymer backbones form complimentary hydrogel building blocks. Dissolution and mixing of these macromers in aqueous solution results in spontaneous, physical crosslinking. Mechanical disruption of the matrix causes dislocation of guest-host molecules triggering a transition from gel to solution. (C) Polymers with constant degree of polymerization of 500 monomeric units and varying densities of guest-host complex-forming groups create stable gels. Increasing density above 15 mol%-modification yielded macromers that were difficult to solubilize and mix, yielding hydrogels that underwent observable syneresis. (D) Oscillatory rheometry of the two initial lead hydrogel formulations revealed correlation between density of Ad and Cd and storage modulus (G') but negligible effect on tan(δ). Rheometry performed at 0.5% strain, 10 Hz frequency. Data expressed as mean ± SD, n=3, unpaired two-tailed t-test, $p<0.01$

A library of polymers was synthesized with variation in degree of polymerization and guest/host group backbone density using the synthesis strategy shown in Figure 4.2.A. The initial polymers were synthesized with a target degree of polymerization of

500 monomeric units (DP500) and a variable ratio of DMA:VDMA in the monomer feed. Variation in the random copolymer monomer mol% of amine-reactive VDMA was used to form a series of DMA-co-β-Cyclodextrin (Cd-Macromer) and DMA-co-Adamantane (Ad-Macromer) with varied backbone density of the Cd/Ad pendant groups. Poly(DMA-*co*-VDMA) was verified by ^{1}H-NMR (Fig A.B.1), and conjugation of pendant guest/host groups to parent polymers was confirmed by FTIR through loss in cyclic VDMA absorbance peak (Fig A.B.2). Polymers bearing more than 20% units of adamantane were insoluble in aqueous solution and were further excluded from characterization (Table A.B.1), Cd-macromers, however, were soluble in PBS for all ratios generated.

We next qualitatively tested the ability of the polymer building blocks in our library to form stable hydrogels. Each lyophilized polymer dissolved rapidly by vortex mixing at room temperature in PBS at 10 wt.% and yielded clear solutions that were easy to transfer using a conventional air-displacement pipette. Equal volumes of Cd-macromer and Ad-macromer solutions were then mixed using a positive-displacement pipette to prepare 10 wt% solutions comprising 5 wt.% of each guest/host macromer. Mixing the two macromers led to a spontaneous and rapid increase in the observable viscosity, suggesting guest-host assembly (Fig 4.2.B). Macromers containing 90:10, 85:15, and 80:20 ratios formed visible hydrogels that remained intact in a glass vial upon inversion (Fig 4.2.C). However, macromers containing an 80:20 ratio were less stable, considerably more difficult to mix, and susceptible to syneresis based on observation of a gel-solution separation. These combined observations led us to exclude 80:20 ratio macromers from further analysis.

We next characterized the mechanical behavior of formulations that qualitatively yielded stable gel formation (90:10 or 85:15 ratio macromers). We used a standard parallel plate rheometer to measure storage modulus (G', associated with internal, elastic forces) and loss modulus (G", associated with internal viscous forces). Rheometry showed that hydrogels formed from 85:15 macromers had a significantly larger G' than hydrogels comprising 90:10 macromers, indicating an increase in stiffness and elasticity directly attributable to the increase in the density of guest-host pendants (Fig 4.2.D). However, neither the 85:15 or 90:10 500 DP macromer-based

systems achieved tan(δ) values that were significantly below 1 (~0.95?). Tan(δ), the ratio of G":G', is an important hydrogel design parameter as it quantifies the dominance of viscous to elastic forces of a material. For injectability purposes, shear thinning hydrogels should ideally have robust linear elastic material properties under low load that are greatly diminished upon application of shear stress, meaning that the tan(δ) should be lower than 1 [4], [19].

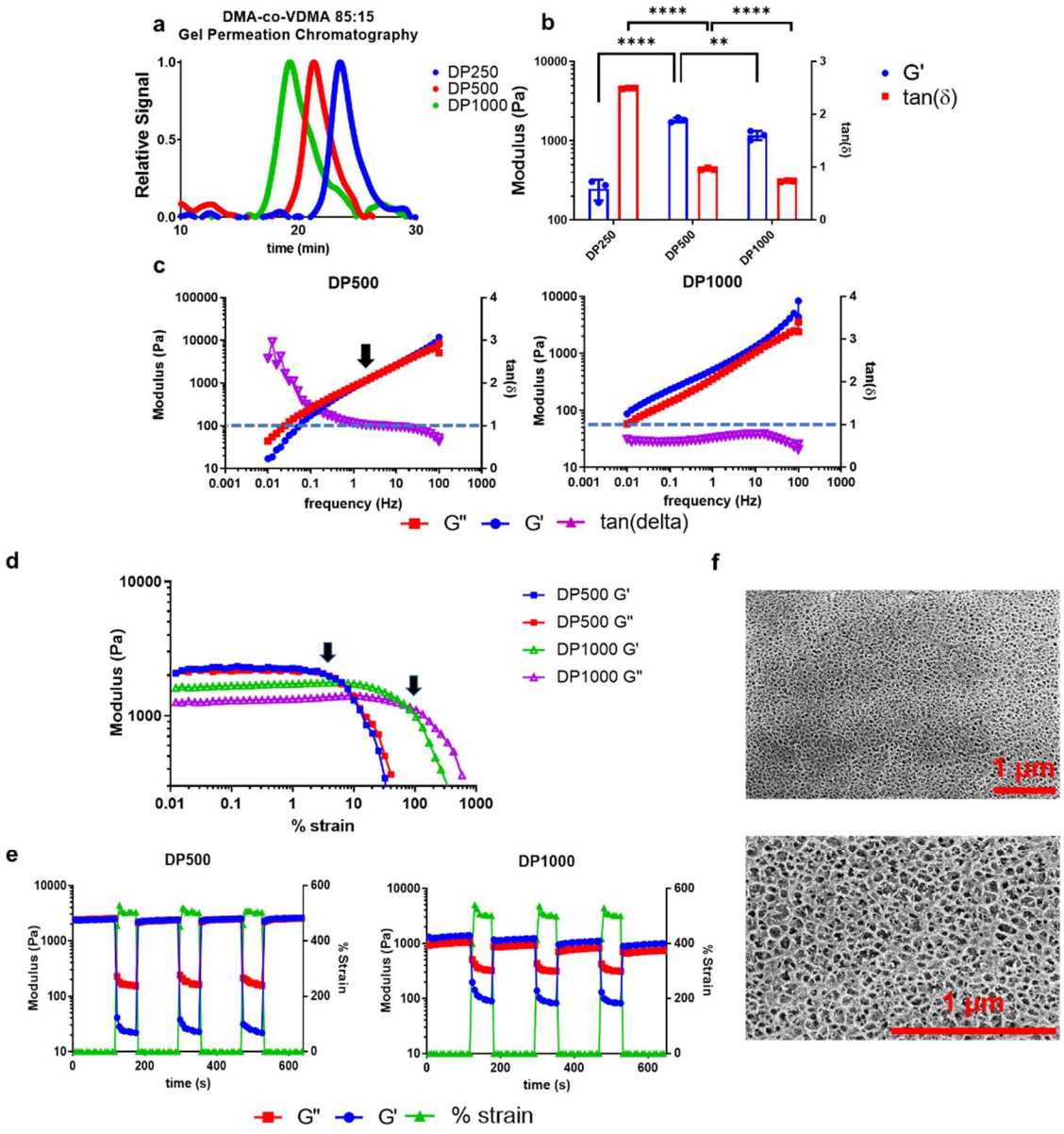

Figure 4.3 Effect of polymer degree of polymerization on mechanical properties for hydrogels comprising polymers with 15 mol% Ad/Cd functionality. (A) Gel permeation chromatography of parent DMA-co-VDMA copolymers demonstrating control over polymer degree of polymerization. (B) Macromer DP affected resultant hydrogel mechanical properties. Oscillatory rheometry performed at 0.5% strain, 10 Hz frequency. Data expressed as mean ± SD, n=3, one-way ANOVA with post-hoc Tukey's multiple comparisons test, $p<0.01$. (C) Stress relaxation of DP500 and DP1000 polymers was assessed by oscillatory frequency sweep measurements. DP1000 hydrogels showed a longer stress relaxation time. Arrow indicates crossover of G' and G". (D) Increasing molecular weight from DP 500 to DP 1000 increased yield strain; arrows indicate % strain where tan(δ)=1 (crossover point of G' and G''). (E) Cyclic measurements of moduli at low and high strain reveal shear-thinning and self-healing behavior of both DP 500 and DP 1000 hydrogels. (F) Cryo-SEM of DP1000 hydrogels revealed a homogenous, nano-porous structure with an average pore size of ~50 nm. Scale bar = 1 μm

4.4.2 Variation of macromer molecular weight to identify lead hydrogel formulation

We hypothesized that mechanical behavior, and tan(δ) in particular, could be further optimized by adjusting the molecular weight of the macromers. Based on its higher storage modulus versus the 90:10 formulation, we focused on the 85:15 composition. Using this monomer ratio, we synthesized a set of polymers with degrees of polymerization of 250 (DP250) and 1000 (DP1000) units to compare to our initialDP500 macromer formulation. RAFT synthesis of these parent polymers yielded unimodal populations by GPC that eluted in the expected, size-dependent manner (Fig 4.3.A).

The DP250 macromers did not yield stable hydrogels with desirable mechanical integrity; G' reduced by approximately an order of magnitude (G'~200 Pa), and tan(δ) increased by approximately 150% (tan(δ) ~2.5) relative to DP500 gels. However, the DP1000 macromers yielded hydrogels with reduced tan(δ) values of approximately 0.75. However, the G' of DP1000 hydrogels was about 35% lower compared to DP500 hydrogels, potentially due to less efficient mixing and guest/host engagement for the larger molecular weight macromers (Fig 4.3.B).

Macromer DP was also found to have effects on other intrinsic hydrogel mechanical properties. Increasing molecular weight was found to increase stress relaxation time. DP250 macromer-based hydrogels showed spontaneous stress relaxation at all frequencies tested; we observed dominant G", tan(δ)>1, regardless of frequency (Fig. A.B.3). DP500-based hydrogels showed slightly longer stress relaxation time, exhibiting dominant G' at and below a frequency of about 1 Hz. Lastly, DP1000 macromer hydrogels showed the longest stress relaxation times, having dominant G' regardless of frequency measured (Fig 4.3.C). Reducing stress relaxation time can increase cell spreading, and increasing this property may minimize hydrogel infiltration by host-cells and therefore reduce immune destruction for cell delivery applications [20].

Furthermore, we compared the effect of macromer molecular weight on yield strain (ε_y), defined by the crossover point of G' and G" (tan(δ)=1), as % strain is increased. We observed that the increase in molecular weight from DP500 to DP1000 led to a 10-fold increase in yield strain; DP500 ε_y~5%, while DP1000 ε_y~50% (Fig

4.3.D). We reasoned that this increase in yield strain would be beneficial to the application of our material by limiting its plastic deformation and potential for catastrophic erosion or loss under physiological loads. This yield strain is also comparable to the adipose tissue of the human omentum, a site with a yield strain of 30% and that is thought to be one of the best locations for implantation of cell therapies [21]. For cell delivery applications, it is also desirable for the cells to remain homogeneously suspended within the biomaterial. Yield mechanics are also relevant to this feature, as low yield stress can predispose the material to cell settling due to gravity [22].

Next, we wanted to determine the self-healing behavior of the leading candidate hydrogels by investigating recovery in modulus following induction of strain beyond the material's yield point. To test this, we cyclically loaded the hydrogels with low (0.5%) and high (500%) strain in an oscillatory time sweep. Both DP500 and DP1000 materials yielded immediately upon application of high strain (G">G', tan(δ)<1) and then recovered instantaneously to their initial moduli following cessation of high strain (G"<G', tan(δ)>1, $G'_i=G'_f$, $G''_i=G''_f$) for at least three cycle (Fig 4.3.E). The hydrogels prepared from the DP250 macromers showed some indicators of self-healing behavior, but this formulation was unstable and showed increased moduli with each progressive cycle in the time sweep.

Due to its emergence as a leading hydrogel candidate based on its mechanical performance, we examined the DP1000 formulation by cryo-SEM to visualize its native, hydrated nano-structure. This hydrogel produced a homogenous, nano-porous structure with pore sizes of approximately 50 nm on average (Fig 4.3.F). We reasoned that this pore size could potentially be ideal for cell delivery in terms of a system that would block entry of the host immune cells, as T cells have a diameter of ~5-7 μm, neutrophils ~12-15 μm, and macrophages ~20-25 μm [23], [24]. Previous studies have shown that host-cellular infiltration into biomaterials correlates to pore size, with larger pores enabling greater infiltration and smaller pore size being ideal for systems used to isolate allografted cells and tissues [25]–[27]. Furthermore, the pore size of 50 nm in the absence of any affinity reactions, is expected to be large enough to enable diffusion of

relevant, therapeutic proteins such as insulin (hydrodynamic radius, r_h=1.5 nm), Factor IX (r_h=3.3 nm), or Factor VIII (r_h=3.8 nm) [28], [29].

Prior to proceeding into cell encapsulation experiments, we sought to ensure cytocompatibility of the DP 1000 hydrogels. In these initial tests, we overlaid the hydrogel onto 3t3 mouse fibroblasts in culture. In comparison to control wells not coated with hydrogel, there were no differences in cell viability, indicating that this hydrogel does not cause contact-associated toxicity to surrounding cells and tissues (Fig A.B.4).

4.4.3 Preparation and characterization of nanoparticle-laden hydrogels

A benefit to these hydrogels being physically crosslinked by guest-host assembly is that they are inherently modular; amenable to building block substitution, enabling facile tuning of the hydrogel properties and functionalities. To explore the adaptability of this system, we sought to integrate drug-loadable nanoparticles (NPs) into the hydrogel matrix.

Toward NP hydrogel loading, we first synthesized a diblock polymer with a NP core-forming poly(ε-caprolactone) (PCL) block and a DMA-co-Ad hydrophilic, NP corona-forming block. To tune and optimize NP integration into the hydrogels, we prepared a small library of NPs with variable percentages of Ad in the corona-forming block (0%, 1% and 10% Ad). For all NPs, the hydrophilic block was maintained at a degree of polymerization of 300 units (PCL_{90}-b-DMA_x-co-Ad_y, x+y=300) (Fig 4.4.A). We found that all candidate polymers produced stable and uniform NPs of approximately 50 nm hydrodynamic diameter with low dispersity by DLS (Fig 4.4.B).

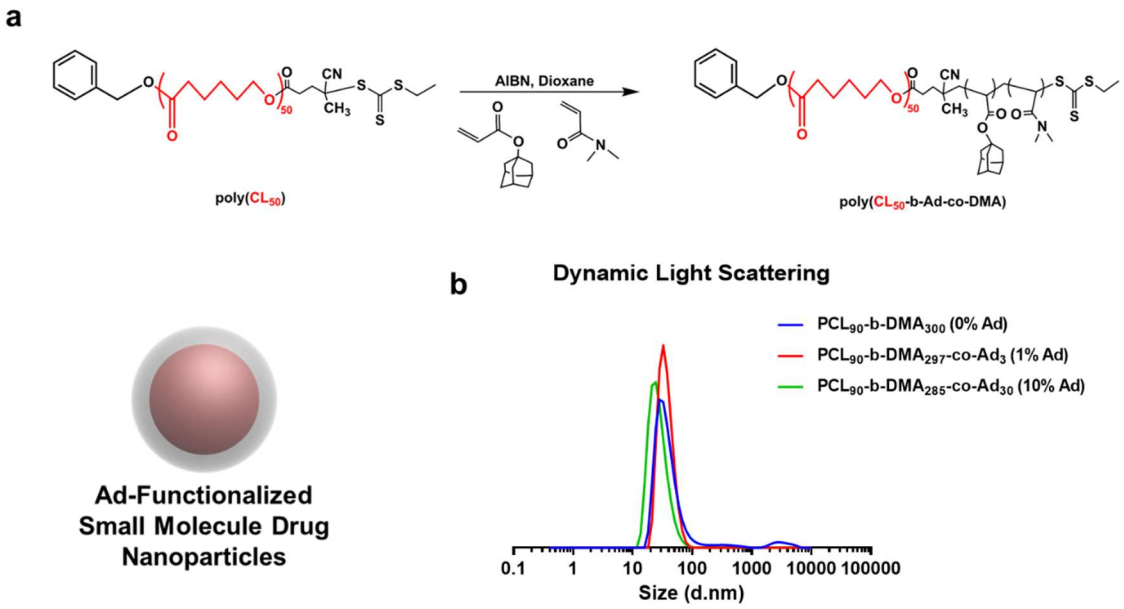

Figure 4.4 Synthesis of adamantane-bearing nanoparticles for hydrogel integration. (A) Scheme for PCL polymerization and chain extension. Nanoparticles were synthesized through polymerization of poly(ε-caprolactone) macro-RAFT chain transfer agent, followed by RAFT polymerization of a random copolymer of DMA-co-1-acryloyloxy-3-hydroxyadamantane (adamantane monomer). (B) Polymers with up to 10% adamantane in the DMA-co-adamantane block form uniformly-sized, monodisperse nanoparticles by DLS

Because these NPs were bearing guest molecule Ad, the NPs were first mixed into the Ad-functionalized macromer prior to mixing with the Cd-functionalized macromer solutions. To account for the addition of guest molecules, we reduced the mass of Ad-macromer by the equivalent mass of NPs added, such that the final hydrogel was 10 wt% (50 mg Cd-Macromer, 40 mg Ad-Macromer, 10 mg NPs to prepare 1 mL hydrogel). Interestingly, at 1 mg/mL, addition of NPs with 0% Ad functionality (PCL_{90}-b-DMA_{300}, 0% Ad) reduced G' by about 38% relative to analogous macromer-only hydrogels. This may be attributable to a small imbalance in Cd and Ad content of the overall system and due to the NPs partially physically blocking the Cd/Ad guest/host complex formation. However, tests on Ad-bearing NPs (PCL_{90}-b-DMA_{297}-co-Ad_3, 1% Ad and PCL_{90}-b-DMA_{270}-co-Ad_{30}, 10% Ad) showed that the functional NPs increased G' in a dose-dependent manner, while not impacting tan(δ) (Fig 4.5.A). We next increased the concentration of 10% Ad NPs within the hydrogel to 10 mg/mL and observed further dose-dependent strengthening of the hydrogel; as NP concentration

increased, G' increased. However, G' differences between 1 mg/mL and no NP control were much larger than 1 mg/mL and 10 mg/mL NP hydrogels suggesting that the strengthening effect does is not linearly related to NP concentration and may saturate (Fig 4.5.B). We used the 10 mg/mL, 10%Ad NP hydrogel for further testing. Yield strain decreased slightly to about 30% strain, but stress relaxation time was indistinguishable from the equivalent material without NPs (Fig 4.5.C). Because this loss in yield strain was not observed for hydrogels with 1 mg/mL of the same particles (Fig A.B.5), we suspect that this reduction might be attributable to interstitial irregularities caused by higher density of nanoparticles. Lastly, we also observed maintenance in self-healing behavior (Fig 4.5.D). These properties in combination with the added possibility of drug delivery led us to consider this our primary candidate material for further testing.

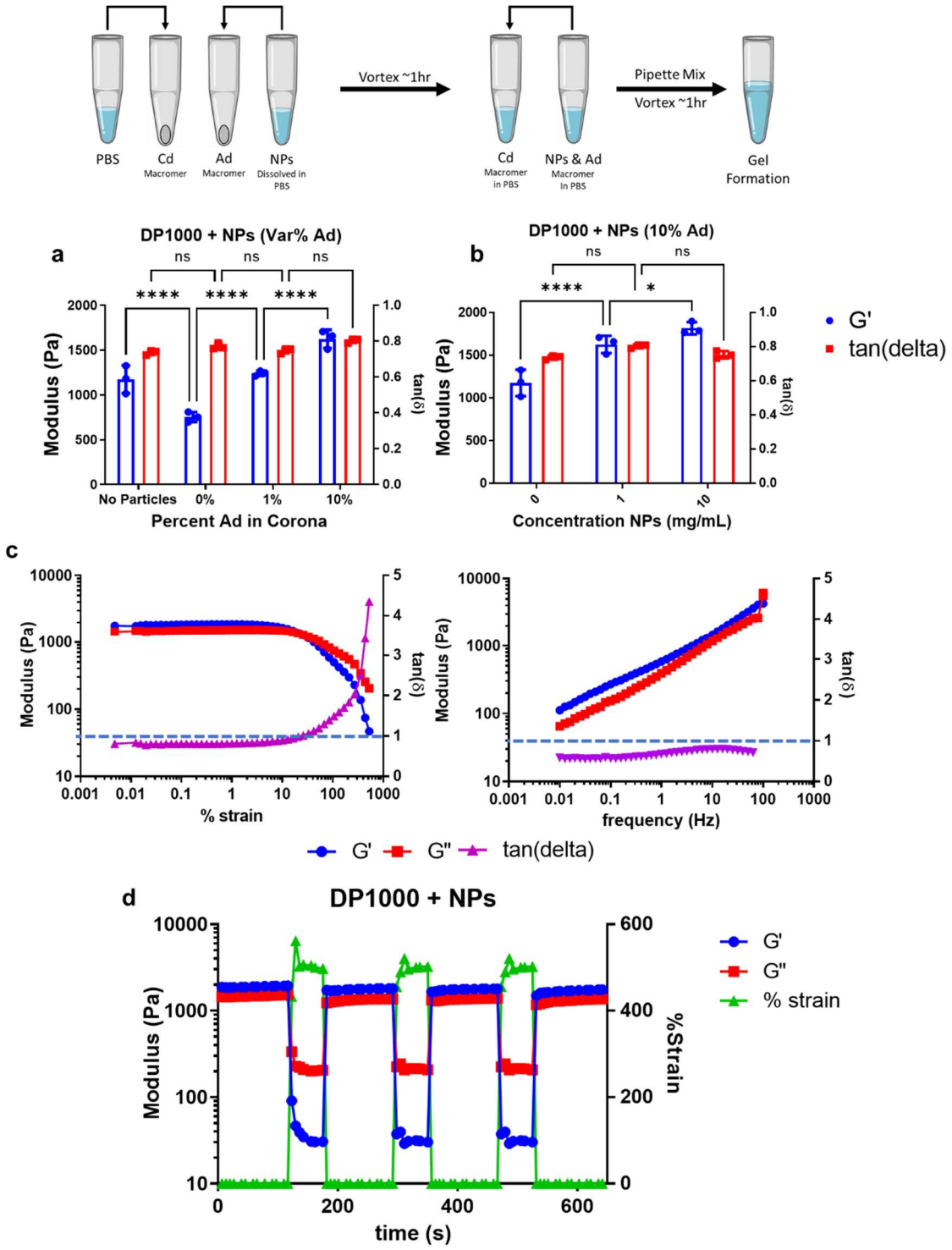

Figure 4.5 Rheometry of nanoparticle-loaded hydrogels. Replacing mass of Ad-functionalized polymer with equivalent mass of Ad-bearing nanoparticles yielded hydrogels of higher moduli, but similar tan(δ), yield strain, stress relaxation, and self-healing behavior. (A) Increasing density of adamantane in corona-forming DMA-co-adamatane block of nanoparticles increased moduli in hydrogels containing 0.1 wt% nanoparticles and overall 10 wt% polymer in solution.

Data expressed as mean ± SD, n=3, one-way ANOVA with post-hoc Tukey's multiple comparisons test, $p<0.01$ (B) Increasing nanoparticle (10% Ad corona) concentration correlated with increase in resultant hydrogel moduli. Data expressed as mean ± SD, n=3, one-way ANOVA with post-hoc Tukey's multiple comparisons test, $p<0.01$ (C) Yield strain decreased with the addition of 10 mg/mL, 10% adamantane nanoparticles to replace equivalent mass of Ad-functional polymer (from 40% to 30% strain to yield). Stress relaxation time differences were indistinguishable within the frequencies measured for the formulations with and without nanoparticles. (D) Self-healing behavior is maintained with the addition of 10 mg/mL, 10% adamantane nanoparticles to replace equivalent mass of Ad-macromer.

Next, we assessed if including Ad on the corona of our particles corresponded to better nanoparticle retention at the hydrogel injection site in vivo. To test this hypothesis, we prepared hydrogels with 10 mg/mL NPs with 10% Ad (NP(+)Ad) or 0% Ad (NP(-)Ad) loaded with hydrophobic Nile Red dye. These hydrogels were injected as 50 µL samples into the abdominal subcutaneous space of mice. The fluorescent signal of the dye was tracked intravitally by IVIS (Fig 4.6.A). By 24 hours, the two groups had diverged, as signal from NP(-)Ad decreased by about 75% on average while signal from NP(+)Ad decreased by only 40%. Overall it took about 24 days for the NP(+)Ad hydrogels to fully release of the Nile red, while NP(-)Ad hydrogels fully releases in approximately 8 days (Fig 4.6.B).

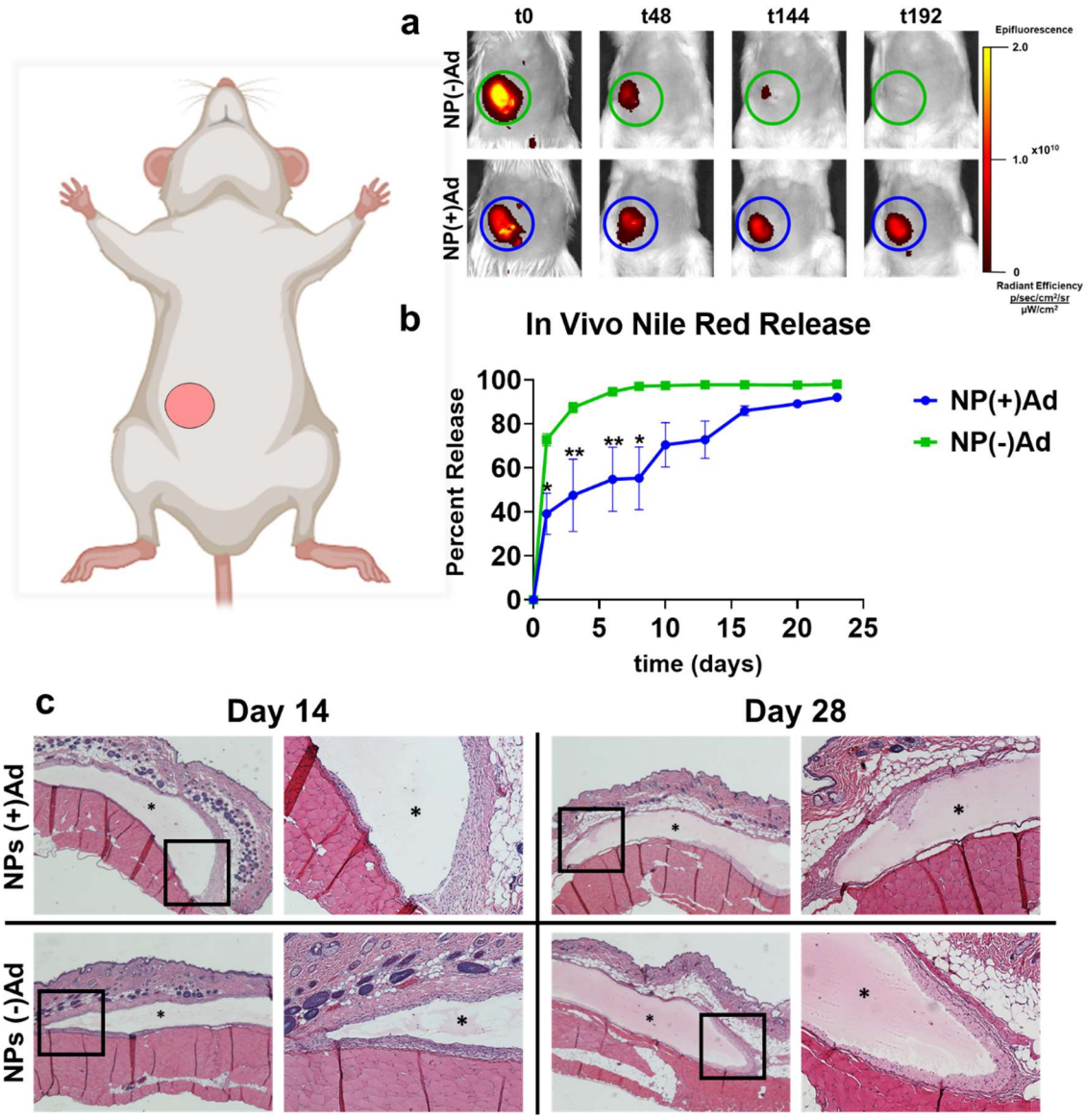

Figure 4.6 Surface functionalization of nanoparticles with Ad sustains their retention at the hydrogel injection site in vivo. (A) Representative images from IVIS intravital imaging to monitor local retention of Nile red-loaded nanoparticles in hydrogels injected subcutaneously. (B) Quantification of cumulative fluorescence loss from the hydrogels in vivo. Data expressed as mean ± SEM, n=4, two-way ANOVA with post-hoc Sidak's multiple comparison test, $p<0.01$ (C) Histology of hydrogels loaded with nanoparticles with or without surface Ad (gel indicated with *). With either type of embedded nanoparticles, the hydrogels are retained intact, block host cell infiltration, and show minimal fibrous encapsulation in subcutaneous compartments for at least 28 dayshost-cell infiltration.

Histological assessment of the hydrogels after 14 and 28 days showed no visible indication of hydrogel degradation or host-cellular infiltration. These results indicate that

NP-encapsulated fluorophore release was due to diffusion out of the matrix rather than hydrogel breakdown. A thin layer of fibrous encapsulation was observed around the hydrogels, and this feature was not apparently impacted by the NP(-)Ad versus NP(+)Ad formulation (Fig 4.6.C). Maintenance of the hydrogel in an inert format with minimal fibrous encapsulation or local immune reaction may offer benefits for use of this system as a tissue filler or for use as an immune isolating material for cell delivery. By limiting host-cell interaction with implanted cells, functionality can potentially be extended for allograft applications. This has been long explored in inert materials such as alginates, studied for their ability to achieve immune cell exclusion [30].

4.4.4 Hydrogel Cell Delivery

To test the performance of this system for generating a cell-based depot intended to provide paracrine effects in vivo, we developed a model system for measuring the ability of encapsulated cells to receive and deliver cues from the external environment. To do so, MSCs derived from C57BL/6J mice were transduced to express secreted embryonic alkaline phosphatase (SEAP) (Fig 4.7.A and Fig 4.7.B) in response to small-molecule doxycycline (dox). SEAP production was found to be doxycycline-dependent in 2D culture (Fig 4.7.C) and in 3D hydrogel (Fig 4.8.A) cultures. After 10 days of hydrogel encapsulation, the cells were imaged via confocal microscopy using calcein-AM (Live, green stain, cell-permeable, assembles within cytoplasm and becomes fluorescent) and ethidium homodimer (Dead, red stain, cell-impermeable, stains cell nucleus). The encapsulated cells were predominantly viable and homogenously distributed throughout the hydrogel with no visible settling overtime (Fig 4.8.B).

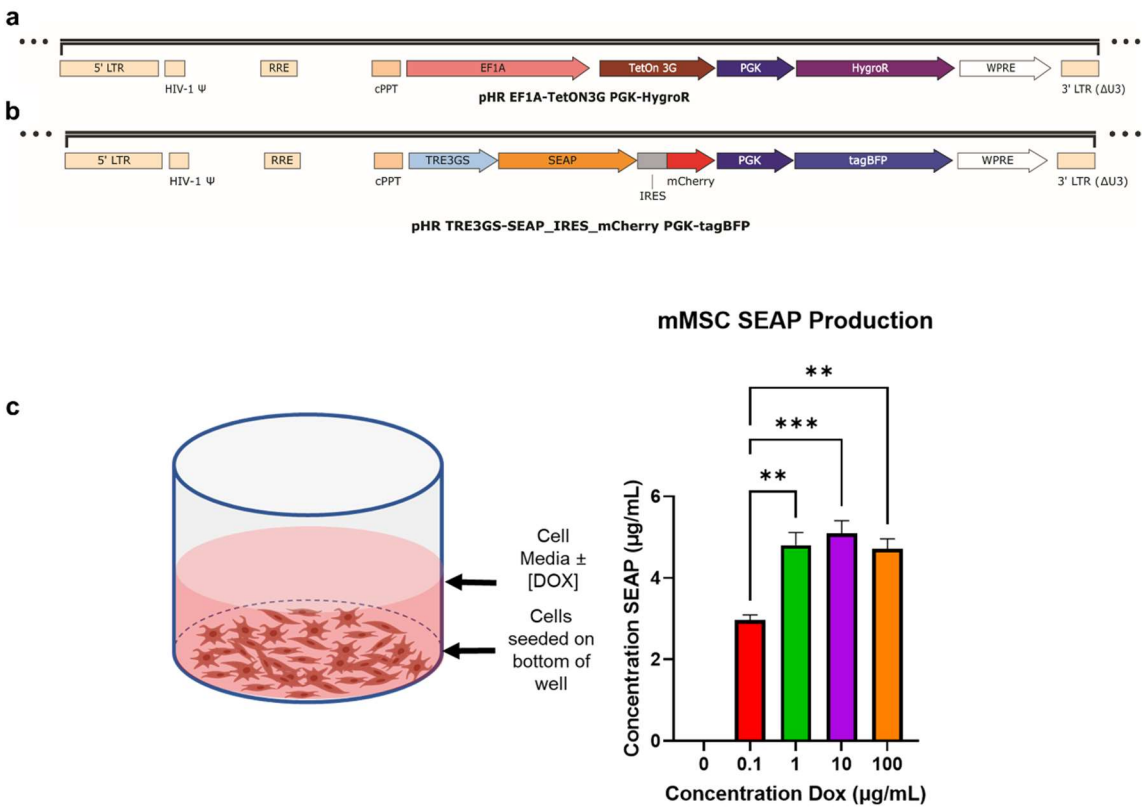

Figure 4.7 Mouse mesenchymal stem cells (mMSCs) were transduced to express doxycycline-induced, secreted embryonic alkaline phosphatase (dox-SEAP) for facile measurement of protein produced by transplanted cells. (A) Transfer plasmid used to produce vectors driving constitutive expression of the dox-responsive transcription factor, TetOn3G (doxycycline). (B) Transfer plasmid encoding inducible expression of SEAP and mCherry in response to TetOn3G activity. LTR: long terminal repeat; RRE: Rev response element; cPPT: central polypurine tract; EF1A: human elongation factor-1α promoter; SEAP: secreted alkaline phosphatase; IRES: internal ribosome entry site; PGK: murine phosphoglycerate kinase-1 promoter; HygroR: hygromycin-resistance transgene; tagBFP: monomeric blue fluorescent protein; WPRE: woodchuck hepatitis virus post-transcriptional regulatory element. (C) SEAP production of mMSCs grown in 2D culture is doxycycline-dependent

We also assessed the effect of cell loading on hydrogel mechanics. Preparing hydrogels with 600 cells/μL led to no significant differences in G' or tan(δ). Loading of 6000 cells/μL (the highest dose tested) led to statistically significant but modest reduction in G' (9% difference) and no changes in tan(δ), signifying that loading of cells had minimal impact on the hydrogel mechanics (Fig 4.8.C). Furthermore, increasing cell concentration led to simultaneous reduction in yield strain and stress relaxation time. (Fig 4.8.D).

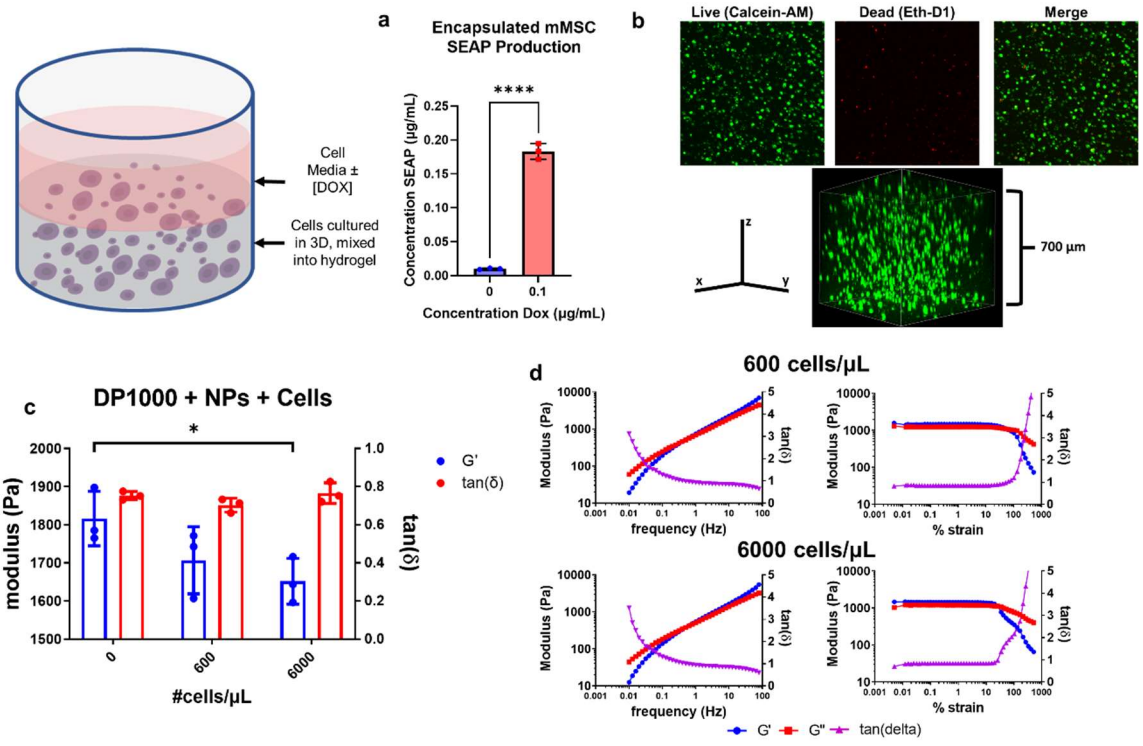

Figure 4.8 Hydrogel encapsulated cells remain viable, respond to small molecule (doxycycline) stimuli, release measurable secreted factors, and do not alter hydrogel mechanics. (A) SEAP secretion into the media of cells encapsulated in gels was doxycycline-dependent. Data expressed as mean ± SD, unpaired two-tailed t-test ****p<0.001 (B) Encapsulated cells were visualized by confocal microscopy using calcein-AM (green, live) and ethidium homodimer (eth-d1, red, dead) stains. Cells were found to be predominantly viable for at least 10 days and remained homogenously distributed throughout the hydrogel. (C) Increasing cell-concentration in hydrogels led to a statistically significant decrease in G' but no differences in tan(δ). Hydrogels with mechanical integrity were formed at all cell concentrations tested. Data expressed as mean ± SD, One way ANOVA with post-hoc Sidak's Multiple Comparison test *p<0.05 (D) Increasing the concentration of cells into hydrogels decreased yield strain and stress relaxation time.

To explore the feasibility of this platform as a potential cell depot in vivo, we injected SEAP-MSC-loaded hydrogels subcutaneously in BALB/C mice, an allogeneic model of cell transplantation. These mice were fed a doxycycline-containing diet to induce SEAP production by the transplanted cells. SEAP signal in the mouse plasma persisted for at least 13 days, while signal from mice receiving cells injected in PBS persisted for only 4 days. However, the lack of diffusional limitations of cells in the PBS excipient led to greater quantity of measurable SEAP production in comparison to cells within the hydrogel. SEAP absorption in the blood from the PBS cell-suspension was

more akin to a bolus injection, while hydrogel-implanted cells resembled first-order delivery (Fig 4.9.A).

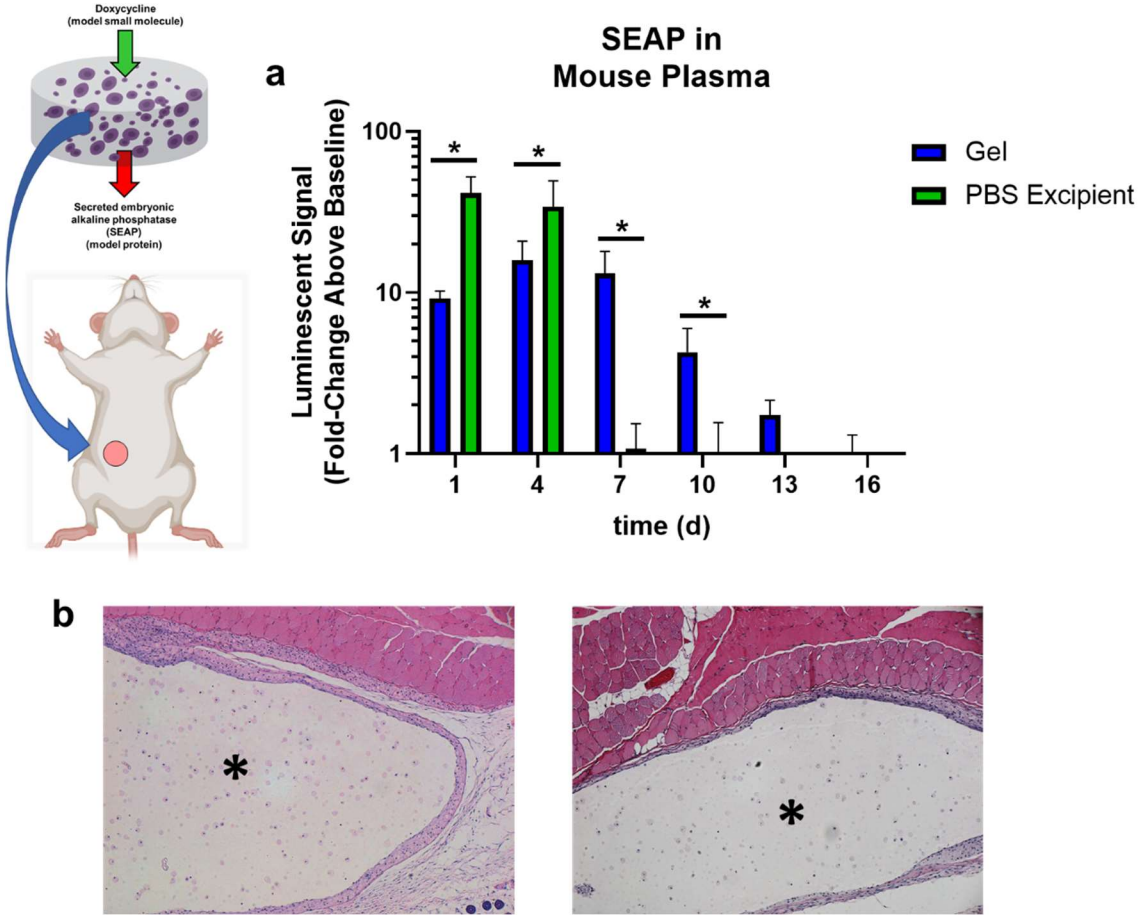

Figure 4.9 Cells encapsulated in hydrogel and delivered subcutaneously in an allogeneic transplant model were retained in the gel and showed longer-persisting paracrine activity than free cells. (A) Signal from protein produced by cells encapsulated within hydrogels persisted in mouse plasma for at least 13 days while signal from cells delivered by PBS excipient persisted for less than 7 days. Data expressed as mean ± SEM, n=4, unpaired two-tailed t-test each day, $p<0.01$ (B) Representative histological sections from cell-laden hydrogels implanted subcutaneously after 21 days showed retention of cells by H&E stain. Gel indicated by *.

Histological examination of the subcutaneously implanted hydrogels at day 21 showed homogenously dispersed cells within the hydrogel with rounded morphology (Fig 4.9.B), similar to the results of our *in vitro* microscopy (Fig 4.8.B). Because we saw no cell infiltration with prior cell-free *in vivo* implantation with this hydrogel (Fig 4.6.C) and only a small reduction in mechanics due to the inclusion of cells, we can assume

that the cells we are visualizing are of transplanted origin. Therefore, the hydrogel acted to retain the cells locally without host-cell invasion and direct contact.

4.3 Conclusion

In summary, we have demonstrated design and production of a fully-synthetic, shear-thinning hydrogel, the effects of modifying guest-host complex density along with molecular weight of the polymer building blocks on mechanical properties by rheometry, and therapeutic potential of this platform. As expected, increasing complex density led to increased elasticity, but had little effect on tan(δ). Increasing molecular weight of the polymer building blocks caused substantial reduction in tan(δ), indicative of stable hydrogel formation. Including nanoparticles surface-modified with adamantane contributed to increased mechanical properties and led to longevity in release in vivo. In the final study of this work, we demonstrated that we could prolong the release of a protein produced by allografted cells encapsulated within our lead candidate hydrogel.

4.7 References

[1] M. Guvendiren, H. D. Lu, and J. A. Burdick, “Shear-thinning hydrogels for biomedical applications,” *Soft Matter*, vol. 8, no. 2, pp. 260–272, Dec. 2011, doi: 10.1039/C1SM06513K.

[2] C. B. Rodell, A. L. Kaminski, and J. A. Burdick, “Rational Design of Network Properties in Guest–Host Assembled and Shear-Thinning Hyaluronic Acid Hydrogels,” *Biomacromolecules*, vol. 14, no. 11, pp. 4125–4134, Nov. 2013, doi: 10.1021/bm401280z.

[3] C. Loebel, C. B. Rodell, M. H. Chen, and J. A. Burdick, “Shear-thinning and self-healing hydrogels as injectable therapeutics and for 3D-printing,” *Nat Protoc*, vol. 12, no. 8, pp. 1521–1541, Aug. 2017, doi: 10.1038/nprot.2017.053.

[4] E. A. Appel, M. W. Tibbitt, M. J. Webber, B. A. Mattix, O. Veiseh, and R. Langer, “Self-assembled hydrogels utilizing polymer–nanoparticle interactions,” *Nat Commun*, vol. 6, no. 1, p. 6295, Feb. 2015, doi: 10.1038/ncomms7295.

[5] A. Sionkowska, “Current research on the blends of natural and synthetic polymers as new biomaterials: Review,” *Progress in Polymer Science*, vol. 36, no. 9, pp. 1254–1276, Sep. 2011, doi: 10.1016/j.progpolymsci.2011.05.003.

[6] J. M. Messman, B. S. Lokitz, J. M. Pickel, and S. M. Kilbey, “Highly Tailorable Materials based on 2-Vinyl-4,4-dimethyl Azlactone: (Co)Polymerization, Synthetic Manipulation and Characterization,” *Macromolecules*, vol. 42, no. 12, pp. 3933–3941, Jun. 2009, doi: 10.1021/ma900316t.

[7] A. L. Facklam, L. R. Volpatti, and D. G. Anderson, “Biomaterials for Personalized Cell Therapy,” *Advanced Materials*, vol. 32, no. 13, p. 1902005, 2020, doi: 10.1002/adma.201902005.
[8] E. Caló and V. V. Khutoryanskiy, “Biomedical applications of hydrogels: A review of patents and commercial products,” *European Polymer Journal*, vol. 65, pp. 252–267, Apr. 2015, doi: 10.1016/j.eurpolymj.2014.11.024.
[9] T. Squillaro, G. Peluso, and U. Galderisi, “Clinical Trials with Mesenchymal Stem Cells: An Update,” *Cell Transplant*, vol. 25, no. 5, pp. 829–848, May 2016, doi: 10.3727/096368915X689622.
[10] E. Eggenhofer, F. Luk, M. H. Dahlke, and M. J. Hoogduijn, “The Life and Fate of Mesenchymal Stem Cells,” *Front Immunol*, vol. 5, p. 148, May 2014, doi: 10.3389/fimmu.2014.00148.
[11] A. Naji, M. Eitoku, B. Favier, F. Deschaseaux, N. Rouas-Freiss, and N. Suganuma, “Biological functions of mesenchymal stem cells and clinical implications,” *Cell. Mol. Life Sci.*, vol. 76, no. 17, pp. 3323–3348, Sep. 2019, doi: 10.1007/s00018-019-03125-1.
[12] M. M. Gabr *et al.*, “From Human Mesenchymal Stem Cells to Insulin-Producing Cells: Comparison between Bone Marrow- and Adipose Tissue-Derived Cells,” *Biomed Res Int*, vol. 2017, p. 3854232, 2017, doi: 10.1155/2017/3854232.
[13] M. A. Ghoneim, A. F. Refaie, B. L. Elbassiouny, M. M. Gabr, and M. M. Zakaria, “From Mesenchymal Stromal/Stem Cells to Insulin-Producing Cells: Progress and Challenges,” *Stem Cell Rev and Rep*, vol. 16, no. 6, pp. 1156–1172, Dec. 2020, doi: 10.1007/s12015-020-10036-3.
[14] C. B. Doering, “Retroviral Modification of Mesenchymal Stem Cells for Gene Therapy of Hemophilia,” in *Gene Therapy Protocols: Production and In Vivo Applications of Gene Transfer Vectors*, J. M. L. Doux, Ed. Totowa, NJ: Humana Press, 2008, pp. 203–212. doi: 10.1007/978-1-59745-237-3_12.
[15] K. Gao *et al.*, “Potential long-term treatment of hemophilia A by neonatal co-transplantation of cord blood-derived endothelial colony-forming cells and placental mesenchymal stromal cells,” *Stem Cell Research & Therapy*, vol. 10, no. 1, p. 34, Jan. 2019, doi: 10.1186/s13287-019-1138-8.
[16] C. B. Rodell *et al.*, “Shear-Thinning Supramolecular Hydrogels with Secondary Autonomous Covalent Crosslinking to Modulate Viscoelastic Properties In Vivo,” *Advanced Functional Materials*, vol. 25, no. 4, pp. 636–644, 2015, doi: https://doi.org/10.1002/adfm.201403550.
[17] A. M. Sisso, M. O’Kelly Boit, and C. A. DeForest, “Self-Healing Injectable Gelatin Hydrogels for Localized Therapeutic Cell Delivery,” *J Biomed Mater Res A*, vol. 108, no. 5, pp. 1112–1121, May 2020, doi: 10.1002/jbm.a.36886.
[18] M. K. Gupta, J. R. Martin, B. R. Dollinger, M. E. Hattaway, and C. L. Duvall, “Thermogelling, ABC Triblock Copolymer Platform for Resorbable Hydrogels with Tunable, Degradation-Mediated Drug Release,” *Advanced Functional Materials*, vol. 27, no. 47, p. 1704107, 2017, doi: https://doi.org/10.1002/adfm.201704107.
[19] M. H. Chen, L. L. Wang, J. J. Chung, Y.-H. Kim, P. Atluri, and J. A. Burdick, “Methods To Assess Shear-Thinning Hydrogels for Application As Injectable Biomaterials,” *ACS Biomater. Sci. Eng.*, vol. 3, no. 12, pp. 3146–3160, Dec. 2017, doi: 10.1021/acsbiomaterials.7b00734.

[20] O. Chaudhuri *et al.*, “Hydrogels with tunable stress relaxation regulate stem cell fate and activity,” *Nature Mater*, vol. 15, no. 3, pp. 326–334, Mar. 2016, doi: 10.1038/nmat4489.
[21] J. D. Weaver *et al.*, “Vasculogenic hydrogel enhances islet survival, engraftment, and function in leading extrahepatic sites,” *Science Advances*, vol. 3, no. 6, p. e1700184, Jun. 2017, doi: 10.1126/sciadv.1700184.
[22] A. K. Grosskopf, G. A. Roth, A. A. A. Smith, E. C. Gale, H. L. Hernandez, and E. A. Appel, “Injectable supramolecular polymer–nanoparticle hydrogels enhance human mesenchymal stem cell delivery,” *Bioengineering & Translational Medicine*, vol. 5, no. 1, p. e10147, 2020, doi: https://doi.org/10.1002/btm2.10147.
[23] H. Tasnim, G. M. Fricke, J. R. Byrum, J. O. Sotiris, J. L. Cannon, and M. E. Moses, “Quantitative Measurement of Naïve T Cell Association With Dendritic Cells, FRCs, and Blood Vessels in Lymph Nodes,” *Frontiers in Immunology*, vol. 9, p. 1571, 2018, doi: 10.3389/fimmu.2018.01571.
[24] A. Tigner, S. A. Ibrahim, and I. Murray, “Histology, White Blood Cell,” in *StatPearls*, Treasure Island (FL): StatPearls Publishing, 2021. Accessed: Sep. 27, 2021. [Online]. Available: http://www.ncbi.nlm.nih.gov/books/NBK563148/
[25] B. K. H. L. Boekema *et al.*, “Effect of pore size and cross-linking of a novel collagen-elastin dermal substitute on wound healing,” *J Mater Sci: Mater Med*, vol. 25, no. 2, pp. 423–433, Feb. 2014, doi: 10.1007/s10856-013-5075-2.
[26] T. A. Desai, D. Hansford, and M. Ferrari, “Characterization of micromachined silicon membranes for immunoisolation and bioseparation applications,” *Journal of Membrane Science*, vol. 159, no. 1, pp. 221–231, Jul. 1999, doi: 10.1016/S0376-7388(99)00062-9.
[27] K. E. La Flamme *et al.*, “Biocompatibility of nanoporous alumina membranes for immunoisolation,” *Biomaterials*, vol. 28, no. 16, pp. 2638–2645, Jun. 2007, doi: 10.1016/j.biomaterials.2007.02.010.
[28] S. S. Jensen, H. Jensen, C. Cornett, E. H. Møller, and J. Østergaard, “Insulin diffusion and self-association characterized by real-time UV imaging and Taylor dispersion analysis,” *Journal of Pharmaceutical and Biomedical Analysis*, vol. 92, pp. 203–210, Apr. 2014, doi: 10.1016/j.jpba.2014.01.022.
[29] R. De Cristofaro *et al.*, “Molecular Aggregation of Marketed Recombinant FVIII Products: Biochemical Evidence and Functional Effects,” *TH Open*, vol. 3, no. 2, pp. e123–e131, May 2019, doi: 10.1055/s-0039-1688413.
[30] M. A. Bochenek *et al.*, “Alginate encapsulation as long-term immune protection of allogeneic pancreatic islet cells transplanted into the omental bursa of macaques,” *Nat Biomed Eng*, vol. 2, no. 11, pp. 810–821, Nov. 2018, doi: 10.1038/s41551-018-0275-1.

CHAPTER 5

FUTURE WORK AND BROADER IMPACTS

5.1 ROS-Responsive Hydrogel Platform

5.1.1 Primary Islet Encapsulation and Demonstration of ROS Protection

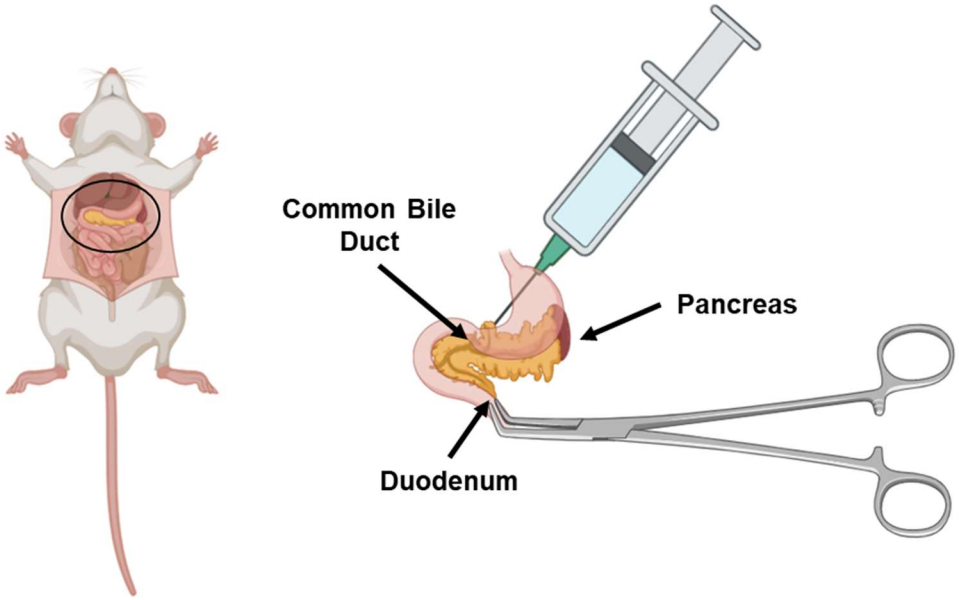

Figure 5.1 Description of surgical technique to access and distend mouse pancreas for isolation of primary islets.

Evolution of this project will require exploration of the hydrogel's ability to prevent ROS-induced toxicity in more clinically relevant, primary islets. Working with the Jacobson Lab (Department of Molecular Physiology and Biophysics Vanderbilt University, Nashville, TN, USA), we have optimized a protocol for islet isolation from mice (Fig 5.1).

Primary islets were harvested from C57B6/J mice through distention of the pancreas *in situ*. Immediately following euthanization by cervical dislocation, the common bile duct was accessed via the ventral abdominal space. The duodenum was clamped using hemostatic forceps to prevent flowthrough, and a solution of collagenase was injected into the pancreas via the common bile duct. The distended pancreas was excised and placed into a warm solution of collagenase and agitated to break apart the

extracellular matrix. The resulting solution yielded intact islets that could be isolated by pipette.

Next, we attempted to repeat the cyto-protection studies optimized in Chapter 3. Islets were mixed into solutions of type-1 collagen and/or antioxidant PDN hydrogel and cultured in media ± H_2O_2. Cells encapsulated with antioxidant hydrogel appeared viable in media containing up to 20 μM H_2O_2 as evidenced by calcein-AM staining. Hydrogels without antioxidant substrate (collagen only control) exhibited increased ethidium-homodimer staining, associated with cell-necrosis. This result holds promise that translation of this platform toward islet encapsulation might be feasible, however studies examining verification of this result are necessary. Follow up studies to this experiment would repeat this method with a quantitative measure of cell viability and also measure insulin production in response to glucose stimulation.

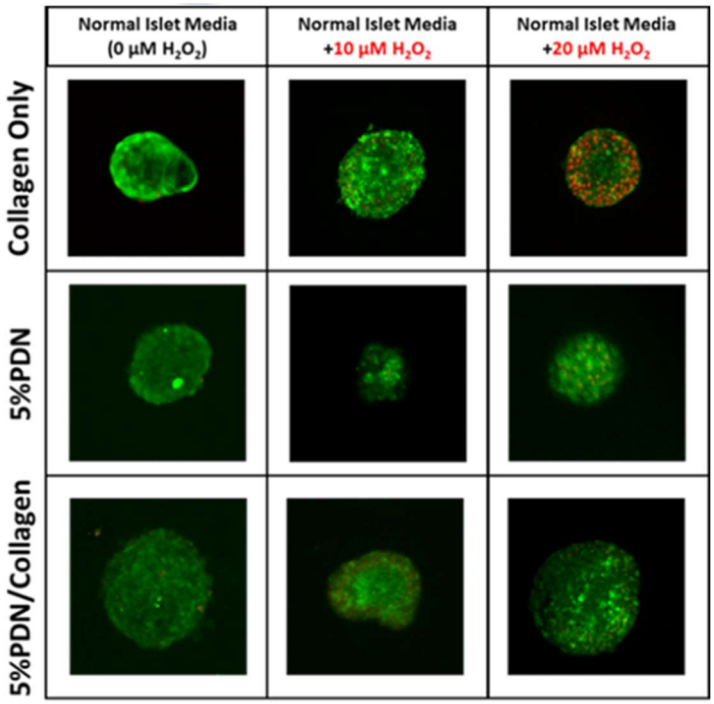

Figure 5.2 Primary islets isolated from C57B6/J mice were encapsulated within hydrogels and challenged with cytotoxic H_2O_2 in vitro. Cells were then stained with LIVE/DEAD stain and assessed by confocal microscopy. DEAD stain became largely apparent in collagen-only control but remained minimal in PDN-inclusive groups suggesting cell-survival.

5.1.2 Antioxidant Hydrogel to Induce Regulatory, Immune Phenotype in Islet Delivery

The central hypothesis of continued work with this hydrogel system is that sustained release of a C-X-C chemokine receptor type 4 (CXCR4) agonist from an injectable hydrogel cell-delivery system with inherent reactive oxygen species (ROS) scavenging will protect against innate, allogeneic, and autoimmune destruction mechanisms and therefore promote long-term transplanted islet function at the omental site. The process of biomaterial/cellular implantation triggers an unavoidable innate immune response that is associated with production of ROS by locally-activated neutrophils and macrophages. The host ROS response is a main source of loss of cell therapies and is especially problematic in islet transplant because the insulin-producing β cells produce unusually low levels of protective, antioxidant enzymes such as catalase, superoxide dismutase, and glutathione peroxidase [1-6].

We plan to leverage our novel antioxidant hydrogel technology for sustained local release of a CXCR4 agonist that will inhibit effector T cell destruction of transplanted allogeneic grafts within non-obese diabetic (NOD) mice. C-X-C motif chemokine 12 ligand (CXCL12) can improve graft acceptance by activating CXCR4, which is expressed on lymphatic cell types such as regulatory T cells (Tregs) and effector T cell populations. Activation of the CXCR4/CXCL12 axis reduces local effector T cell quantity and recruits Tregs [9-12]. We hypothesize that sustained, local activation of the CXCR4/CXCL12 axis by a synthetic CXCR4 agonist will induce a local immuno-tolerogenic environment. Rather than utilize an expensive and potentially unstable CXCL12 recombinant protein, we intend to deliver a new, synthetic CXCR4 agonist, NUCC-390. NUCC-390 has shown promise in in vitro but has yet to be tested in vivo [13]. Unlike competing hydrogel technologies, the PDN formulation provides sustained release of hydrophobic small molecules and potentially enables our goal of achieving long-term allogeneic islet survival without systemic immunosuppression.

Immune rejection and cell sourcing are the key limitations to clinical islet transplant success for Type 1 diabetes. Breakthroughs in stem cell derivation of insulin-producing cells suggests that the cell sourcing problems in diabetes cell therapies will be eventually solved [14-18]. Therefore, the current work focuses on exploration of cell-

encapsulating biomaterials that can abrogate the cytotoxic impact of the innate, acquired, and auto-immune responses to create long-term graft acceptance of allogeneic cell sources at the extra-hepatic, omentum site in recipients with auto-immune type 1 diabetes. This work will focus on proof of concept with transplantation of primary islets with the anticipation of eventual adaptation for delivery of alternative cell sources.

We propose to focus this project on allogeneic transplant into the rigorous NOD recipient mouse model to best mimic the three main immune systems barriers against successful clinical islet transplant (innate, auto-immune, and allo-immune) [19, 20]. The innate immune response accounts for the destruction of approximately 60% of transplanted islets [21, 22]. This is because innate immune neutrophils and macrophages are acutely recruited post-transplant, and these cells create a burst of ROS that are cytotoxic to islets. Characteristic to the NOD model, and clinically relevant to T1D pathology, is the selective, autoimmune destruction of pancreatic β-cells characterized by B and T lymphocytes [23]. Furthermore, we will do species non-matched transplant of C3H mouse donor islets, which normally triggers allogeneic adaptive immunity, creating targeted lymphocytes against specific graft-related antigens. We seek to determine whether, in this most rigorous and clinically-representative model, we can locally produce tolerance over both the innate and adaptive immune systems to generate stable cure with allogeneic cell transplants into autoimmune-diabetic recipients without requiring chronic, systemic immune suppression.

The proposed work will focus on transplant into the omentum. Historically-used hepatic transplant of islets as developed in the Edmonton protocol suffers from graft loss through induction of the instant blood mediated inflammatory reaction and hypoxia [24-27]. There has been a research shift toward developing extra-hepatic islet transplantation sites/technologies. The earliest work focused on physically blocking immune cells with alginate coatings, but this approach historically suffers from foreign body reaction, causing fibrous tissue encapsulation, blocking glucose/insulin transport, and triggering islet dysfunction/death [28-30]. Recent focus has shifted toward

biomaterial scaffolds that provide a temporary support for the islets and are gradually resorbed as the islets graft with the host [31-41]. We will focus on leveraging our hydrogel for transplant into the epidydimal fat pad (mouse equivalent of omentum). The omentum is highly vascular (reducing hypoxic death) and has been confirmed to be a clinically viable islet transplant site in humans that is potentially superior to intrahepatic delivery [41-44]. Current clinical work using the omentum site delivers the islets within a polymerized fibrin gel, which requires subsequent systemic immune-suppression [42, 43]. We propose to replace the fibrin gel with our technology to provide sustained, local immunosuppression and drug release capabilities.

5.2 Shear-Thinning Hydrogel Platform

5.2.1 Shear-Thinning Hydrogels for RNA Interference

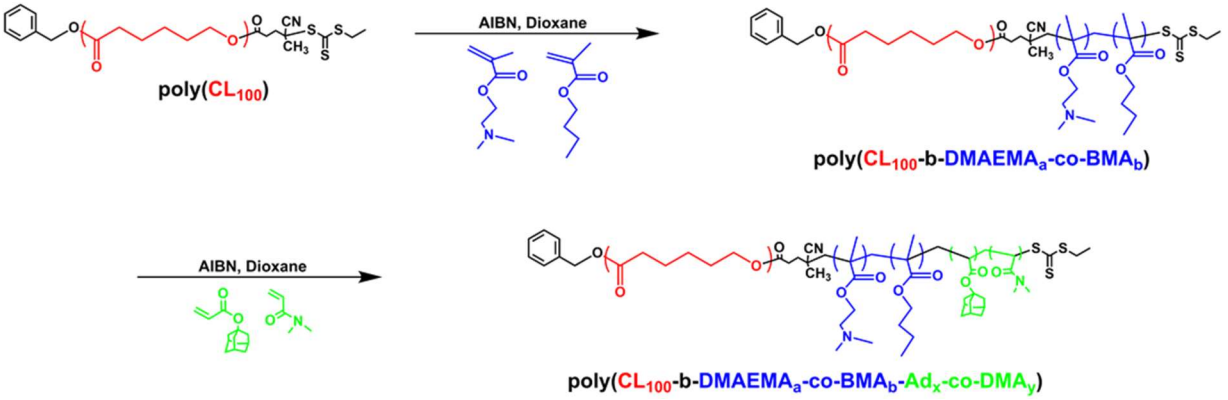

Figure 5.3 Synthesis scheme for siRNA-condensing nanoparticles based upon iterative chemistry of diblock nanoparticles previously optimized.

The crystalline-core, PCL nanoparticles compatible with the material shown in Chapter 4 can be loaded with small-molecule drugs. However, we've recently become interested in modifying its architecture to enable packaging of siRNA. Targeted siRNA therapy is a method of post-transcriptional gene silencing; it temporarily blocks the production of a specific protein by acting directly on the cell-circuitry [45]. We have previously shown efficacy of poly[(ethylene glycol)-*b*-[(butyl methacrylate)-*co*-(2-(dimethylamino)ethyl methacrylate)]] (PEG-*b*-p(BMA-*co*-DMAEMA), PEG-DB) as a suitable delivery vehicle for siRNA *in vivo* [46], and modification of this preexisting platform to include surface-functionalized adamantane might make it amenable to this hydrogel system.

We were first interested in adding siRNA-condensing block, BMA-*co*-DMAEMA (DB), between the core and corona of our preexisting nanoparticles to iterate upon the chemistry we've already optimized (Fig 5.3). Thus, we set out to create a library of polymers to test and fine-tune block lengths and composition. Each monomerically-defined polymer that was prepared is shown in Table 5.1.

poly(CL$_{120}$-b-DMAEMA-co-BMA-b-DMA)

CL #Repeats	DMAEMA	BMA	DMA
120	60	60 (50%)	100
120	60	60 (50%)	200
120	105	60 (40%)	100
120	105	60 (40%)	200
120	115	50 (30%)	100
120	115	50 (30%)	200

Table 5.1 Monomeric units of each block to prepare siRNA-condensing nanoparticle library.

Next, we examined the efficacy of each particle to silence genes *in vitro* by measuring reduction in the expression of luciferase. Luciferase (Luc), as previously described in Chaper 3, can be expressed in mammalian cells by viral transduction, and generates measurable bioluminescence when exogenously stimulated with substrate luciferin. Therefore, to test gene-silencing potential of all these particles in high-throughput, we treated Luc+ 3t3s with nanoparticles carrying Luc siRNA and compared this to a scrambled siRNA with no effect on luciferase production. At a 200 nM dose of siRNA, particles containing 50% B were the only species that didn't lead to overt toxicity defined by total loss in bioluminescent signal from Luc siRNA- and scrambled siRNA-treated samples. Only the 50% B nanoparticle with the shorter corona (100 units of DMA) showed efficacy, reducing bioluminescent signal from Luc siRNA and maintaining signal in scrambled siRNA in comparison to untreated controls. However, gold-standard, Lipofectamine® was twice as effective at knocking down Luc signal; only a 100 nM dose of siRNA was needed to achieve similar silencing, suggesting potential of these nanoparticles to act as a siRNA carrier, but perhaps inefficiently (Fig 5.4). DLS revealed homogeneity in micelle formation with low dispersity and particle size of about 50 nm (Fig A.C.1). Particles were loaded with Luc siRNA at variable N:P and 95% of siRNA was loaded at N:P of 2, demonstrating highly-efficient siRNA packaging (Fig A.C.2).

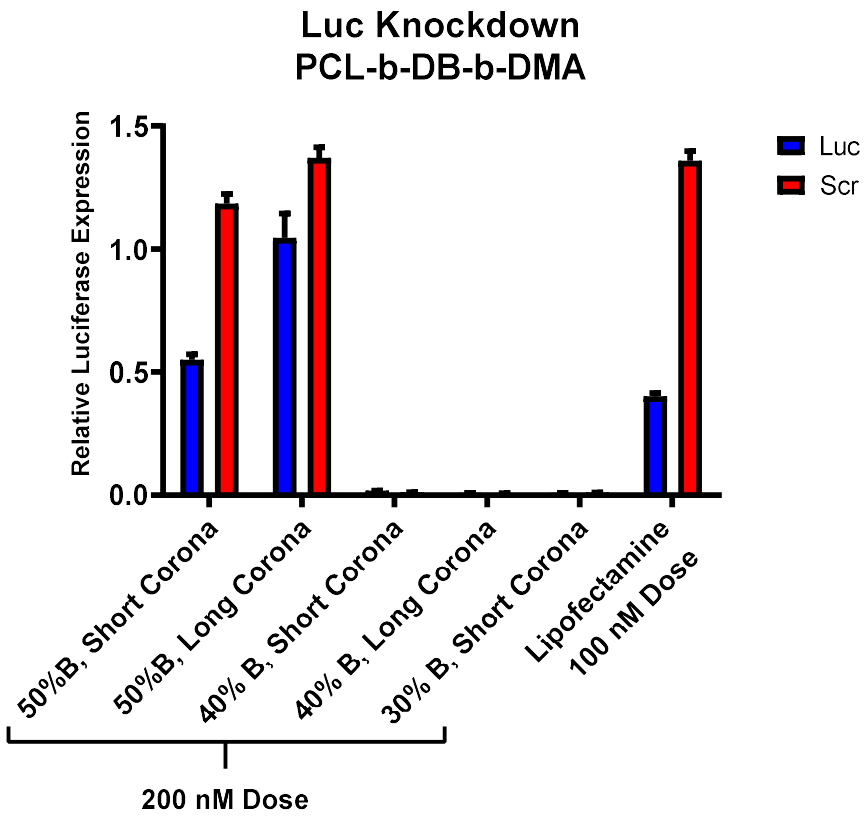

Figure 5.4 Luc knockdown by siRNA loaded into PCL-b-DB-b-DMA library. All nanoparticles except 50%B species were cytotoxic. 50%B with short DMA corona led to approximately 50% knockdown of Luc signal.

When challenged with 25 U/mL of Heparin, 50% B nanoparticles with a short DMA corona rapidly de-complexed from siRNA in comparison to heparin-negative and PEG-DB controls, indicating poor stability under physiological conditions (Fig 5.5). Therefore, we chose to change the chemistry of our nanoparticle to be most analogous to PEG-DB, preparing a diblock particle with only DB-b-DMA-co-Ad. Considering previous work [46-48], we chose to explore DB-core nanoparticles with DMA coronas of either 10K or 5K molecular weight (Fig 5.6.A). 10%Ad was used for both species prepared in unison with prior results for PCL-b-DMA-co-Ad particles from Chapter 4. Both nanoparticles rapidly lysed red blood cells at pH 6.8 and even further at pH 6.2, demonstrating suitable endosomal disruption by acidic lysis (Fig 5.6.B). 10K Corona particles reduced Luc signal by ~75%, compared to PEG-DB control that reduced Luc signal by 50% and 5K Corona particles that exhibited toxicity (Fig 5.6.C). DLS of 10K

Corona nanoparticles showed homogenous, uniform particle populations with low dispersity (Fig A.C.3), while 5K Corona particles was highly disperse and nonuniform (Fig A.C.4). The combination of these results led to exclusion of 5K particles from further analysis. 10K Corona particles were loaded with Luc siRNA at variable N:P and 98% of siRNA was loaded at N:P of 2, demonstrating highly efficient siRNA packaging (Fig A.C.5).

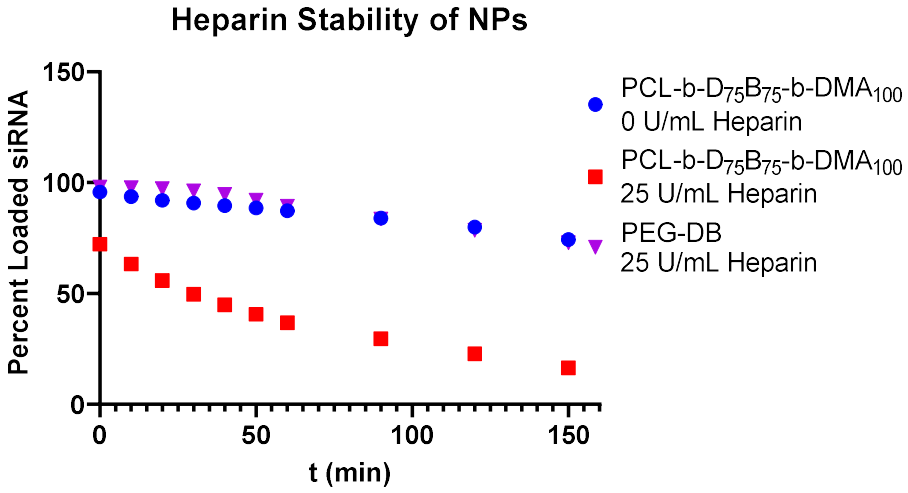

Figure 5.5 PCL-b-DB-b-DMA nanoparticles rapidly dissociate from siRNA cargo under heparin challenge.

Future work will incorporate 10K Corona DB-b-DMA-co-Ad nanoparticles into the shear-thinning hydrogel network in a similar manner to PCL-b-DMA-co-Ad particles. We will optimize gene-silencing of this siRNA hydrogel in an *in vivo* subcutaneous model through silencing of housekeeping gene, GAPDH to demonstrate a hydrogel platform capable of RNA interference.

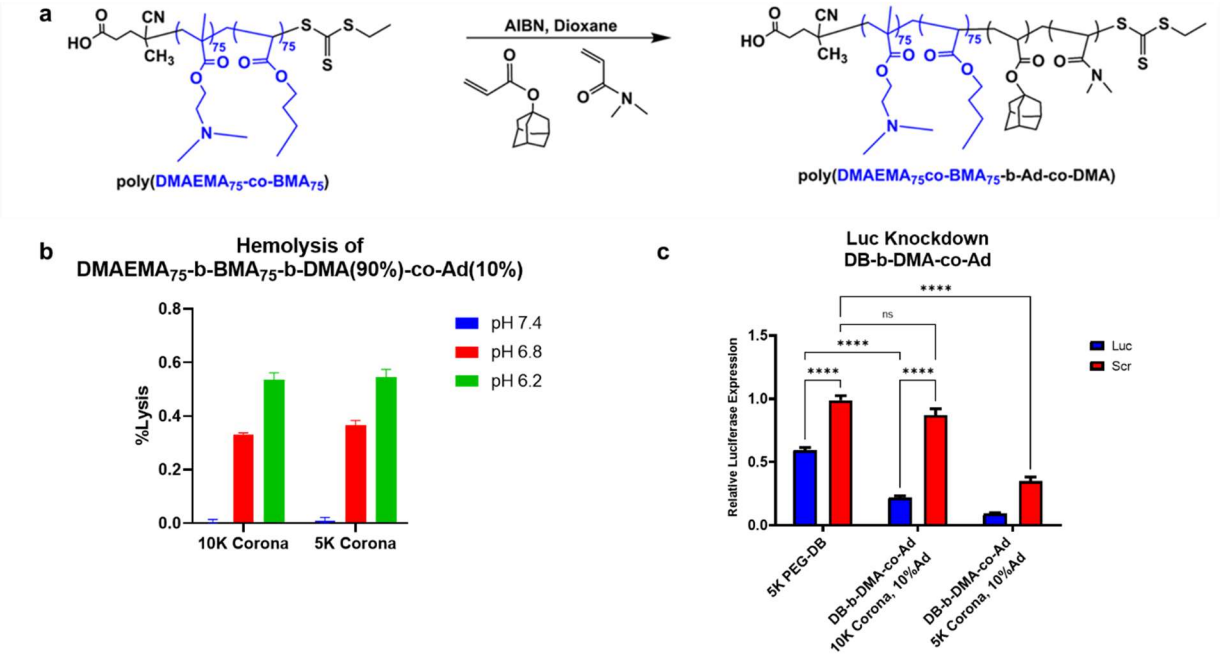

Figure 5.6 Synthesis and characterization of DB-b-DMA-co-Ad nanoparticles (A) Synthesis scheme for DB-b-DMA-co-Ad by RAFT polymerization (B) Both 10K and 5K corona nanoparticles show pH responsive activity at pH 6.8 (C) 10K corona nanoparticles loaded with Luc siRNA reduced Luc signal by ~65% and significantly greater than to 5K PEG-DB, however 5K corona nanoparticles showed toxicity. Data expressed as mean ± SEM, two-way ANOVA with post-hoc Sidak's multiple comparison test, * $p<0.01$

5.2.2 Preparation of a Natural-Synthetic Composite

The modular nature of the synthetic shear-thinning hydrogel prepared in Chapter 4 enables the substitution of its matrix-building blocks with new components to prepare composites. Within reason, any material that can display Cd or Ad can be exchanged in any quantity with the preexisting matrix. Including variable concentrations of hyaluronic acid, which has been previously demonstrated as compatible with our guest-host matrix [49], may improve our system for host cell infiltration to improve revascularization of the grafted cells.

To test this hypothesis, we will utilize hyaluronic-acid with Ad side-pendants as and prepare a new set of hydrogels that incorporate this new component at different ratios within the fully synthetic matrix. This new library of hydrogels will be tested as previously described in Chapter 4 and optimized composition will: (1) tune *in vivo* cell

infiltration such that revascularization can occur as measured by Ki-67 and (2) increase longevity of delivered-cell produced protein, SEAP, in plasma.

5.2.3 Conformal Coating of Silicone Implants

Over 1 million silicone protheses are implanted yearly worldwide, and about 3% of these will result in reoperation due to fibrosis [50]. Recent work by Noskovicova et. al., demonstrated that softening the surface of silicone implants to a modulus of approximately 2 kPa (identical to G' values of the shear thinning gel introduced in Chapter 4) led to reduced collagen deposition, myofibroblast activation and TGF-β1 expression, indicative of abrogated fibrosis. Soft silicone implants are often fabricated to include a rigid outer shell to help them maintain their shape and prevent shear failure, and based upon this stiffness-dependence of fibrotic encapsulation, coating with a soft material may improve outcomes [51].

Silicone can be easily modified to present surface hydroxyls by UV-irradiation [50]. Therefore, by revisiting analogous chemistry for Cd-NH2 synthesis presented in Chapter 4, we can activate these OH- groups by tosylation and directly conjugate adamantylamine to prepare an Ad-functionalized surface. Deposition of our shear-thinning hydrogel system onto this surface will prepare an adhered interface with tunable properties.

In chapter 4, we demonstrated month-long small molecule drug release from our hydrogel by incorporating matrix-adherent nanoparticles, and we will explore the utility of persistent delivery of antifibrotic drug, pirfenidone. Pirfenidone is currently used for treatment of idiopathic pulmonary fibrosis and its suppression mechanism of fibrotic overgrowth is believed to be associated with the MUC1 bioactivation pathway [52]. It is currently in clinical trials as a topical for scleroderma [53] but has yet to be explored in the context of internal, localized applications even though it’s believed to have tremendous potential in transplantation [54]. To this end, we will explore differences in fibrotic overgrowth of silicone implants using the model and readouts demonstrated by Noskovicova et. al. [51].

5.3 References

1. Bloch, K., et al., Catalase expression in pancreatic alpha cells of diabetic and non-diabetic mice. Histochemistry and Cell Biology, 2007. **127**(2): p. 227-232.
2. Chen, H., X. Li, and P.N. Epstein, MnSOD and Catalase Transgenes Demonstrate That Protection of Islets From Oxidative Stress Does Not Alter Cytokine Toxicity. 2005.
3. Gurgul, E., et al., Mitochondrial catalase overexpression protects insulin-producing cells against toxicity of reactive oxygen species and proinflammatory cytokines. Diabetes, 2004. **53**(9): p. 2271-80.
4. Li, X., H. Chen, and P.N. Epstein, Metallothionein protects islets from hypoxia and extends islet graft survival by scavenging most kinds of reactive oxygen species. J Biol Chem, 2004. **279**(1): p. 765-71.
5. Mysore, T.B., et al., Overexpression of glutathione peroxidase with two isoforms of superoxide dismutase protects mouse islets from oxidative injury and improves islet graft function. Diabetes, 2005. **54**(7): p. 2109-2116.
6. Xu, B., J.T. Moritz, and P.N. Epstein, Overexpression of catalase provides partial protection to transgenic mouse beta cells. Free Radical Biology and Medicine, 1999. **27**(7-8): p. 830-837.
7. O'Grady, K.P., et al., Drug-Free ROS Sponge Polymeric Microspheres Reduce Tissue Damage from Ischemic and Mechanical Injury. 2017.
8. Gupta, M.K., et al., Cell Protective, ABC Triblock Polymer-Based Thermoresponsive Hydrogels with ROS-Triggered Degradation and Drug Release. Journal of the American Chemical Society, 2014.
9. Chen, T., et al., Alginate Encapsulant Incorporating CXCL12 Supports Long-Term Allo- and Xenoislet Transplantation Without Systemic Immune Suppression. American Journal of Transplantation, 2015. **15**(3): p. 618-627.
10. McCandless, E.E., et al., CXCL12 limits inflammation by localizing mononuclear infiltrates to the perivascular space during experimental autoimmune encephalomyelitis. Journal of Immunology, 2006. **177**(11): p. 8053-8064.
11. Meiron, M., et al., CXCL12 (SDF-1 alpha) suppresses ongoing experimental autoimmune encephalomyelitis by selecting antigen-specific regulatory T cells. Journal of Experimental Medicine, 2008. **205**(11): p. 2643-2655.
12. Righi, E., et al., CXCL12/CXCR4 Blockade Induces Multimodal Antitumor Effects That Prolong Survival in an Immunocompetent Mouse Model of Ovarian Cancer. Cancer Research, 2011. **71**(16): p. 5522-5534.
13. Mishra, R.K., et al., Discovery and characterization of novel small-molecule CXCR4 receptor agonists and antagonists. Scientific Reports, 2016. **6**.
14. Konagaya, S. and H. Iwata, Reproducible preparation of spheroids of pancreatic hormone positive cells from human iPS cells: An in vitro study. Biochim Biophys Acta, 2016. **1860**(9): p. 2008-16.
15. Vegas, A.J., et al., Long-term glycemic control using polymer-encapsulated human stem cell-derived beta cells in immune-competent mice. Nat Med, 2016. **22**(3): p. 306-11.
16. Pagliuca, F.W., et al., Generation of functional human pancreatic beta cells in vitro. Cell, 2014. **159**(2): p. 428-39.

17. Kroon, E., et al., Pancreatic endoderm derived from human embryonic stem cells generates glucose-responsive insulin-secreting cells in vivo. Nat Biotechnol, 2008. **26**(4): p. 443-52.
18. Baetge, E.E., Production of beta-cells from human embryonic stem cells. Diabetes Obes Metab, 2008. **10 Suppl 4**: p. 186-94.
19. Moore, D.J., et al., Resistance to anti-CD45RB-induced tolerance in NOD mice: mechanisms involved. Transplant International, 2004. **17**(5): p. 261-269.
20. Pearson, T., et al., NOD congenic mice genetically protected from autoimmune diabetes remain resistant to transplantation tolerance induction. Diabetes, 2003. **52**(2): p. 321-326.
21. Evgenov, N.V., et al., In vivo imaging of immune rejection in transplanted pancreatic islets. Diabetes, 2006. **55**(9): p. 2419-28.
22. Huang, X., et al., Resolving the conundrum of islet transplantation by linking metabolic dysregulation, inflammation, and immune regulation. Endocrine Reviews, 2008. **29**(5): p. 603-630.
23. Pearson, J.A., F.S. Wong, and L. Wen, The importance of the Non Obese Diabetic (NOD) mouse model in autoimmune diabetes. Journal of Autoimmunity, 2016. **66**: p. 76-88.
24. Moberg, L., et al., Production of tissue factor by pancreatic islet cells as a trigger of detrimental thrombotic reactions in clinical islet transplantation. Lancet, 2002. **360**(9350): p. 2039-2045.
25. Johansson, H., et al., Tissue factor produced by the endocrine cells of the islets of Langerhans is associated with a negative outcome of clinical islet transplantation. Diabetes, 2005. **54**(6): p. 1755-1762.
26. Berman, D.M., et al., Interference with tissue factor prolongs intrahepatic islet allograft survival in a nonhuman primate marginal mass model. Transplantation, 2007. **84**(3): p. 308-315.
27. Bennet, W., et al., Isolated human islets trigger an instant blood mediated inflammatory reaction: Implications for intraportal islet transplantation as a treatment for patients with type 1 diabetes. Upsala Journal of Medical Sciences, 2000. **105**(2): p. 125-133.
28. de Vos, P., et al., Alginate-based microcapsules for immunoisolation of pancreatic islets. Biomaterials, 2006. **27**(32): p. 5603-17.
29. Vegas, A.J., et al., Combinatorial hydrogel library enables identification of materials that mitigate the foreign body response in primates. Nat Biotechnol, 2016. **34**(3): p. 345-52.
30. Veiseh, O., et al., Size- and shape-dependent foreign body immune response to materials implanted in rodents and non-human primates. Nat Mater, 2015. **14**(6): p. 643-51.
31. Andrades, P., et al., Subcutaneous pancreatic islet transplantation using fibrin glue as a carrier. Transplantation Proceedings, 2007. **39**(1): p. 191-192.
32. Blomeier, H., et al., Polymer scaffolds as synthetic microenvironments for extrahepatic islet transplantation. Transplantation, 2006. **82**(4): p. 452-459.
33. Brady, A.-C., et al., Proangiogenic Hydrogels Within Macroporous Scaffolds Enhance Islet Engraftment in an Extrahepatic Site. Tissue Engineering Part A, 2013. **19**(23-24): p. 2544-2552.

34. Dufour, J.M., et al., Development of an ectopic site for islet transplantation, using biodegradable scaffolds. Tissue Engineering, 2005. **11**(9-10): p. 1323-1331.
35. Gibly, R.F., et al., Extrahepatic islet transplantation with microporous polymer scaffolds in syngeneic mouse and allogeneic porcine models. Biomaterials, 2011. **32**(36): p. 9677-9684.
36. Jiang, K., et al., Local release of dexamethasone from macroporous scaffolds accelerates islet transplant engraftment by promotion of anti-inflammatory M2 macrophages. Biomaterials, 2017. **114**: p. 71-81.
37. Pedraza, E., et al., Macroporous Three-Dimensional PDMS Scaffolds for Extrahepatic Islet Transplantation. Cell Transplantation, 2013. **22**(7): p. 1123-1135.
38. Perez-Basterrechea, M., et al., Plasma-Fibroblast Gel as Scaffold for Islet Transplantation. Tissue Engineering Part A, 2009. **15**(3): p. 569-577.
39. Phelps, E.A., et al., Vasculogenic bio-synthetic hydrogel for enhancement of pancreatic islet engraftment and function in type 1 diabetes. Biomaterials, 2013. **34**(19): p. 4602-4611.
40. Salvay, D.M., et al., Extracellular matrix protein-coated scaffolds promote the reversal of diabetes after extrahepatic islet transplantation. Transplantation, 2008. **85**(10): p. 1456-1464.
41. Weaver, J.D., et al., Vasculogenic hydrogel enhances islet survival, engraftment, and function in leading extrahepatic sites. Science Advances, 2017. **3**(6).
42. Berman, D.M., et al., Bioengineering the Endocrine Pancreas: Intraomental Islet Transplantation Within a Biologic Resorbable Scaffold. Diabetes, 2016. **65**(5): p. 1350-1361.
43. Hamad, O.A., et al., Platelets, complement, and contact activation: partners in inflammation and thrombosis. Adv Exp Med Biol, 2012. **946**: p. 185-205.
44. Jacobs-Tulleneers-Thevissen, D., et al., Human islet cell implants in a nude rat model of diabetes survive better in omentum than in liver with a positive influence of beta cell number and purity. Diabetologia, 2010. **53**(8): p. 1690-1699.
45. Setten, R. L., Rossi, J. J. & Han, S. The current state and future directions of RNAi-based therapeutics. Nat Rev Drug Discov 18, 421–446 (2019).
46. Werfel, T. A. et al. Combinatorial optimization of PEG architecture and hydrophobic content improves ternary siRNA polyplex stability, pharmacokinetics, and potency in vivo. Journal of Controlled Release 255, 12–26 (2017).
47. Miteva, M. et al. Tuning PEGylation of mixed micelles to overcome intracellular and systemic siRNA delivery barriers. Biomaterials 38, 97–107 (2015).
48. Kilchrist, K. V. et al. Gal8 Visualization of Endosome Disruption Predicts Carrier-Mediated Biologic Drug Intracellular Bioavailability. ACS Nano 13, 1136–1152 (2019).
49. Rodell, C. B., Kaminski, A. L. & Burdick, J. A. Rational Design of Network Properties in Guest–Host Assembled and Shear-Thinning Hyaluronic Acid Hydrogels. Biomacromolecules 14, 4125–4134 (2013).
50. Lam, M., Migonney, V. & Falentin-Daudre, C. Review of silicone surface modification techniques and coatings for antibacterial/antimicrobial applications to improve breast implant surfaces. Acta Biomaterialia 121, 68–88 (2021).

51. Noskovicova, N. et al. Suppression of the fibrotic encapsulation of silicone implants by inhibiting the mechanical activation of pro-fibrotic TGF-β. Nat Biomed Eng 1–20 (2021).
52. Ballester, B., Milara, J. & Cortijo, J. Pirfenidone anti-fibrotic effects are partially mediated by the inhibition of MUC1 bioactivation. Oncotarget 11, 1306–1320 (2020).
53. Rodríguez-Castellanos, M., Tlacuilo-Parra, A., Sánchez-Enríquez, S., Vélez-Gómez, E. & Guevara-Gutiérrez, E. Pirfenidone gel in patients with localized scleroderma: a phase II study. Arthritis Research & Therapy 16, 510 (2014).
54. Dosanjh, A. Pirfenidone: Anti-fibrotic agent with a potential therapeutic role in the management of transplantation patients. European Journal of Pharmacology 536, 219–222 (2006).

CHAPTER 6

CONCLUSION

In sum, the work outlined in this dissertation shows the reduction to practice of a ROS-responsive hydrogel system, and presents a novel platform for a synthetic, shear-thinning hydrogel for cell- and drug-delivery. We've demonstrated that the presence of an antioxidant hydrogel can preserve cells from ROS-mediated toxicity, and future work will aim to combine this inherent property with a small molecule drug for long term preservation as a cellular graft in vivo. We also showed our work on the development of a shear-thinning hydrogel system by tuning composition and polymer architecture, which directly influenced intrinsic properties. Inclusion of matrix-bound nanoparticles into the shear-thinning structure enabled prolonged drug-release in vivo. Furthermore, cells encapsulated within the shear-thinning hydrogel displayed improved longevity in trophic factor production by detection of a systemic protein.

APPENDIX A

SUPPLEMENTARY MATERIAL AND FIGURES FOR CHAPTER 3

A.A.1 Selection of collagen concentration to be used in composite

To determine the optimal concentration of collagen to be used in our polymer-collagen composites, we used NIH 3t3 fibroblasts that were stably transduced to express luciferase. Four acid-solubilized rat-tail, type 1 collagen (T1C) solutions were prepared by diluting a 4 mg/mL collagen solution (stock concentration) to 3, 2, 1 mg/mL. Fibroblasts were grown in a T-75 flask using normal cell medium (NCM). Once the cells reached confluence, they were dissociated with 0.05% Trypsin EDTA and centrifuged at 300 g. The medium was aspirated off the resulting cell pellet, and the cells were resuspended in ~3 mL of NCM. Next, the cells were counted, and ~250,000 cells were dispensed into four 2 mL tubes. The T1C solutions were then pH-neutralized using the included neutralization solution at the volumes specified in the instructions.

The tubes were then centrifuged again at 300 g, and the media overtop of the resulting cell pellets was vacuumed off and replaced with 500 mL of either 4, 3, 2, or 1 mg/mL T1C solutions. The cell pellets were then pipetted and mixed thoroughly into the collagen solutions. Next, 50 mL of each collagen/cell solution was pipetted into the bottom of a black-walled 96-well plate in five replicates each. The 96-well plate was placed in the cell incubator at 37°C, 5% CO_2 for 30 min to allow the collagen to gel. Two hundred microliters of NCM was dispensed overtop of the gels in each well, and the 96-well plate was returned to the incubator.

After 48 h, each well was given 150 mL of 37°C NCM containing 0.45 mg/mL d-Luciferin monopotassium salt and the plate was returned to the cell incubator. After 10 min, the plate was placed on a heated stage set to 37°C in an IVIS imaging system, and total luminescent flux was read for 2 min. Based upon our results of growing fibroblasts in T1C, we saw that viability was highest in the 1 and 2 mg/mL solutions (Fig A.A.1). We chose to use the 2 mg/mL solution for our experiments because the 1 mg/mL solution did not form a robust gel. We felt that the concentration should be high enough to enable testing of collagen-only gels as a control in subsequent experiments.

A.A.2 MIN6 Luminescent Signal and Cell Number Relationship

To confirm the direct correlation between cell number and luminescent output of MIN6 cells stably transduced to express luciferase, a serial dilution of cells was performed. Mouse insulinoma pancreatic β-cells (MIN6) below passage 10 and stably transduced to express luciferase and mApple fluorescent protein were seeded into a tissue culture flask at a density of $1.5x10^4$ cells/cm2 and cultured at 37°C, 5% CO_2 for ~4 days or until confluent. The cells were dissociated with 0.25% trypsin for 5 min, suspended in NCM, and centrifuged at 300 g for 5 minutes to form a pellet. The medium was aspirated, and the pelleted cells were resuspended in NCM to a density of $1.8x10^6$ cells/mL. Cells were serially diluted into separate tubes with media, preparing two-fold dilutions each step for six steps. The last tube had no cells and only media to act as a zero-luminescence control.

Next, 200 mL of the solutions of the varying cell densities were pipetted into the wells of a black-walled 96-well plate in triplicate. The plate was then placed in an incubator set to 37°C, 5% CO_2 overnight to allow the cells to adhere. The next morning the plate was removed from the incubator. The media overtop of the cells was aspirated, replaced with 200 mL of 37°C NCM containing 0.45 mg/mL d-Luciferin monopotassium salt, and the plate was returned to the cell incubator. After 10 min, the plate was placed on a heated stage set to 37°C in an IVIS imaging system, and total luminescent flux was read for 2 min.

Based upon the luminescent output, we were able to see a clear increase in luminescence as the cell number was increased (Fig A.A.2). Therefore, we can reasonably assume that this luminescent output relates directly to the number of viable cells in culture.

A.A.3 Injectability of Cell-Laden T1C/PDN Hydrogel Composite

First, 30 mg of lyophilized PDN polymer was weighed and dissolved in 950 mL of 0.2 wt.% acid-solubilized T1C (3 wt.% polymer solution) and allowed to dissolve for 48 h at 4°C. Next, the PDN/T1C solution was brought to neutral pH using 50 mL of the included neutralization solution, and 250,000 NIH 3t3 fibroblasts stably transduced to

express luciferase were pelleted and dispersed into 500 mL of the solution. The cell-laden PDN solution was carefully drawn into a 1-mL syringe through a 16G needle and then injected onto a 100-mm cell culture petri dish that was placed on a hot plate set to 37°C. The dish was moved to the cell incubator for 30 min. After 30 min, the dish was placed back onto the hot plate set to 37°C, and 10 mL of NCM at 37°C containing 0.45 mg/mL d-Luciferin monopotassium salt was added. After 10 min, the dish was placed on a heated stage set to 37°C in an IVIS imaging system, and total luminescent flux was read for 30 s. The dish was then moved back to the hot plate set to 37°C, and the supernatant was replaced with 5 mL of phosphate-buffered saline (PBS) that was prewarmed to 37°C. This washing step was repeated twice more to ensure removal of the d-Luciferin monopotassium salt. Next, 5 mL was aspirated from the dish and replaced with NCM prewarmed to 37°C. The dish was then incubated at 37C, 5% CO_2 for 24 h.

After 24 h of incubation, the media was aspirated out of the dish and again replaced with 10 mL of NCM containing 0.45 mg/mL d-Luciferin monopotassium. After 10 min, the dish was placed on a heated stage set to 37°C in an IVIS imaging system, and total luminescent flux was read for 30 s. When NIH 3t3 fibroblasts were mixed into a PDN hydrogel+collagen composite and injected through a 16G syringe onto a 100-mm petri dish, luminescent measurements demonstrated that the viable cells were exclusively associated with the injected hydrogel, and that viability was maintained for 24 h in culture (Fig A.A.5).

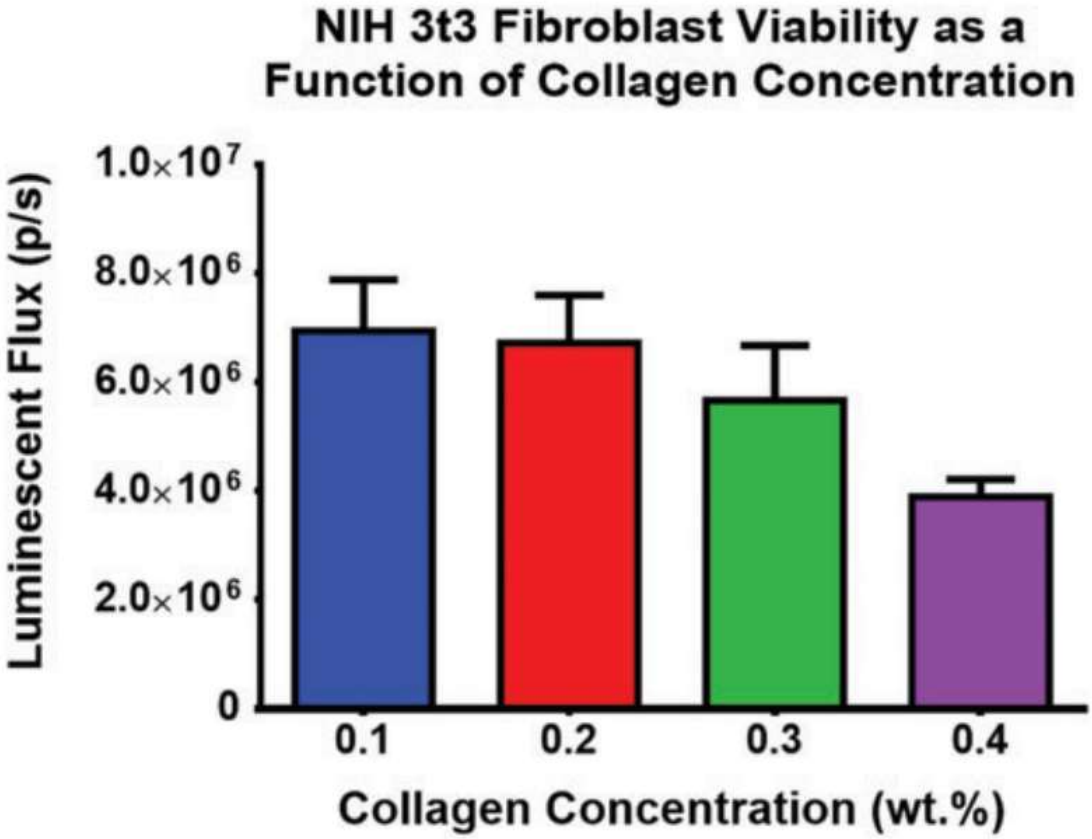

Figure A.A.1 Higher concentrations of collagen lead to decreased cell number of encapsulated 3t3 fibroblasts after 48 h (n = 3, data expressed as mean ± standard error of the mean).

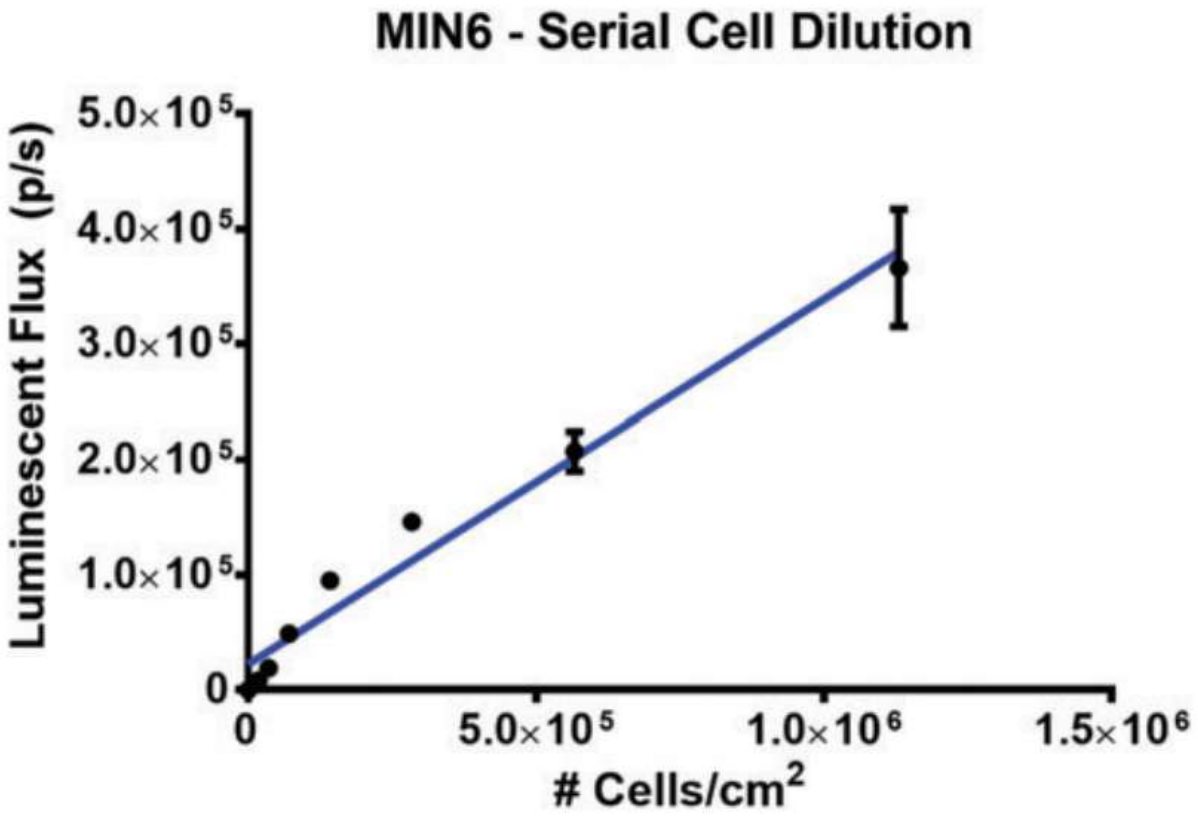

Figure A.A.2. Increasing luminescent signal is directly correlated to increase in cell number (data expressed at mean ± standard error of the mean, linear regression analysis, $R^2 = 0.9216$).

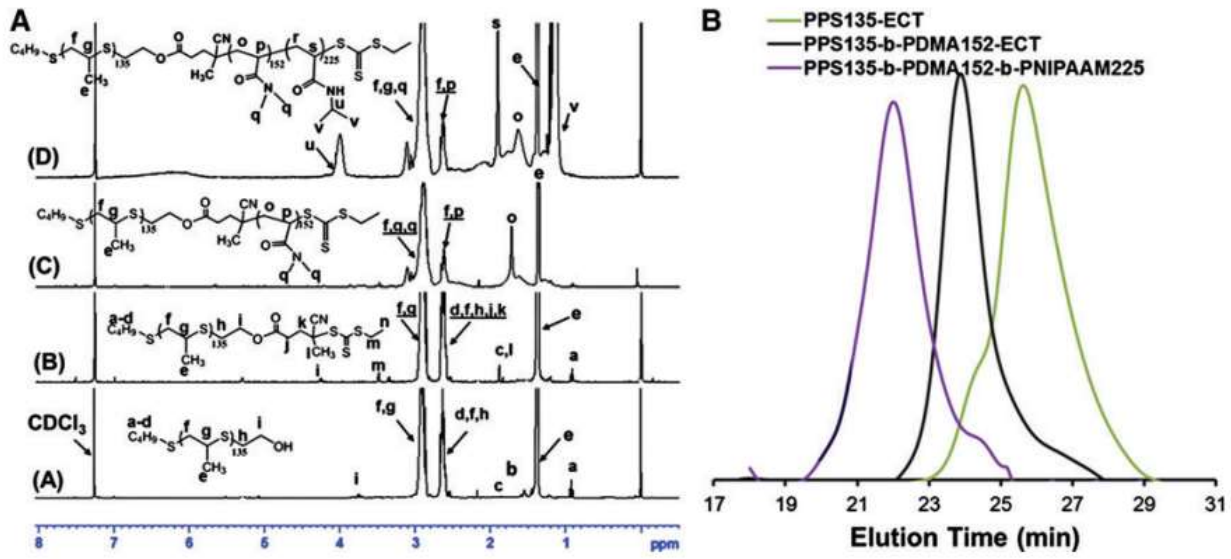

Figure A.A.3 PPS_{135}-b-$PDMA_{152}$-b-$PNIPAAM_{225}$ was successfully synthesized. (A) ^{1}H nuclear magnetic resonance spectra show successful incorporation of all three monomers that comprise the triblock architecture. (B) Gel permeation chromatography trace shows successful stepwise incorporation of each successive polymer block into the triblock copolymer.

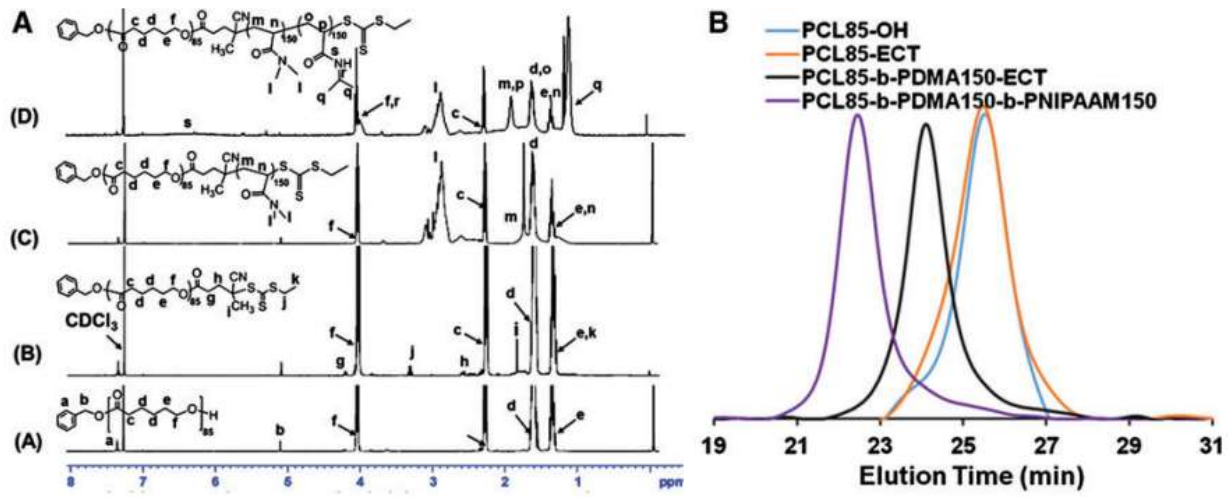

Figure A.A.4 PCL_{85}-b-$PDMA_{150}$-b-$PNIPAAM_{150}$ was successfully synthesized. (A) ^{1}H nuclear magnetic resonance spectra show successful incorporation of all three monomers that comprise the triblock architecture. (B) Gel permeation chromatography trace shows successful stepwise incorporation of each successive polymer block into the triblock copolymer.

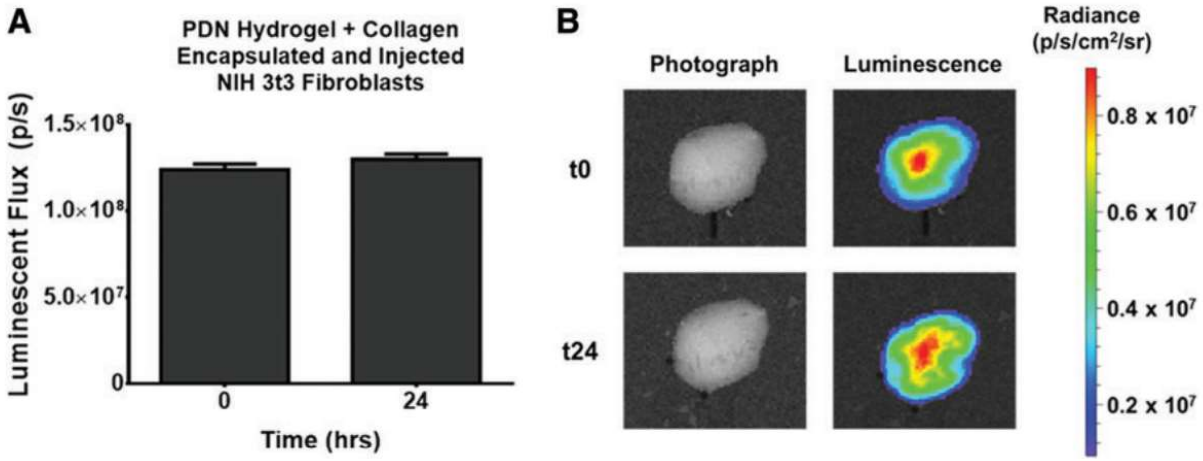

Figure A.A.5 Fibroblasts suspended within PDN hydrogel+collagen composite precursors and injected through a 16G needle onto a heated surface remained exclusively associated with the gelled material and viable for at least 24 h. (A) Luminescent flux readings of NIH 3t3 fibroblasts indicate that all of the cells injected through the syringe remained viable (data expressed at total flux ± SD). (B) Images showing thermogelled hydrogel composite and overlaid luminescent radiance density at the start of the experiment and 24 h later. SD, standard deviation.

APPENDIX B

SUPPLEMENTARY FIGURES FOR CHAPTER 4

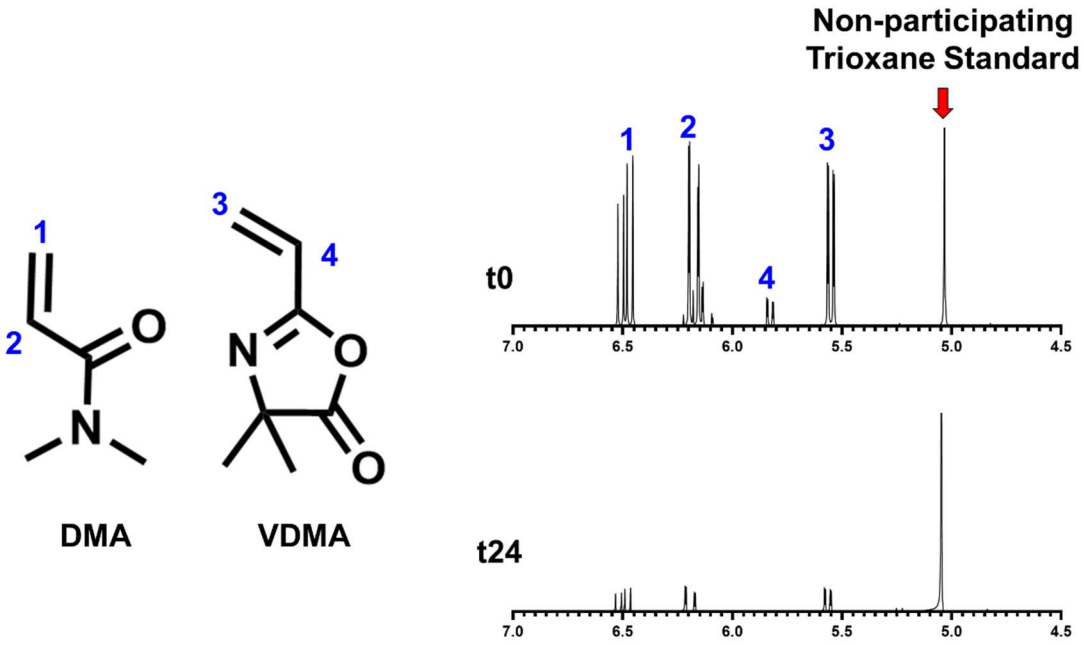

Figure A.B.1 Representative ^{1}H-NMR of DMA-co-VDMA polymerization. Samples were taken of reaction mixture prior to (t0) and after (t24) polymerization and submitted for ^{1}H-NMR and compared to non-participating trioxane standard to derive monomer conversion and degree of polymerization.

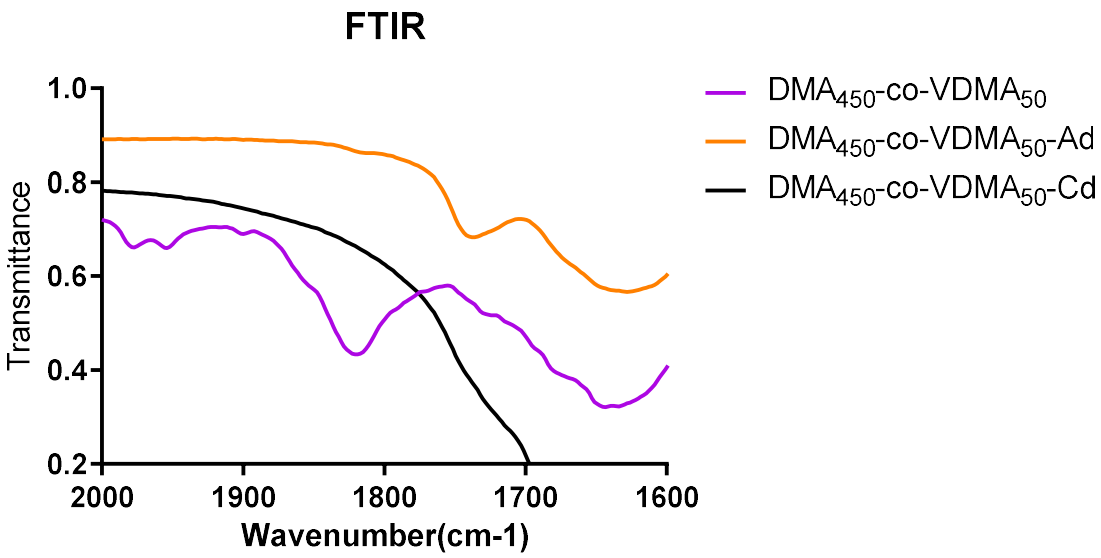

Figure A.B.2 Representative IR-transmittance spectra of pre- and post-modified polymer via VDMA ring-opening. Cyclic-VDMA creates an absorbance peak at ~1825/cm, which disappears following ring-opening modification with primary amine-bearing guest-host molecules.

Target Composition (Ratio)	Actual Composition (Ratio)	Degree of Polymerization	Observation
DMA_{450}-co-$VDMA_{50}$ (90:10)	DMA_{445}-co-$VDMA_{55}$ (89:11)	~500	Gel Formation
DMA_{425}-co-$VDMA_{75}$ (85:15)	DMA_{412}-co-$VDMA_{78}$ (83:17)	~490	Gel Formation
DMA_{400}-co-$VDMA_{100}$ (80:20)	DMA_{382}-co-$VDMA_{108}$ (78:22)	~490	Gel Formation
DMA_{375}-co-$VDMA_{125}$ (75:25)	DMA_{346}-co-$VDMA_{134}$ (72:28)	~480	Ad-Macromer insoluble in PBS
DMA_{350}-co-$VDMA_{150}$ (70:30)	DMA_{280}-co-$VDMA_{140}$ (66:34)	~420	Ad-Macromer insoluble in PBS

Table A.B.1 Composition and subjective gel assessment of hydrogel library

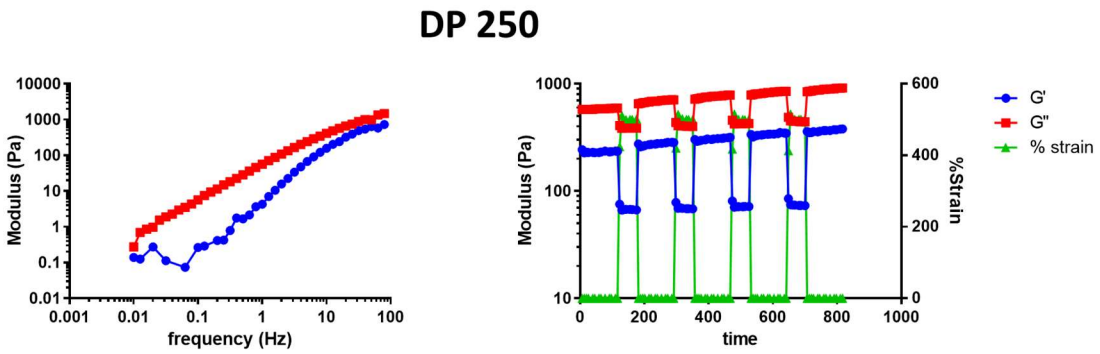

Figure A.B.3 Rheometry of DP250 hydrogel. (A) Stress relaxation time for DP250 was shorter than gels prepared from polymers of larger DP as evidenced by frequency sweep; tan(δ)>1 at all frequencies measured (B) Self-healing mechanical behavior was inconsistent with repeated cycling of strain; moduli progressively increased with respect to strain cycle.

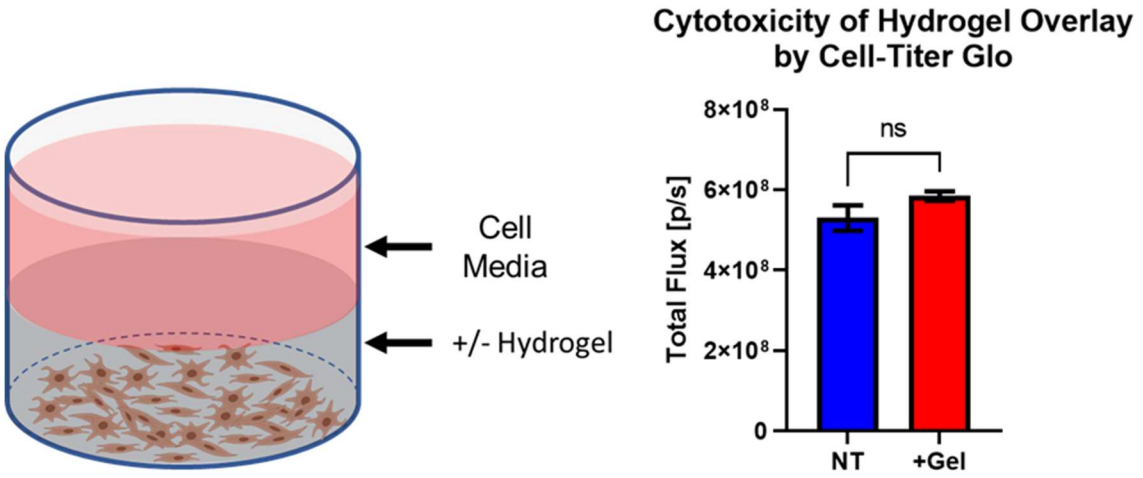

Figure A.B.4 DP1000 hydrogel was non-cytotoxic as evidenced by Cell-Titer Glo® assay of overlaid 3t3 cells in 2D culture in comparison to no hydrogel control. Data expressed as mean ± SD, n=3, unpaired two-tailed t-test

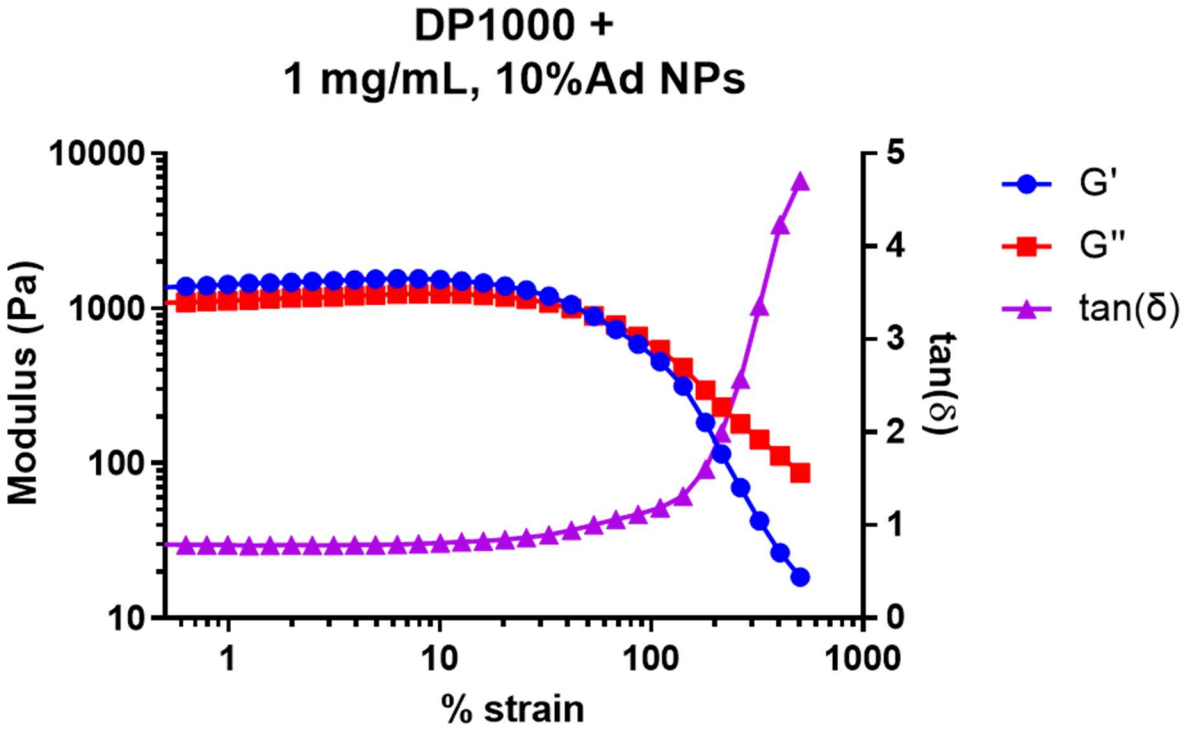

Figure A.B.5 DP1000 hydrogels with 1 mg/mL, 10% Ad NPs demonstrate yield strain at approximately 50% strain.

APPENDIX C

SUPPLEMENTARY FIGURES FOR CHAPTER 5

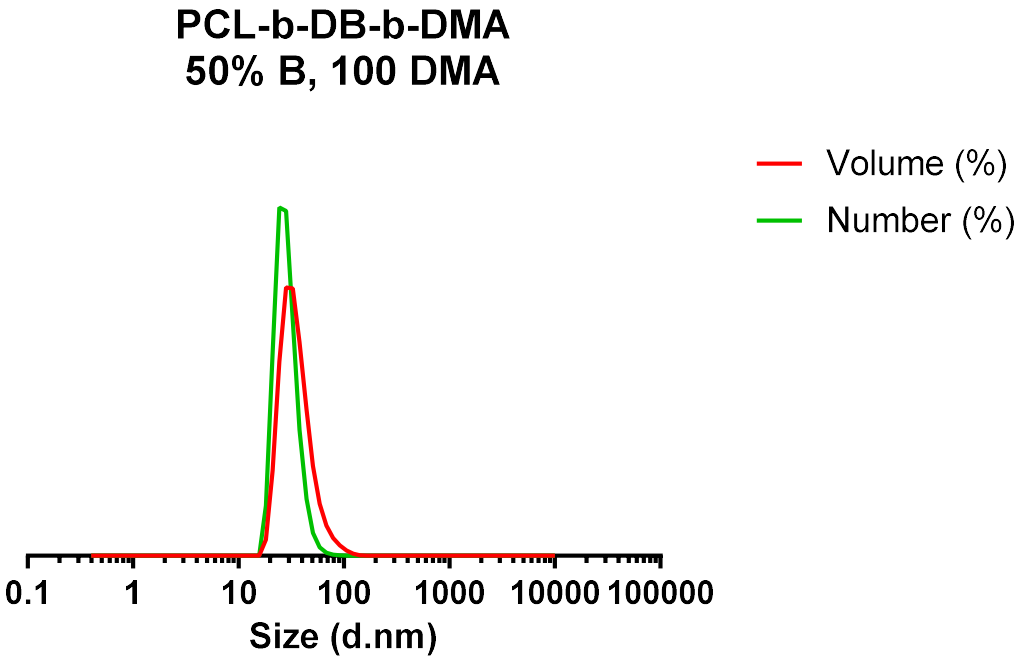

Figure A.C.1 Triblock PCL-b-DB-b-DMA nanoparticles (50%B, 100 units DMA), form homogenous nanoparticles with low dispersity, approximately 50 nm in hydrodynamic diameter

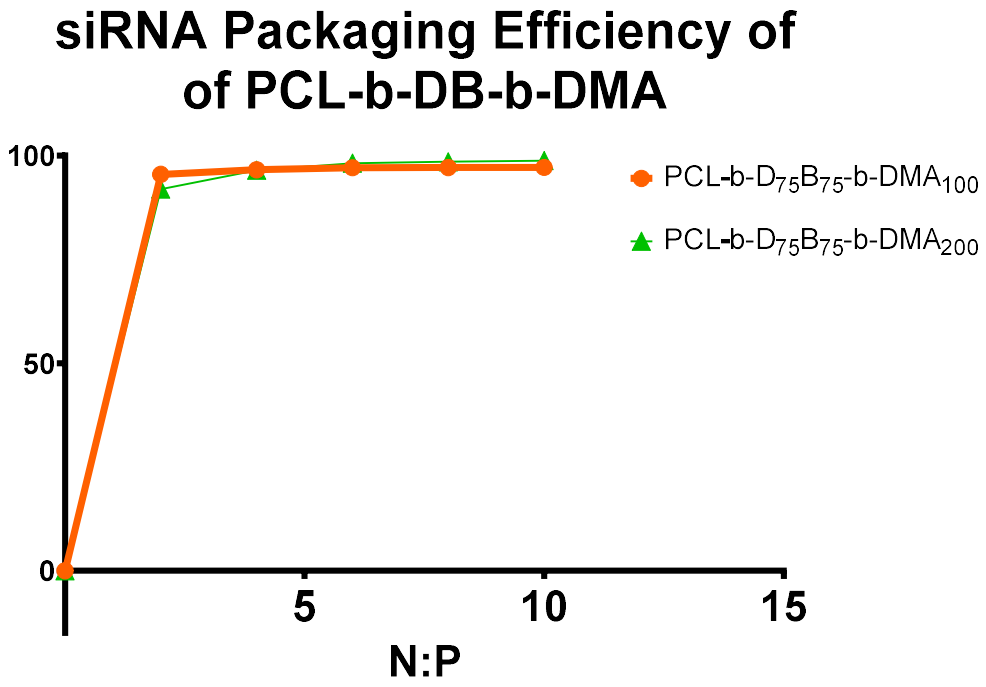

Figure A.C.2 Triblock PCL-b-DB-b-DMA nanoparticles (50%B, 100 or 200 units DMA) efficiently load siRNA with N:P of 2 loading about 95% of siRNA.

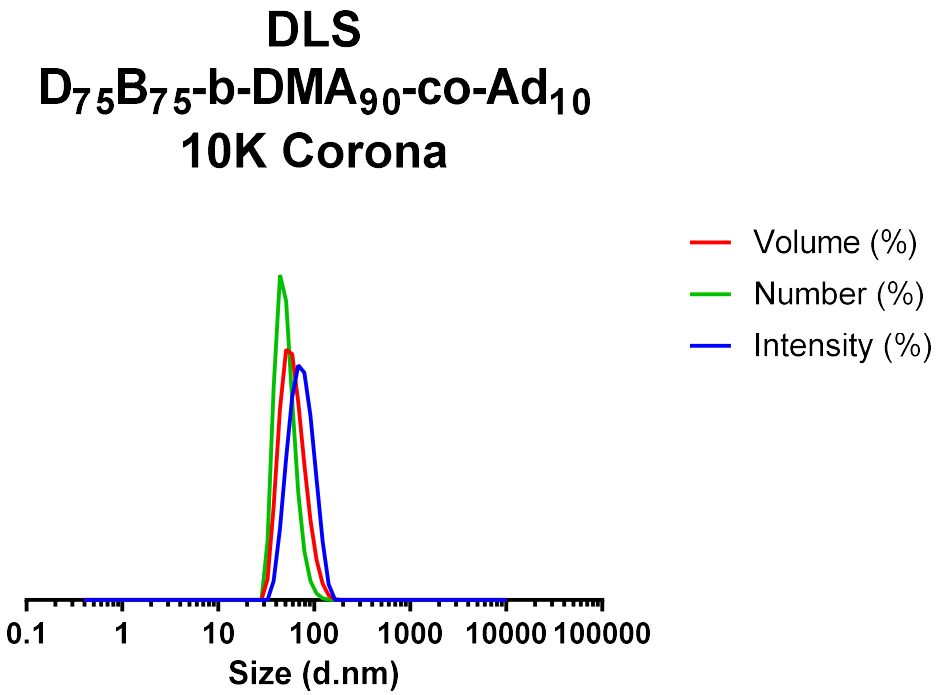

Figure A.C.3 Diblock DB-b-DMA-co-Ad nanoparticles (10K corona), form homogenous nanoparticles with low dispersity, approximately 75 nm in hydrodynamic diameter

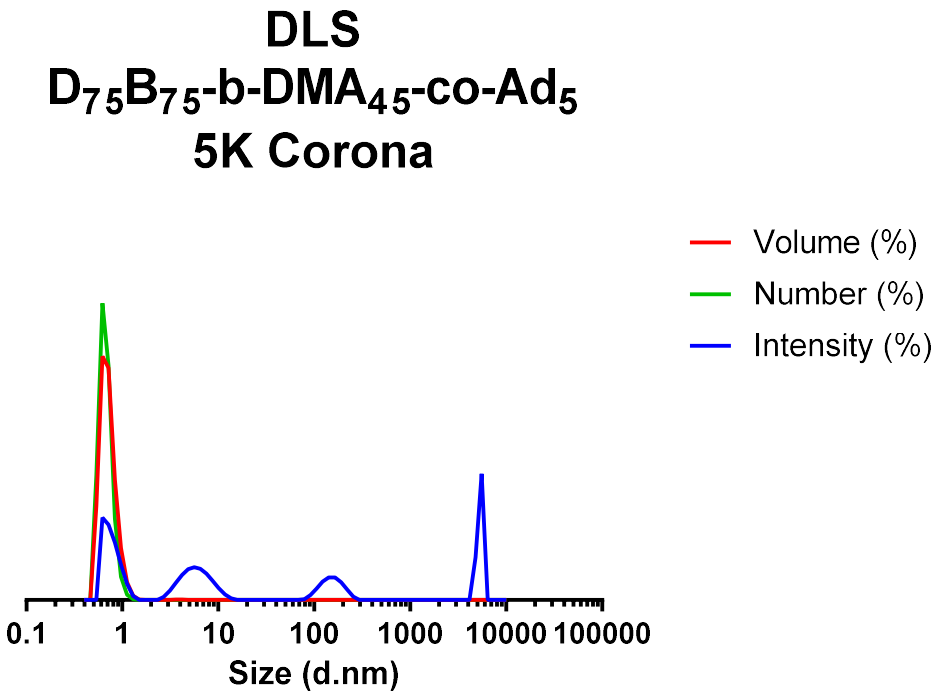

Figure A.C.4 Diblock DB-b-DMA-co-Ad nanoparticles (5K corona) do not form stable nanoparticles

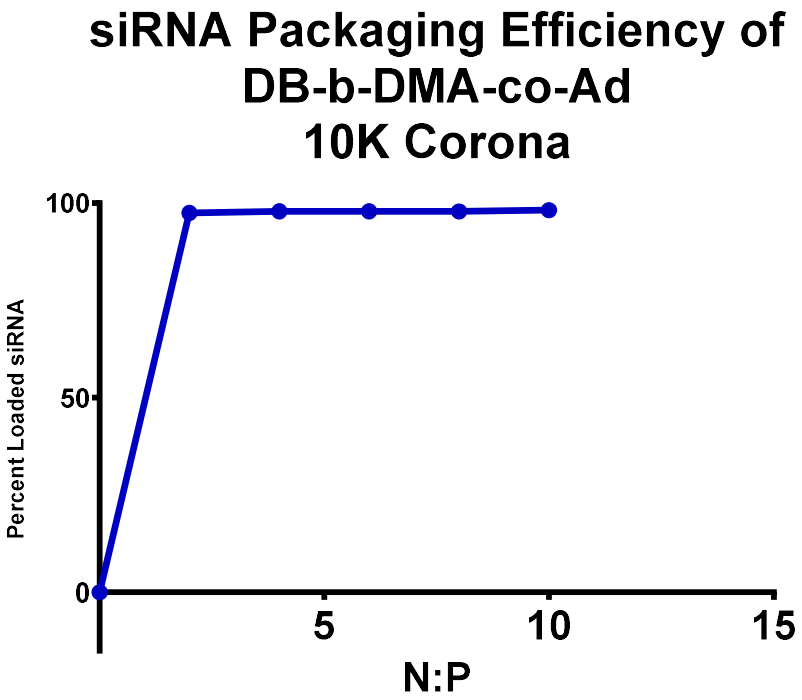

Figure A.C.5 Diblock DB-b-DMA-co-Ad nanoparticles (10K Corona) efficiently load siRNA with N:P of 2 loading about 98% of siRNA.